

**mgr inż. Magdalena Długołęcka**

**„Wyzwania związane z charakteryzacją metodami fluorescencyjnymi pęcherzyków zewnątrzkomórkowych do zastosowań klinicznych na przykładzie płynu z płukania oskrzelowo-pęcherzykowego i osocza pacjentów z podejrzeniem niedrobnokomórkowego raka płuc”**

**Rozprawa na stopień doktora nauk medycznych i nauk o zdrowiu  
w dyscyplinie nauki medyczne**

Promotor: dr hab. n. med. n. o zdr. Małgorzata Czystowska-Kuźmicz

Katedra i Zakład Biochemii WUM



Obrona rozprawy doktorskiej przed Radą Dyscypliny Nauk Medycznych  
Warszawskiego Uniwersytetu Medycznego

Warszawa 2024 r.

**Słowa kluczowe:**

Pęcherzyki zewnątrzkomórkowe, barwienie fluorescencyjne, fluorescencyjna analiza śledzenia nanocząstek, cytometria przepływowa w nanoskali, płyn z płukania oskrzelowo-pęcherzykowego, niedrobnokomórkowy rak płuc

**Keywords:**

Extracellular vesicles, fluorescent staining, fluorescence nanoparticle tracking analysis, nanoscale flow cytometry, bronchoalveolar lavage fluid, non-small cell lung cancer



## Projekty badawcze:

1. NAWA PPI/APM/2019/1/00051/V/00001
2. NCN OPUS 14 2017/27/B/NZ6/01990
3. NAWA BPI/PST/2021/1/00071/U/00001
4. Medical University of Warsaw, Grant Młodego Badacza 1WK/2/M/MB/N/22/22



NARODOWE CENTRUM NAUKI

## Podziękowania

*Składam serdecznie podziękowania*

*Promotorowi*

*Pani dr hab. n. med. n. o zdr. Małgorzacie Czystowskiej-Kuźmich  
za nadzór merytoryczny, wartościowe uwagi i sugestie oraz życzliwą pomoc  
przy przygotowaniu pracy doktorskiej, a także w codziennej pracy badawczej.*

*Dziękuję Pracownikom Katedry i Zakładu Biochemii WUM*

*za życzliwość i wsparcie.*

*Dziękuję Rodzinie*

*za pomoc, motywację, wyrozumiałość i ciągle podnoszenie na duchu.*

## **Wykaz publikacji stanowiących pracę doktorską:**

1. Długolecka M, Szymanski J, Zareba L, Homoncik Z, Domagala-Kulawik J, Polubiec-Kownacka M, et al. Characterization of Extracellular Vesicles from Bronchoalveolar Lavage Fluid and Plasma of Patients with Lung Lesions Using Fluorescence Nanoparticle Tracking Analysis. *Cells*. 2021;10(12).
2. Długolecka M, Czystowska-Kuźmich M. Factors to consider before choosing EV labeling method for fluorescence-based techniques. *Front. Bioeng. Biotechnol. Sec. Nanobiotechnology*. Volume 12 – 2024.

Łączna punktacja cyklu:

Impact factor: 11,96

Punkty MNiSW: 240

## Spis treści

Słowa kluczowe:.....	2
Keywords: .....	2
Projekty badawcze:.....	3
Podziękowania.....	3
Wykaz publikacji stanowiących pracę doktorską:.....	5
Wykaz stosowanych skrótów .....	7
Streszczenie .....	8
Abstract .....	11
Wstęp.....	14
Pęcherzyki zewnątrzkomórkowe jako nośniki informacji.....	14
Postępy w Diagnostyce i Leczeniu Raka Płuc .....	14
Charakteryzacja EVs z wykorzystaniem metod fluorescencyjnych .....	16
Założenia i cel pracy.....	18
Kopie opublikowanych prac.....	20
Podsumowanie i wnioski.....	22
Bibliografia.....	27
Oświadczenia współautorów publikacji .....	29

## Wykaz stosowanych skrótów

BALF – płyn z płukania oskrzelowo-pęcherzykowego (ang. *Bronchoalveolar Lavage Fluid*) pobrany odpowiednio z płuca objętego zmianą chorobową/nowotworem (cBALF) oraz z płuca nieobjętego zmianą chorobową (oBALF)

Cryo-TEM – kriogeniczna transmisyjna mikroskopia elektronowa (ang. *Cryogenic transmission electron microscopy*)

EVs – pęcherzyki zewnątrzkomórkowe (ang. *Extracellular Vesicles*)

f-NTA – fluorescencyjna analiza śledzenia nanocząstek (ang. *Fluorescence Nanoparticle Tracking Analysis*)

NDRP – niedrobnokomórkowy rak płuc (ang. *non-small cell lung cancer*, NSCLC)

nFC – cytometria przepływowa w nanoskali (ang. *Nanoscale Flow Cytometry*)

SEC – chromatografia wykluczenia (ang. *Size Exclusion Chromatography*, SEC)

## Streszczenie

**Wyzwania związane z charakteryzacją metodami fluorescencyjnymi pęcherzyków zewnątrzkomórkowych do zastosowań klinicznych na przykładzie płynu z płukania oskrzelowo-pęcherzykowego i osocza pacjentów z podejrzeniem niedrobnokomórkowego raka płuc.**

Ostatnie badania pokazują, że małe pęcherzyki zewnątrzkomórkowe (ang. *Extracellular Vesicles*, EVs) wydzielane przez wszystkie typy komórek, są zaangażowane w komunikację międzykomórkową poprzez przenoszenie białek, lipidów i materiału genetycznego między komórkami oraz że odzwierciedlają stan fizjologiczny komórek parentalnych. EVs występują we wszystkich typach płynów biologicznych, przez co można je pobrać od pacjentów w sposób małoinwazyjny w postaci tzw. „płynnej biopsji” jako źródło biomarkerów diagnostycznych czy prognostycznych różnych chorób.

Jednakże, z uwagi na swoją heterogenność oraz małe rozmiary, wykorzystanie EVs jako biomarkerów nastrocza wielu problemów technicznych. Większość metod charakteryzacji stosowanych w przypadku komórek nie może zostać użyta w przypadku EVs. W ostatnich latach powstało kilka nowych metod, dedykowanych analizie wielkości, stężenia i molekularnego składu EVs. Szczególnie przydatne wydają się być metody fluorescencyjne, takie jak fluorescencyjna analiza śledzenia nanocząstek (ang. *Fluorescence Nanoparticle Tracking Analysis*, f-NTA) oraz cytometria przepływowa w nanoskali (ang. *Nanoscale Flow Cytometry*, nFC). Pozwalają one na odróżnienie EVs od tła i czynników zakłócających typu lipoproteiny i korona białkowa, szczególnie częste przy izolacji EVs z płynów biologicznych. Wciąż jednak metody te wymagają optymalizacji oraz walidacji by można było je wykorzystać do dokładnej i rzetelnej analizy EVs, która jest podstawą rozwoju przyszłościowych zastosowań EVs jako biomarkerów w praktyce klinicznej.

W niniejszej pracy podjęto próbę optymalizacji i walidacji analizy ilościowej oraz fenotypowej EVs izolowanych z płynów biologicznych - osocza oraz płynu z płukania oskrzelowo-pęcherzykowego (ang. *Bronchoalveolar Lavage Fluid*, BALF), z użyciem metody f-NTA – jednej z najnowszych metod charakteryzacji pęcherzyków zewnątrzkomórkowych. Te badania oryginalne zostały opublikowane jako Publikacja nr. 1 przedstawionego cyklu. Celem badań było opracowanie protokołu izolacji EVs z wymienionych płynów biologicznych oraz protokołu barwienia fluorescencyjnego do dokładnej analizy stężenia oraz składu molekularnego (obecność tetraspanin) EVs metodą f-NTA pod kątem przyszłych zastosowań

EVs jako biomarkerów diagnostycznych i/lub prognostycznych. Jako przykład schorzenia o dużym znaczeniu klinicznym wybrano niedrobnokomórkowy rak płuc (NDRP) – po pierwsze z uwagi na istniejące już doniesienia o możliwej roli EVs jako biomarkerów dla tego typu nowotworu, po drugie z uwagi na możliwość pozyskania od pacjentów z podejrzeniem NDRP wspomnianych dwóch typów płynu biologicznego, osocza i BALF.

Opracowano i zoptymalizowano metodę izolacji EVs z BALF oraz warunki barwienia fluorescencyjnego barwnikiem lipidowym oraz przeciwciałami specyficznymi dla wybranych tetraspanin jako biomarkerów małych EVs pod kątem późniejszej analizy f-NTA. Porównując pomiary wszystkich cząstek w świetle widzialnym NTA z pomiarami EVs po barwieniach fluorescencyjnych dowiedziono, że znakowanie fluorescencyjne dla specyficznych markerów pęcherzyków, takich jak tetraspaniny, jest niezbędne do identyfikacji „prawdziwych” EVs izolowanych z zanieczyszczonych, heterogenicznych próbek biologicznych oraz do precyzyjnej i wiarygodnej analizy ilościowej i molekularnej EVs. Wykazano przy tym silny wpływ zanieczyszczeń takich jak lipoproteiny na barwienia fluorescencyjne i następującą analizę f-NTA EVs. Ponadto ważnym rezultatem pracy była pierwsza tak kompleksowa charakteryzacja ilościowa i jakościowa EVs pochodzących z BALF tak obszernej grupy pacjentów z NDRP (34 pacjentów) przy użyciu klasycznych metod charakteryzacji EV jak i nowatorskiej metody f-NTA. Wykazano, że EVs pochodzące z osocza różnią się wielkością, stężeniem i profilem tetraspanin od tych obecnych w BALF. Co ciekawe, wbrew oczekiwaniom nie stwierdzono różnic dotyczącej wielkości, stężenia i fenotypu EVs pochodzących z płuca chorego (objętego zmianą nowotworową) oraz z płuca zdrowego. W obrębie badanej grupy 34 pacjentów na tym etapie badań nie stwierdzono korelacji między mierzonymi parametrami EVs a dostępnymi danymi klinicznymi.

Podsumowując, pokazano, że znakowanie fluorescencyjne EVs dla określonych markerów pęcherzyków w połączeniu z analizą NTA w trybie rozproszenia i fluorescencji umożliwia precyzyjne określenie stężenia, rozmiaru, dystrybucji i fenotypu powierzchni „prawdziwych” EV izolowanych z heterogenicznych płynów biologicznych. Przeprowadzona analiza f-NTA EVs pochodzących z BALF w porównaniu z EVs pochodzącymi z osocza ujawniła, że metoda ta jest odpowiednia tylko dla stosunkowo czystych próbek EVs izolowanych z BALF lub z nadsącza z hodowli komórkowych. W przypadku preparatów EVs z osocza lub surowicy, o bardzo niskich poziomach EVs w stosunku do zanieczyszczających lipoprotein, konieczne jest wpięrw usunięcie tych zanieczyszczeń, przed barwieniem fluorescencyjnym i analizą f-NTA. Zagadnienia związane z optymalizacją i weryfikacją fluorescencyjnych metod analizy

pęcherzyków zewnątrzkomórkowych do przyszłych zastosowań klinicznych wraz z kompleksowym przeglądem aktualnie dostępnego piśmiennictwa na ten temat zostały przedstawione w Publikacji nr. 2 cyklu, która stanowi część pogładową niniejszej pracy doktorskiej.

Szczegółowe poznanie profilu EVs z BALF na bazie przedstawionego w pracy protokołu analizy f-NTA pozwoli na identyfikację potencjalnych markerów diagnostycznych i prognostycznych i może przyczynić się do stworzenia bardziej spersonalizowanych, skuteczniejszych terapii przeciwnowotworowych.



## Abstract

**Challenges in characterization of extracellular vesicles by fluorescence-based methods for clinical applications using bronchoalveolar lavage fluid and plasma from patients with suspected non-small cell lung cancer as examples.**

Recent studies show that small Extracellular Vesicles (EVs), secreted by all cell types, are involved in intercellular communication by transferring proteins, lipids and genetic material between cells and reflect the physiological state of the parent cells. EVs are found in all types of biological fluids and can therefore be collected from patients in a minimally invasive manner as a so-called "liquid biopsy" as a source of diagnostic or prognostic biomarkers for various diseases.

However, due to their heterogeneity and small size, the use of EVs as biomarkers poses many technical problems. Most characterization methods used for cells cannot be applied to EVs. In recent years, several new methods have been developed to analyze the size, concentration and molecular composition of EVs. Fluorescence-based methods, such as fluorescent nanoparticle tracking analysis (f-NTA) and nanoscale flow cytometry (nFC) appear to be particularly useful. They make it possible to distinguish EVs from background and interfering factors such as lipoproteins and the protein corona, which are particularly common when EVs are isolated from biological fluids. However, these methods need to be optimized and validated to be used for accurate and reliable analysis of EVs, which is the basis for developing future applications of EVs as biomarkers in clinical practice.

In the present study, we attempted to optimize and validate the quantitative and phenotypic analysis of EVs isolated from biological fluids (plasma and bronchoalveolar lavage fluid, BALF) using the f-NTA method, one of the latest cutting-edge methods for characterizing extracellular vesicles. This original research was published as Publication No.1 of the presented series. The purpose of this research was to develop a protocol for the isolation of EVs from biological fluids and a fluorescent staining protocol for the accurate analysis of the concentration and molecular composition (presence of tetraspanins) of EVs by the f-NTA method, in terms of future applications of EVs as diagnostic and/or prognostic biomarkers. Non-small cell lung cancer (NSCLC) was chosen as an example of a disease of high clinical relevance, firstly because of existing reports on the possible role of EVs as biomarkers for this

type of cancer, and secondly because of the possibility of obtaining of the previously mentioned two types of biological fluids, plasma and BALF, from patients with suspected NSCLC.

A method for isolation of EVs from BALF and conditions for fluorescent staining with a lipid dye and antibodies specific for selected tetraspanins as biomarkers of small EVs were developed and optimized for subsequent f-NTA analysis. By comparing measurements of all particles visible under scatter light NTA with measurements of EVs after fluorescent staining, it was demonstrated that fluorescent labeling for specific vesicle markers such as tetraspanins is essential for the identification of "true" EVs isolated from contaminated heterogeneous biological samples and for precise and reliable quantitative and molecular analysis of EVs. The strong influence of contaminants such as lipoproteins on fluorescent staining and subsequent f-NTA analysis of EVs was demonstrated. In addition, an important result of the work was a first such comprehensive quantitative and qualitative characterization of BALF-derived EVs from such a large group of NSCLC patients (34 patients) using classical EV characterization methods as well as the novel f-NTA method. Plasma-derived EVs were shown to differ in size, concentration and tetraspanin profile from those present in BALF. Interestingly, contrary to expectations, no differences in size, concentration and phenotype were found between EVs derived from the diseased lung (affected by the cancer lesion) and the healthy lung. Within the study group of 34 patients at this stage of the study, no correlation was found between the measured EV parameters and available clinical data.

In conclusion, fluorescent immunolabeling of EVs for specific vesicle markers in combination with NTA analysis in scatter and fluorescence modes allows precise determination of the concentration, size, distribution and surface phenotype of "true" EVs isolated from heterogeneous biological fluids. An f-NTA analysis of BALF-derived EVs compared to plasma-derived EVs showed that this method is only suitable for relatively pure EV samples isolated from BALF or cell culture filtrate. For plasma- or serum-derived EV preparations with very low levels of EVs relative to contaminating lipoproteins, it is necessary to first remove these contaminants prior to fluorescent staining and f-NTA analysis. Issues related to the optimization and validation of fluorescence-based methods for the analysis of extracellular vesicles for future clinical applications, together with a comprehensive review of the currently available literature on the subject, are presented in Publication No. 2 of the series, as the review part of this dissertation.

A detailed understanding of the profile of EVs from bronchoalveolar lavage fluid (BALF) on the basis on the f-NTA analysis protocol presented in this work will allow the identification of potential diagnostic and prognostic markers and may contribute to the development of more personalized, more effective cancer therapies.

# Wstęp

## Pęcherzyki zewnątrzkomórkowe jako nośniki informacji

W ostatnich latach wiele uwagi poświęcono badaniom nad nośnikami informacji między komórkami, jakimi są uwalniane z komórek małe pęcherzyki zewnątrzkomórkowe (ang. *Extracellular Vesicles*, EVs) wielkości 30-300 nm (1). W hodowlach *in vitro* zaobserwowano wytwarzanie EVs przez większość typów komórek. *In vivo* wykazano ich obecność we krwi, w płynie z płukania oskrzelowo-pęcherzykowe (ang. *Bronchoalveolar Lavage Fluid*, BALF), w płynie stawowym, w moczu, w ślinie, w płynie mózgowo-rdzeniowym, w wodach płodowych oraz w mleku (2). W skład pęcherzyków wchodzi między innymi mRNA, miRNA, białka i lipidy z komórki, z której pochodzą. EVs są wytwarzane zarówno przez komórki prawidłowe, jak i patologiczne (3). EVs pochodzenia nowotworowego uczestniczą w procesie regulacji mikrośrodowiska guza, poprzez transfer białek i materiału genetycznego między komórkami. Co ciekawe, w stanach patologicznych ich liczba rośnie, a więc zwiększone stężenie EVs w krwi czy innych płynach biologicznych może być wczesnym markerem diagnostycznym dla nowotworu w ramach w tzw. płynnej biopsji (4-6).

## Postępy w Diagnostyce i Leczeniu Raka Płuc

Rak płuc jest agresywnym nowotworem złośliwym o bardzo niekorzystnym rokowaniu z dużym odsetkiem zgonów. Każdego roku 1.8 miliona ludzi na świecie jest diagnozowanych, a 1.6 miliona ludzi umiera z powodu tej choroby. Pięcioletnie przeżycie waha się między 4 a 17% (7). Najczęstsze postaci raka płuc to niedrobnokomórkowy rak płuca (NDRP) oraz drobnokomórkowy rak płuca (DRP), występujące odpowiednio w ok. 80 i ok. 20% przypadków. Z kolei najczęstsze typy NDRP to rak gruczołowy i rak płaskonabłonkowy (8). Z uwagi na długotrwały rozwój bez widocznych objawów, choroba ta jest często rozpoznawana dopiero w zaawansowanym stadium, kiedy niemożliwe jest już leczenie chirurgiczne. Wczesne biomarkery diagnostyczne mogłyby znacznie poprawić wykrywalność tego nowotworu i umożliwić wdrożenie wczesnego leczenia, kiedy rokowania są dużo korzystniejsze. W licznych pracach wykazano, że dla wielu typów nowotworów, w tym też dla NDRP, takimi wczesnymi potencjalnymi markerami mogą być EVs (9, 10). Z uwagi na to, że komórki nowotworowe wydzielają znacznie więcej EVs w porównaniu do komórek zdrowych, pacjenci z różnymi nowotworami charakteryzują się zwiększonym stężeniem EVs pochodzenia nowotworowego w różnych płynach biologicznych, jak np. krew obwodowa, które można analizować w mało inwazyjny sposób. W przypadku pacjentów z podejrzeniem NDRP są oni

kierowani na bronchoskopię diagnostyczną. Podczas tej procedury może zostać im dodatkowo wykonane płukanie oskrzelowo-pęcherzykowe i pobrany BALF, w którym EVs, ze względu na bliskość guza, mogą pojawiać się na wcześniejszym etapie choroby i w wyższym stężeniu niż w krwi obwodowej, a także mogą one lepiej odwzorowywać skład mikrośrodowiska nowotworu. Spodziewano się więc, że EVs pochodzące z osocza, a tym bardziej z BALF, mogą być dobrym kandydatem na wczesny marker diagnostyczny dla NDRP.

Do niedawna jedynym stosowanym rozwiązaniem stosowanym w terapii NDRP były chemioterapia i radioterapia (7, 11). Dzięki zgłębianiu biologii nowotworów i rozwoju nowoczesnych technik badawczych, coraz lepiej rozumiane są przyczyny oraz mechanizmy rozwoju chorób nowotworowych, a dzięki temu można projektować coraz bardziej dopasowane i skuteczniejsze terapie. Postęp ten umożliwia tworzenie leczenia spersonalizowanego (terapię biologiczne/terapię celowane) (12, 13). Przykładem terapii celowanych są leki będące inhibitorami receptora naskórkowego czynnika wzrostu (ang. EGFR), takie jak Osimertinib oraz zastosowanie Lorlatinibu, który jest inhibitorem kinazy chłoniaka anaplastycznego (ang. ALK) (13). Leki te hamują rozwój choroby nowotworowej, można je stosować w domu w postaci tabletek i mają mniej skutków ubocznych niż chemioterapia czy radioterapia. Niestety tego typu terapie sprawdzają się tylko u niewielkim odsetku pacjentów, u których stwierdzono określone mutacje genetyczne. Co więcej, pomimo początkowej poprawy, z czasem u tych pacjentów wytwarza się lekooporność i następuje dalsza progresja choroby.

W ostatnim czasie w leczeniu NDRP zaczęła być stosowana immunoterapia - nowe podejście terapeutyczne wykorzystujące inhibitory punktów kontrolnych (np. szlak PD-1/PD-L1), które wzmacniają naturalną reakcję immunologiczną do walki z nowotworem (14). Przykładami leków tego typu są Pembrolizumab i Durvalumab (15, 16). Niestety skuteczność immunoterapii u poszczególnych pacjentów jest bardzo zróżnicowana i prawdopodobnie silnie zależy od stopnia supresji układu odpornościowego, szczególnie w mikrośrodowisku nowotworu. Dodatkowo, stosowanie tego typu terapii często wiąże się z zwiększonym ryzykiem silnie toksycznego działania (17). Terapię tę należy dobierać pod kątem statusu immunologicznego danego pacjenta. Poznanie składu molekularnego EVs, które są odzwierciedleniem wydzielających je komórek, także komórek immunologicznych, może pozwolić na określenie stopnia immunosupresji u danego pacjenta i zdecydować, czy immunoterapia będzie u niego skuteczna. Zbadanie i monitorowanie profilu EVs u konkretnych pacjentów w trakcie terapii może więc dostarczyć informacji o odpowiedzi na leczenie i pozwolić na ewentualne modyfikacje terapii (18-23). Stąd też szczegółowe poznanie

liczby i profilu EVs z BALF, a w szczególności EVs pochodzenia nowotworowego, może przyczynić się do stworzenia bardziej spersonalizowanych, skuteczniejszych terapii przeciwnowotworowych w NDRP.

### **Charakteryzacja EVs z wykorzystaniem metod fluorescencyjnych**

Aby móc wykorzystywać obecne w płynach biologicznych pacjentów EVs jako biomarkery diagnostyczne lub prognostyczne, konieczne jest opracowanie wiarygodnych i powtarzalnych protokołów ich izolacji i analizy ilościowej i jakościowej. Ze względu na mały rozmiar i dużą heterogenność pęcherzyków obecnych w płynach biologicznych, a także na trudności w uniknięciu zanieczyszczeń w postaci agregatów białek, lipoprotein czy białkowej korony podczas izolacji EVs z płynów biologicznych, konieczne jest odpowiednie opracowanie i walidacja metod izolacji oraz charakteryzacji EVs.

Przed przeprowadzeniem procesu analizy EVs, w większości wypadków należy przeprowadzić proces separacji pęcherzyków od innych składników znajdujących się w płynach biologicznych. Metody stosowane rutynowo do izolacji EVs z hodowli komórkowych w przypadku płynów biologicznych muszą zostać zoptymalizowane indywidualnie do każdego płynu biologicznego, z uwagi na jego unikalny skład i właściwości, w tym obecność składników zakłócających pomiar oraz zróżnicowany rozmiar oraz profil białkowy EVs. W zależności od typu płynu biologicznego, stosuje się różne metody izolacji.

W przypadku osocza najczęściej stosowaną metodą jest chromatografia wykluczenia (ang. *Size Exclusion Chromatography*, SEC) (24), która pozwala frakcjonować cząstki ze względu na ich wielkość. Istotne jest, że liczba lipoprotein w osoczu jest o kilka rzędów wielkości większa niż liczba EVs, a lipoproteiny mogą być współizolowane z EVs podczas procesu separacji, co prowadzi do potencjalnego zanieczyszczenia lub zakłócenia procesu barwienia EVs. SEC pozwala na oddzielenie lipoprotein o średniej i małej gęstości (IDL i LDL) oraz lipoprotein o dużej gęstości (HDL) ze względu na ich różnicę w wielkości, ale nie usuwa lipoprotein o bardzo małej gęstości (VLDL) i chylomikronów (25-28). Niezależnie od metody izolacji, udowodniono że w przypadku próbek osocza zaleca się pobieranie próbek krwi na czczo w celu zmniejszenia zanieczyszczenia lipoproteinami (29). W przypadku analizy śledzenia nanocząstek (NTA), w jej konwencjonalnej wersji z pomiarem w świetle widzialnym (tzw. ang. *'scatter mode'*) nie można odróżnić EVs od lipoprotein a także od agregatów białek czy innych zanieczyszczeń o podobnej wielkości. Przedstawiona poniżej Publikacja nr. 1 jest jedną z pierwszych prac potwierdzających tę tezę i pokazującą różnice w pomiarach EVs

z użyciem NTA z udziałem światła rozproszonego oraz z użyciem zmodyfikowanej wersji NTA w trybie fluorescencji (ang. *Fluorescence Nanoparticle Tracking Analysis*, f-NTA), Dodatkowo, ostatnio zauważono, że znakowanie samymi barwnikami lipofilowymi nie pozwala odróżnić EVs od lipoprotein oraz, że lipoproteiny wpływają na dokładność i specyficzność znakowania (26), co też zweryfikowano w przedstawionej pracy.

BALF ma zupełnie inny skład i dostępną klinicznie objętość w stosunku do osocza, dlatego wymaga innego podejścia w przypadku izolacji EVs. Płyn ten charakteryzuje się wysoką lepkością, utrudniającą stosowanie metody SEC, dodatkowo BALF nie zawiera lipoprotein, czy wysokiego stężenia białek, które zakłócałyby późniejszy pomiar. W czasie opracowywania metody nie było dostępnej metody SEC dla dużych objętości płynu, a próby zagęszczenia go nie powiodły się ze względu na jego wysoką lepkość. Z uwagi na doniesienia literaturowe zdecydowano się więc w tym przypadku zastosować ultrawirowanie (UC) do izolacji EVs (30).

Bezpośredni pomiar małych EVs za pomocą konwencjonalnej cytometrii przepływowej jest niemożliwy, ponieważ ich rozmiar jest poniżej granicy wykrywalności instrumentów (31-33). Co więcej, ich mały rozmiar ma również pewne implikacje na sposób znakowania fluorescencyjnego EVs oraz wymusza często inne procesy barwienia i płukania niż w przypadku komórek.

Aby sprostać tym wyzwaniom, opracowano kilka bardzo czułych metod, które są w stanie bezpośrednio mierzyć EV znakowane fluorescencyjnie. Najczęściej stosowanymi metodami są f-NTA i cytometria przepływowa w nanoskali (ang. *Nanoscale Flow Cytometry*, nFC). Dodatkowo, niedawno pojawiły się inne metody, które mogą być stosowane w ograniczonym zakresie do charakteryzacji EV, takie jak te oparte na tzw. bezpośredniej stochastycznej rekonstrukcji optycznej (dSTORM) lub tzw. jednocząsteczkowym interferometrycznym sensorze obrazowania odbiciowego (ang. *Single-Particle Interferometric Reflectance Imaging Sensor*, SP-IRIS) połączonym z mikroskopią fluorescencyjną.

Dodatkowo, z uwagi na małe rozmiary EVs, często pokrywające się wielkością z czynnikami zakłócającymi zawartymi w próbce, takimi jak lipoproteiny oraz składniki tła (agregaty białek, kryształy soli), konieczne jest przeprowadzenie różnych pomiarów kontrolnych (zbadanie samego tła, buforu, liza próbki w celu sprawdzenia specyficzności sygnału, itd.), aby prawidłowo zweryfikować wyniki. W przeciwieństwie do standardowego NTA, które mierzy liczbę wszystkich cząstek obecnych w roztworze, metody fluorescencyjnej analizy EVs pozwalają na odróżnienie EVs od zanieczyszczeń oraz tła próbki.

## Założenia i cel pracy

Dotychczasowe badania sugerują, że profil EVs w płynach biologicznych może zostać wykorzystany do wczesnego wykrywania nowotworów oraz późniejszego monitorowania immunologicznego oraz kontroli postępów w terapii w przypadku NDRP (9, 10, 18).

Praca ta ma na celu:

- Opracowanie metody izolacji EVs z BALF.
- Porównanie ilościowe i jakościowe profilu EVs z krwi i BALF.
- Porównanie cBALF z oBALF - czy nowotwór wpływa na całe płuca, czy są to odrębne środowiska?
- Określenie czy ilość EVs w krwi i/lub BALF może być markerem diagnostycznym?
- Przegląd dostępnych metod analizy EVs z wykorzystaniem technik fluorescencyjnych.
- Przedstawienie zalet i wad poszczególnych metod fluorescencyjnych.
- Przedstawienie różnic między barwieniem komórek, a EVs.
- Określenie wpływu metody izolacji oraz zanieczyszczeń na uzyskane wyniki.

Niniejsza rozprawa obejmuje cykl dwóch publikacji. W Publikacji nr. 1 przedstawiono dostępne metody izolacji EVs z płynów biologicznych oraz szczegółowo uzasadniono wybór metod izolacji EVs w przypadku krwi obwodowej i BALF 34 pacjentów z podejrzeniem NDRP. Następnie przeprowadzono szczegółową charakteryzację EVs wyizolowanych z BALF oraz krwi obwodowej za pomocą metod Western Blot, Cryo-TEM oraz cytometrii opartej na kulkach magnetycznych, zgodnie z wytycznymi Międzynarodowego Towarzystwa Pęcherzyków Zewnątrzkomórkowych (34). Ponadto przeprowadzono pomiar stężenia, wielkości, a także charakteryzację pęcherzyków z wykorzystaniem barwienia membranowego oraz za pomocą przeciwciał na specyficzne białka egosomalne (CD63, CD9, CD81) nowatorską metodą f-NTA. Porównano wyniki dla płuca objętego zmianami chorobowymi, płuca zdrowego oraz osocza. Przeprowadzono także eksperymenty kontrolne, tj. analizę f-NTA próbek EVs po lizie, po usuwaniu lipoprotein oraz po usunięciu subpopulacji EVs zawierających tetraspaniny. Dokonano także próby korelacji wyników z danymi klinicznymi pacjentów. Przeprowadzone badania pozwoliły na zaobserwowanie kluczowych parametrów mających wpływ na dane uzyskane w wyniku analizy EVs z użyciem metod fluorescencyjnych



i pozwoliły na późniejsze przygotowanie pracy przeglądowej omawiającej wszystkie te parametry.

W Publikacji nr. 2 szczegółowo omówiono metodykę jaką powinno się zastosować przy analizie EVs za pomocą metod fluorescencyjnych, aby uzyskać jak najbardziej rzetelne informacje o właściwościach EVs do późniejszego zastosowania EVs jako biomarkerów w aplikacjach klinicznych. Prześladowano istniejące metody fluorescencyjne pozwalające na określenie wielkości i stężenia EVs oraz na charakteryzację ich składu. Szczegółowo omówiono czynniki jakie należy wziąć pod uwagę planując analizę EVs, tak aby wyniki oddawały miarodajne informacje na temat wielkości, stężenia oraz składu i funkcjonalności EVs. Uwzględnienie przedstawionych czynników przy fluorescencyjnej analizie EVs, pozwoli w dłuższej perspektywie, na prowadzenie lepszej jakości badań naukowych oraz uzyskanie bardziej zweryfikowanych informacji, które można zastosować do medycznych aplikacji, w tym do płynnej biopsji w NDRP.

## **Kopie opublikowanych prac**

1. Długolecka M, Szymanski J, Zareba L, Homoncik Z, Domagala-Kulawik J, Polubiec-Kownacka M, et al. Characterization of Extracellular Vesicles from Bronchoalveolar Lavage Fluid and Plasma of Patients with Lung Lesions Using Fluorescence Nanoparticle Tracking Analysis. *Cells*. 2021;10(12).

## Article

# Characterization of Extracellular Vesicles from Bronchoalveolar Lavage Fluid and Plasma of Patients with Lung Lesions Using Fluorescence Nanoparticle Tracking Analysis

Magdalena Dlugolecka <sup>1</sup>, Jacek Szymanski <sup>2,3</sup>, Lukasz Zareba <sup>3</sup>, Zuzanna Homoncik <sup>3</sup>,  
Joanna Domagala-Kulawik <sup>4</sup>, Malgorzata Polubiec-Kownacka <sup>5</sup> and Malgorzata Czystowska-Kuzmicz <sup>3,\*</sup>

<sup>1</sup> Chair and Department of Biochemistry, Doctoral School, Medical University of Warsaw, Banacha 1, 02-097 Warsaw, Poland; magdalena.dlugolecka@wum.edu.pl

<sup>2</sup> Faculty of Chemistry, Warsaw University of Technology, Noakowskiego 3, 00-664 Warsaw, Poland; j.szymanski1997@gmail.com

<sup>3</sup> Chair and Department of Biochemistry, Medical University of Warsaw, Banacha 1, 02-097 Warsaw, Poland; lukaszzareba01@gmail.com (L.Z.); homoncik.zuzanna@gmail.com (Z.H.)

<sup>4</sup> Department of Internal Medicine, Pulmonary Diseases and Allergy, Medical University of Warsaw, Banacha 1a, 02-097 Warsaw, Poland; jdomagala@wum.edu.pl

<sup>5</sup> Department of Surgery, Institute of Tuberculosis and Lung Diseases, Plocka 26, 01-138 Warsaw, Poland; m.polubiec@igichp.edu.pl

\* Correspondence: mczystowska@wum.edu.pl



**Citation:** Dlugolecka, M.; Szymanski, J.; Zareba, L.; Homoncik, Z.; Domagala-Kulawik, J.; Polubiec-Kownacka, M.; Czystowska-Kuzmicz, M. Characterization of Extracellular Vesicles from Bronchoalveolar Lavage Fluid and Plasma of Patients with Lung Lesions Using Fluorescence Nanoparticle Tracking Analysis. *Cells* **2021**, *10*, 3473. <https://doi.org/>

Academic Editor: Lucas Treps

Received: 18 October 2021

Accepted: 7 December 2021

Published: 9 December 2021

**Publisher's Note:** MDPI stays neutral with regard to jurisdictional claims in published maps and institutional affiliations.



**Copyright:** © 2021 by the authors. Licensee MDPI, Basel, Switzerland. This article is an open access article distributed under the terms and conditions of the Creative Commons Attribution (CC BY) license (<https://creativecommons.org/licenses/by/4.0/>).

**Abstract:** The current lack of reliable methods for quantifying extracellular vesicles (EVs) isolated from complex biofluids significantly hinders translational applications in EV research. The recently developed fluorescence nanoparticle tracking analysis (FL-NTA) allows for the detection of EV-associated proteins, enabling EV content determination. In this study, we present the first comprehensive phenotyping of bronchopulmonary lavage fluid (BALF)-derived EVs from non-small cell lung cancer (NSCLC) patients using classical EV-characterization methods as well as the FL-NTA method. We found that EV immunolabeling for the specific EV marker combined with the use of the fluorescent mode NTA analysis can provide the concentration, size, distribution, and surface phenotype of EVs in a heterogeneous solution. However, by performing FL-NTA analysis of BALF-derived EVs in comparison to plasma-derived EVs, we reveal the limitations of this method, which is suitable only for relatively pure EV isolates. For more complex fluids such as plasma, this method appears to not be sensitive enough and the measurements can be compromised. Our parallel presentation of NTA-based phenotyping of plasma and BALF EVs emphasizes the great impact of sample composition and purity on FL-NTA analysis that has to be taken into account in the further development of FL-NTA toward the detection of EV-associated cancer biomarkers.

**Keywords:** fluorescence nanoparticle tracking analysis; extracellular vesicles; bronchoalveolar lavage fluid; plasma; non-small-cell lung cancer

## 1. Introduction

In recent years, a lot of attention has been given to studies of extracellular vesicles (EVs) as a potential diagnostic and prognostic biomarker for many diseases including cancer. Since tumor-derived EVs can be found in large numbers in the biological fluids of cancer patients and their molecular cargo represents the tumor genotype and phenotype, they have undergone extensive research as a new variant of a liquid biopsy in cancer treatment [1].

In the case of non-small cell lung cancer (NSCLC), the bronchopulmonary lavage fluid (BALF) seems to be a good source of EVs from the tumor microenvironment [2]. BALF is currently extensively studied as a source of lung cancer-specific genetic or protein biomarkers [3]. Some reports suggest that BALF-derived biomarkers might be superior to

serum biomarkers because they appear earlier during the cancer progression and at the higher concentrations [4]. The same can be true for BALF-derived EVs. Because of tumor proximity, EVs released by tumor cells may appear in BALF in the earlier disease stage and the higher concentration than in peripheral blood and reflect the tumor microenvironment more accurately. Therefore, a thorough study on the composition and function of BALF-EVs, representing EVs from the tumor microenvironment in NSCLC patients, can contribute to the development of biomarkers for patient therapy.

To develop clinically-viable EV-based diagnostic or prognostic screening assays, accurate and reproducible methods to evaluate the total concentration, size distribution, and single-particle phenotyping of EVs are urgently needed. Precise analysis of particles as small as EVs presents many technical challenges. In 1903, Prof. Richard Zsigmondy introduced the “Ultramicroscope”, which uses scattering light to visualize nanosized particles [5]. Thanks to this invention, many years later, dynamic light scattering (DLS) was developed [6]. It allowed for the calculation of the average size of nanosized particles but was unable to track individual particles simultaneously [7]. Within the last decade, nanoparticle tracking analysis (NTA) has emerged as the state-of-the-art method for the size and concentration characterization of exosomes and extracellular vesicles, overcoming the downfalls of the DLS method [7,8]. Particles are visualized by laser light, and the scattered light is recorded by a sensitive camera (CMOS/CCD) placed under the 90° angle to the irradiated plane [9]. This angle allows for the detection and tracking of the Brownian motion of particles sized from 10 to 1000 nm. Particles are detected, and their path is recorded. Using the Einstein–Stokes equation, the hydrodynamic diameter (size) of each particle present in the device’s cell unit is calculated [8,10]. Single NTA-based measurements in scatter mode allow for the quantification and size determination of nanosized particles, usually in the range of 40–1000 nm. However, they are unable to distinguish between EVs and other particles within their size range including protein aggregates, cell debris components, and lipoproteins [10]. Unfortunately, none of the currently available EV separation methods from biological fluids such as BALF or plasma is able to fully purify EVs from these contaminations. Therefore, the NTA-based scatter signal can only provide an estimation of the total particle number of EV-enriched fractions obtained from biological fluids. Recently, more advanced NTA instruments allowing for fluorescence detection have been developed. The number of membranous particles that likely represent EVs after staining with fluorescent lipophilic dyes or the number of specific exosomes or EV populations after fluorescent antibody staining for specific markers can be estimated in fluorescence mode [11].

Here, we have undertaken one of the first attempts at a comprehensive phenotypical characterization of BALF-EVs in comparison to plasma EVs. First, we characterized both EV types using established analytical methods such as western blotting, cryo-TEM, and bead-assisted flow cytometry, following the MISEV 2018 recommendations and standards [12]. Next, we performed NTA measurements in both scatter mode and fluorescence mode using the ZetaView device (Particle Metrix, Inning am Ammersee, Germany). The EVs were stained with the lipophilic dye Cell Mask Deep Red (CMDR, Thermo Fisher Scientific, Waltham, MA, USA) and fluorescence-labeled antibodies against some tetraspanins as typical exosome markers. Such analysis allowed us to determine the actual number and size of true EVs and investigate their composition in more detail (e.g., by determining the percentage of classical exosomes). Hereby, we developed an experimental setup based on fluorescence nanoparticle tracking analysis (FL-NTA) that can reveal the amount of bona fide EVs in isolates from heterogeneous particle solutions such as biological fluids.

## 2. Materials and Methods

### 2.1. Patients

The study group consisted of 34 patients (16 men and 18 women) consecutively enrolled with indications for BAL. The inclusion criterion was suspicion of lung cancer. During the diagnostic procedure, all patients were before anti-cancer treatment. Exclusion

criteria involved contraindication to bronchoscopy, lack of patient agreement, ongoing anti-cancer treatment, immunosuppressive therapy, and infection. Patients were 42–80 years old, and the mean age was 66. Twenty-five patients were later confirmed with NSCLC after the diagnostic procedure. Three patients needed further diagnostics (two with no continuity of observation and one had the suspicion of NSCLC). Six patients turned out to have a different diagnosis than NSCLC including sarcoidosis, SCLC, and Pecoma cancer. The material (BALF and whole blood) was collected at the Institute of Tuberculosis and Lung Diseases in Warsaw from fasted patients. Ten mL of each patient's whole blood was collected in vacuum blood collection tubes with EDTA (Vacutest Kima, cat. 13060, Arzergrande, Italy) and mixed. Within 1 h, the blood was transported at room temperature to the Medical University of Warsaw for plasma separation.

## 2.2. BAL-Procedure

BAL was performed according to recommendations of the Polish Respiratory Society [13] at the Institute of Tuberculosis and Lung Diseases in Warsaw. A 100 mL sample of saline (at body temperature) was injected in 20 mL doses via a bronchofiberscope to the small bronchus, leading to the lesion affected by cancer (cBALF) and symmetrically to the same segment of the opposite lung (oBALF). The mean volume of recovered fluid was  $30.5 \text{ mL} \pm 9.2 \text{ mL}$ . The exclusion criteria for further BAL fluid analysis were: recovery fluid less than 30%, presence of more than 10% of epithelial cells, blood contamination, macroscopically visible mucus. After the BAL-procedure, BALF was transported at  $4 \text{ }^\circ\text{C}$  within 1 h to the Medical University of Warsaw for further processing.

### 2.2.1. Choosing EV Separation Method

For plasma EVs, we used centrifugation and homemade size-exclusion chromatography (SEC) columns and for BALF EVs, we chose differential ultracentrifugation as a suitable isolation method. The selection of isolation methods is described in detail in Section 4.1.

### 2.2.2. Separation of EVs from Plasma of BAL Patients Using Homemade Mini-SEC Columns

Plasma was obtained from the patient's whole blood sample by density centrifugation with the Lymphoprep™ (Stemcell, Köln, Germany) gradient as described before [14]. Briefly, about 5 mL of Lymphoprep™ was pipetted into a 15 mL tube, and the 5 mL of undiluted blood was carefully layered over the Lymphoprep™. The tubes were centrifuged (Eppendorf 5804R centrifuge and swing out rotor A-4-44, Hamburg, Germany) at  $750 \times g$  for 30 min at room temperature (RT) with a disabled brake. After the centrifugation step, the upper layer of plasma was carefully aspirated with a Pasteur pipette to a new tube. After another centrifugation step (Eppendorf 5804R centrifuge and fixed-angle rotor F-45-30-11) at  $2000 \times g$  for 10 min at RT, the supernatant was centrifuged again (Eppendorf 5804R centrifuge and fixed-angle rotor F-45-30-11) at  $10,000 \times g$  for 30 min at  $4 \text{ }^\circ\text{C}$ . Finally, the plasma was filtered using a  $0.22\text{-}\mu\text{m}$  filter (qpore, PES-membrane, Heidelberg, Germany), aliquoted, and either stored frozen at  $-80 \text{ }^\circ\text{C}$  until further processing or directly used for EV-isolation. The homemade mini-SEC columns were prepared as described by Ludwig et al. [15] using Sepharose CL-2B (GE Healthcare, cat.17-0140-01, Chicago, IL, USA). Columns were stored at  $4 \text{ }^\circ\text{C}$  filled with PBS (Gibco, cat. 70011-036, Invitrogen, Waltham, MA, USA, diluted with MiliQ water to  $1 \times$ ) with 0.05% sodium azide (Acros Organics, cat. 190381000, Antwerp, Belgium) as a preservative. Columns were reused up to three times. A 1 mL aliquot of the precleared and filtered plasma was thawed and applied to the mini-SEC column. After the sample entered the column, 2 mL of PBS (Lonza, Basel, Switzerland) was added, and 3 mL of void volume was collected (fractions 1–3, 1 mL each). Then, 4 mL of PBS was added, and EV-enriched fractions (1 mL each) were collected in separate tubes. EV fractions 5 and 6 were pooled (see Figure S1). Plasma EVs were either immediately analyzed or concentrated by centrifugation (Merck, Amicon® Ultra-2 mL Centrifugal Filters, Darmstadt, Germany; Eppendorf 5804R centrifuge and swing out rotor

A-4-44) at  $4000\times g$  for about 30 min at RT, and stored in 10  $\mu\text{L}$  aliquots at  $-80\text{ }^{\circ}\text{C}$  until further processing. The mean volume of the concentrated EV fraction was  $111.6 \pm 40.4\ \mu\text{L}$ .

### 2.2.3. Separation of EVs from BALF Using Differential Ultracentrifugation

BALF from the lung affected with either cancer or another lesion (cBALF) and from the opposite lung (oBALF) was strained through gauze and precleared by centrifugation (Eppendorf 5804R centrifuge and swing out rotor S-4-72) at  $1000\times g$  for 10 min at RT and then at  $2500\times g$  for 20 min at RT. Then, to break down the mucus, 2.5 mg of DTT (Sigma-Aldrich, Saint Louis, MO, USA, in water solution) was added, and the samples were shaken at 600 RPM  $37\text{ }^{\circ}\text{C}$  for 30 min. Afterward, samples were centrifuged (Beckman Coulter Optima XPN-80 Ultracentrifuge and SW32 Ti Swinging-Bucket rotor, Brea, CA, USA; Beckman Coulter tubes 355631) at  $25,000\times g$  for 40 min at RT. After that, the supernatant was collected and filtered using a  $0.22\ \mu\text{m}$  filter (Sartorius or GF, cellulose acetate double-membrane, Göttingen, Germany). Then, EVs were pelleted by ultracentrifugation at  $110,000\times g$  for 2 h at  $4\text{ }^{\circ}\text{C}$  ( $k_{\text{adj}} = 511.3$ ). The EV-pellet was washed by ice-cold PBS and further centrifuged (Type 70.1 Ti Fixed-Angle Titanium Rotor; Beckman Coulter tubes 355603) at  $110,000\times g$  for 1 h at  $4\text{ }^{\circ}\text{C}$  ( $k_{\text{adj}} = 522.6$ ). The EV-pellet was dissolved in PBS according to the starting BALF volume (at least 20  $\mu\text{L}$  of PBS for every 1 mL of BALF) and stored in 10  $\mu\text{L}$  aliquots at  $-80\text{ }^{\circ}\text{C}$  until further processing. The mean volume of concentrated EV fraction was  $77.0 \pm 25.3\ \mu\text{L}$ .

### 2.3. Immunocapture and Fluorescence Labeling of EVs for Flow Cytometry

An aliquot of BALF-EVs corresponding to 2 mL of BALF or 50  $\mu\text{L}$  of nonconcentrated plasma-EVs (pooled fraction 5 and 6, 20  $\mu\text{g}$  of protein) were bound to CD63, CD9, and CD81 coated Dynabeads (Invitrogen, cat. 10606D, 10620D, and 10622D, respectively) following the manufacturer's protocol. Briefly, the EV sample volume was adjusted to 100  $\mu\text{L}$  using isolation buffer (PBS with 0.1% BSA, filtered through a  $0.22\ \mu\text{m}$  filter). Then, 20  $\mu\text{L}$  of Dynabeads were washed with isolation buffer and added to each EV sample. Samples were incubated ON with shaking (600 RPM) at  $4\text{ }^{\circ}\text{C}$ . The following day, the Dynabead-bound EVs were stained with either the specific markers (see Supplementary Table S1) or the isotype controls for 1 h at RT with mild shaking (600 RPM), then washed with isolation buffer and analyzed by flow cytometry.

### 2.4. Flow-Cytometric Analysis of EVs

Flow cytometry was performed on a BD FACSVerser 8 Color Flow Cytometer (BD, Franklin Lakes, NJ, USA) with BD FACSuite Software v.1.0.6. FCS files were then analyzed with FlowJo Software (LLC, Ashland, OR, USA). The stained bead-coupled EVs were resuspended in 150  $\mu\text{L}$  PBS. A single-bead gate was set based on the FCS and SSC scatter and a minimum of 1500 beads were acquired. Gating strategies are shown in Figure S2.

### 2.5. Western Blotting of EVs

The protein content of the EVs separated from BALF, and the EVs concentrated from pooled fractions 5–6 from plasma was measured with the BCA Protein Assay Kit (Pierce, cat.23227) according to the manufacturer's instructions. The EV amount corresponding to 100  $\mu\text{L}$  of plasma or 4 mL of BALF was taken for SDS-PAGE. Samples were denatured for 5 min at  $95\text{ }^{\circ}\text{C}$  in reducing sample buffer (homemade). Proteins were separated on a 12% acrylamide gel and transferred into a nitrocellulose  $0.2\ \mu\text{m}$  membrane (GE Healthcare, Chicago, IL, USA), then blocked with either 5% non-fat milk (Sigma-Aldrich) or 5% BSA (Sigma-Aldrich) at RT for 1 h. Incubation with primary antibodies (recognizing Calnexin, Tsg101, Syntenin, CD9, or CD81, see Supplementary Table S1) was performed ON at  $4\text{ }^{\circ}\text{C}$ , followed by incubation with appropriate secondary HRP-conjugated antibodies (see Supplementary Table S1) for 2 h at room temperature. The chemiluminescence signal was achieved using the SuperSignal West Femto Maximum Sensitivity Substrate (Thermo Fisher Scientific, cat. 34095). Image acquisition was performed using a ChemiDoc Imager (Biorad,

Hercules, CA, USA) with Image Lab Software (Biorad). Experiments were repeated at least three times.

### 2.6. Transmission Electron Microscopy

Imaging of EVs was conducted with the use of cryogenic transmission electron microscopy. Two to three  $\mu\text{L}$  of each sample (concentrated EVs from plasma, cBALF-EVs, and oBALF-EVs of one patient) were vitrified in liquid ethane using the Thermo Fisher Scientific Vitrobot (blot time = 2 s, blot force = 0, blot total = 1) on TEM grids (Lacey Carbon or Quantifoil R2/2 copper, 200 mesh), previously glow-discharged (30 s, 25 mA) in a PELCO EasiGlow system. The grid freezing was conducted immediately before placing them into the Thermo Fisher Scientific cryo-electron microscope Glacios 200 kV in cryogenic conditions. For data analysis, EPU 2.7 software for single particle analysis and ImageJ software were used. For imaging, a Falcon3EC camera in linear mode without single-frame fractionation was used with a total electron dose per sample of  $50 \text{ e}/\text{\AA}^2$ , defocus  $-3.0 \mu\text{m}$ ,  $-2.5 \mu\text{m}$ ,  $-2.0 \mu\text{m}$ . For the Lacey carbon grid, a magnification of  $72,000\times$  with a pixel size  $0.19 \text{ nm}$  ( $1.9 \text{ \AA}$ ) and of  $52,000\times$  with a pixel size  $0.24 \text{ nm}$  ( $2.4 \text{ \AA}$ ) was used, and for the Quantifoil R2/2 grid, a magnification of  $92,000\times$  with pixel size  $0.15 \text{ nm}$  ( $1.5 \text{ \AA}$ ) was used.

### 2.7. NTA-Scatter Measurement

EV size distribution profiles and concentration measurements in EV samples separated from BALF and plasma (nonconcentrated pooled fraction 5 and 6) were obtained using the ZetaView PMX220 (Particle Metrix) instrument equipped with a 488 and 640 nm laser and ZetaView 8.05.11 SP4 software. In accordance with the ZetaView manual, polystyrene 100 nm beads (Particle Metrix) were used for the daily calibration and instrument performance check. EV samples were diluted in PBS (Lonza) to obtain approximately 350 particles per frame. This concentration was chosen as an optimal concentration of EVs for the labeling experiments. The measurements in scatter mode were performed at RT at 11 positions in two cycles with the following settings for plasma and BALF-EVs—Sensitivity: 80, Shutter: 100, Minimal Brightness: 30, Trace length: 15, Min Area: 10, Max Area: 1000 nm/Class: 5, Classes/Decade: 64, Resolution: medium. The camera sensitivity was adjusted to also detect dim particles at a minimal background noise (measured in PBS). All settings were kept the same for all analyzed samples of a given sort (BALF-EVs, plasma-EVs) to minimize variability. At least three measurements of each sample were performed. For the daily calibration and reproducibility measurements, the following commercially available beads were used: (Particle Metrix, cat no 110-0020), YG488 beads (FluoSpheres™ Carboxylate-Modified Microspheres, Invitrogen, cat. no. F8803, lot.1835064), and DR660 beads (FluoSpheres™ Carboxylate-Modified Microspheres, Invitrogen, cat. no. F8807, lot.1893532). For all beads, the manufacturer's dedicated settings for scatter measurements were used:

PS100 beads—Sensitivity: 60, Shutter: 100, Minimal Brightness: 30, Trace length: 15, Min Area: 10, Max Area: 1000 nm/Class: 5, Classes/Decade: 64, Resolution: medium.

YG488 and DR660 beads—Sensitivity: 60, Shutter: 100, Minimal Brightness: 30, Trace length: 15, Min Area: 5, Max Area: 1000 nm/Class: 5, Classes/Decade: 64, Resolution: medium.

The day-to-day repeatability and precision of the size and concentration measurements in scatter mode were quantified by performing daily measurements of the 100 nm PS100 beads and calculating the coefficient of variation (Supplementary Figure S3c,f).

#### 2.7.1. Fluorescent Labeling of EVs

For membrane labeling of EVs, the lipophilic membrane dye CMDR (Invitrogen) was used. The CMDR concentration for labeling was optimized experimentally on plasma-EVs (non-concentrated and concentrated) and BALF-EVs (see Supplementary Figure S4). The optimal final concentration for NTA, which ensured maximal EV-staining with a particle size corresponding to the size measured in scatter and a minimal background (only CMDR

in PBS), was established as 4 ng/mL (Supplementary Table S1). The antibody concentration for tetraspanin-labeling and FL-NTA was adjusted by performing serial dilutions of antibodies in PBS and measurement in FL-NTA. The highest antibody concentration, which did not give high background, was chosen for each antibody as the optimal final dilution for the NTA measurement (Supplementary Table S1).

### 2.7.2. Fluorescence-NTA

Prior to immunolabeling, all EV samples were measured in scatter mode to establish particle concentration. Before staining, predilution of EV sample/antibody/dye was prepared if needed. The EV-sample's predilution was adjusted to achieve the highest concentration in range (about 350 particles per frame) for measurement in the scatter mode after final dilution post-labeling and differed according to the original concentration of a given EV sample. Fluorescence labeling was performed using prediluted EVs and prediluted antibody/CMDR in an approximately 9:1 ratio in a total volume of 10–50  $\mu$ L for 2 h at RT in the dark. Then, the EVs were further diluted in PBS (usually 1:1000) and measured on NTA at RT at 11 positions in one cycle with the following settings:

For staining with antibodies:

F488, Sensitivity: 95, Shutter: 100, Minimal Brightness: 25, Trace length: 7, Min Area: 10, Max Area: 1000 nm<sup>2</sup>/Class: 5, Classes/Decade: 64, Resolution: medium.

For staining with CMDR:

F640, Sensitivity: 91, Shutter: 100, Minimal Brightness: 25, Trace length: 7, Min Area: 10, Max Area: 1000 nm<sup>2</sup>/Class: 5, Classes/Decade: 64, Resolution: medium. All immunolabeled samples were first evaluated in fluorescence mode with the function "low bleach" on, immediately followed by evaluation in scatter mode to minimize photobleaching. At least three measurements of each sample were performed.

For YG488 beads:

F488, Sensitivity: 80, Shutter: 100, Minimal Brightness: 20, Trace length: 7, Min Area: 5, Max Area: 1000 nm<sup>2</sup>/Class: 5, Classes/Decade: 64, Resolution: medium.

For DR660 beads:

F640, Sensitivity: 80, Shutter: 100, Minimal Brightness: 20, Trace length: 7, Min Area: 5, Max Area: 1000 nm<sup>2</sup>/Class: 5, Classes/Decade: 64, Resolution: medium.

The day-to-day repeatability and precision of the size and concentration measurements in fluorescence mode were quantified by performing daily measurements of the YG488 and DR660 beads and calculating the coefficient of variation (Figure S3a,b,d–f).

The isolation procedures and analysis methods of plasma and BALF-EVs used in this study are summarized in Figure 1.



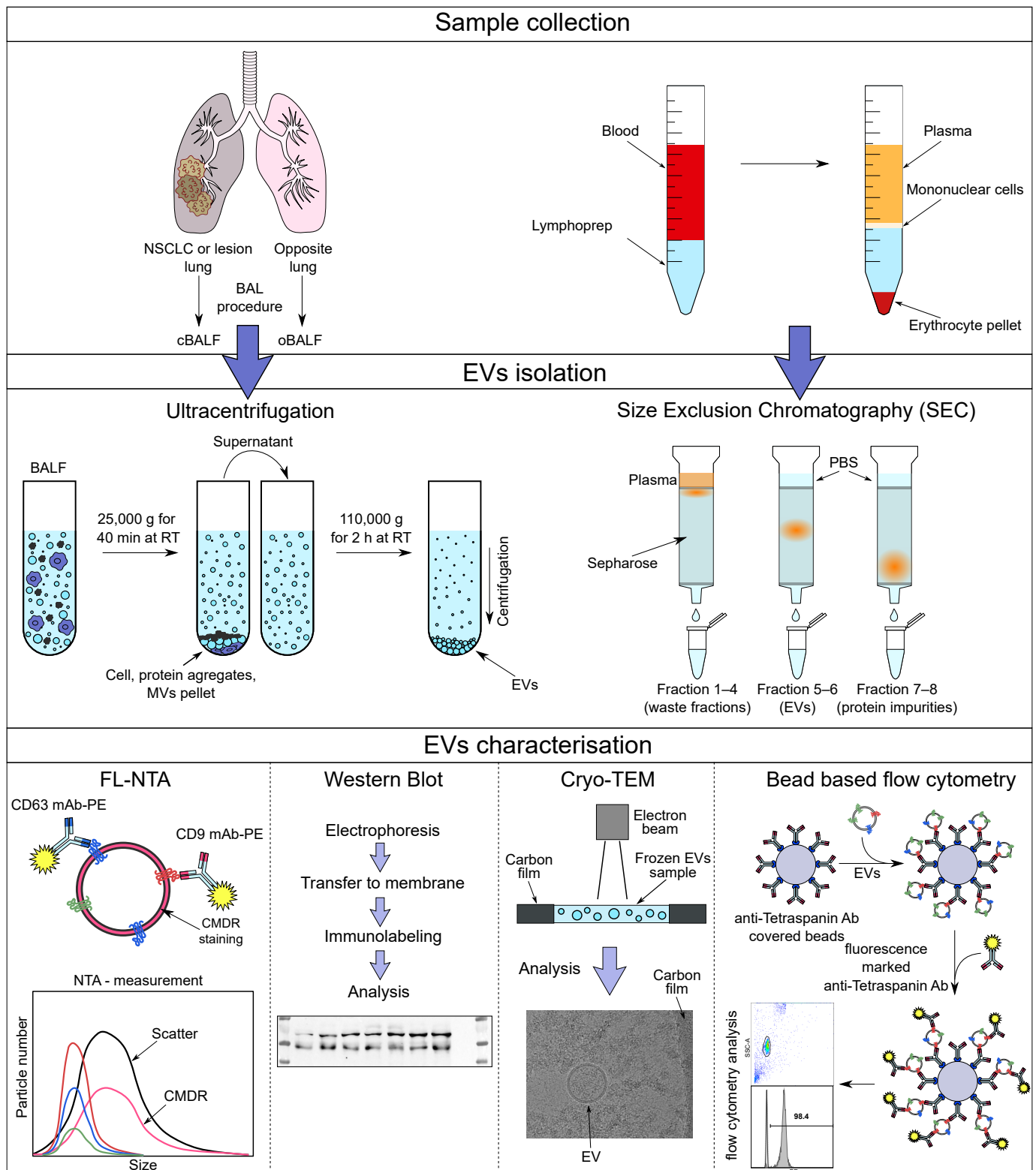


Figure 1. Summary of EV characterization methodology.

2.8. Lysis of EVs

RIPA lysis buffer (Millipore, cat. no. 20-188, Merck) was used to lyse EVs obtained from the cell line NCI-H1975 (Hansa BioMed Life Sciences, cat. nr. HBM-NCI-H1975-100/5, Tallinn, Estonia). The 9 µL mixtures of EVs, after immunolabeling with CD9, CD63, CD81, and CMDR antibodies individually, were divided, and half of each was filled with PBS

to the total volume of 1 mL to obtain optimal 1:1500 EV dilution. NTA-fluorescence was performed as described previously. The residues were incubated with 0.5  $\mu$ L RIPA (10% solution) on ice for 30 min. After the lysis, PBS was added to the total 1 mL volume of each sample, giving the same optimal EV dilution, and FL-NTA measurements were repeated. The control sample was prepared in the same way, but RIPA was replaced with PBS for 30 min incubation on ice. Additionally, an appropriate dilution of RIPA in PBS was prepared to check whether RIPA solution alone interferes with NTA.

### 2.9. Subcellular Particles (Particularly Lipoproteins) Removal

Removal of subcellular particles was performed using the ExoQuick-LP for Lipoprotein Pre-Clear & Exosome Isolation Kit (System Biosciences, cat. no. EXOLP5A-1, Palo Alto, CA, USA) according to the manufacturer's instructions with some modifications. Briefly, plasma was centrifuged at  $2000\times g$  for 10 min, RT, and then the supernatant was centrifuged at  $10,000\times g$  for 30 min at 4 °C. The supernatant was filtered through a 0.22  $\mu$ m filter (q pore, PES-membrane). Subsequently, to remove any trace amounts of fibrinogen, thrombin from human plasma (Sigma-Aldrich, cat. no. 605190-100U-M) was added (final concentration 5 U/mL) and incubated for 5 min, RT, mixing gently. The supernatant was collected after centrifugation at 10,000 rpm for 5 min, RT, and 100  $\mu$ L of the supernatant was added to beads prepared earlier according to the manufacturer's instruction. Then, the sample was incubated for 3 h at 4 °C with rotation and then placed on a magnetic separator DynaMag-2 (Invitrogen, cat. no. 12321D) for 2 min, RT to remove bead-bound lipoproteins. The lipoprotein-cleared plasma sample was transferred into a new tube. Next, both the cleared plasma sample and control sample (plasma after only double centrifugation and filtration) were filled with PBS up to 1 mL and isolated using homemade mini-SEC columns, as described above. Next, the concentration of EVs from the cleared plasma sample (-LP) and control sample (CTRL) was measured by NTA. Finally, the diluted samples were labeled in the dark for 2 h at RT. Then, the FL-NTA measurements were performed.

### 2.10. Removal of Selected EV Populations by Immunomagnetic Isolation

We performed a magnetic separation of EV-subpopulations based on the expression of tetraspanins of a patient's BALF-EVs sample with subsequent NTA measurements. BALF-EVs were isolated from the patient's BALF using the method described above. CD63-specific (Invitrogen, Exosome-Human CD63 Isolation/Detection Reagent) and CD9-specific (Invitrogen, Exosome-Human CD9 Flow Detection Reagent) magnetic beads were washed with an assay buffer (PBS with 0.1% BSA), according to the manufacturer's instructions using a magnetic rack (Invitrogen, DynaMag™-2 Magnet). In the next step, two separate samples for every bead-type consisting of 10  $\mu$ L of the patient's BALF-EVs sample, 90  $\mu$ L of assay buffer, and 40  $\mu$ L of the washed CD63 or CD9 specific beads, respectively, were prepared. The samples were mixed overnight (Topscien, TMM-5 Magic Mixer, Jiangshan, Ningbo, China) at 4 °C. The following day, the samples were spun for a few seconds and placed on the magnetic rack for 2 min to separate beads from the solution. Thereafter, the solutions were collected (unbound EV populations), and scatter and FL-NTA measurements were performed to detect CD63+, CD9+, and CMDR+ EVs. Furthermore, the residual magnetic beads were eluted from the adhered exosomes by incubation for 30 min at RT in 100  $\mu$ L elution buffer (System Biosciences, Exo-Flow Elution Buffer). Subsequently, eluted magnetic beads were separated by placing the sample on a magnetic rack for 2 min. The residual fluid with exosomes was collected (eluted CD63+ and CD9+ populations) and underwent the same NTA measurements as samples from the unbound populations. A control sample represented the same unseparated patient-derived EVs. Additionally, we prepared a background control sample consisting of PBS instead of the patient's EVs and 60  $\mu$ L of both magnetic beads that underwent the same magnetic separation protocol.

### 2.11. Statistical Analysis

Statistical analysis was conducted using Excel (Microsoft, Redmond, WA, USA), GraphPad Prism (San Diego, CA, USA), and Statistica Software (StatSoft, Tibco, Palo Alto, CA, USA). The  $p$  value  $< 0.05$  was considered significant. The quantitative analysis of data from NTA measurements was performed as follows:

Samples were measured in three repetitions. All samples were measured in scatter mode before and after labeling with dyes. Peak size (Mode—the value of size that appears most often in the collected statistical data analyzed by the Zeta View software) was chosen as the particle size in most samples. When the Mode could not be calculated by the instrument software, the Median (X50) size was taken for calculations. The mean concentration of EVs in the original sample was calculated and presented as the concentration of particles per 1 mL of plasma or 1 mL of BALF, respectively. The distribution of data was tested using the Shapiro–Wilk test. In the case of a normal distribution of the data, the paired two-tailed student's  $t$ -test for dependent variables for comparisons of the concentrations and sizes of plasma EVs and BALF EVs was conducted. When there was no normal distribution of the data, the Wilcoxon matched pairs signed rank test for dependent variables was conducted. Nonparametric correlations of Spearman were calculated for associations between the concentration of particles and protein concentration.

### 2.12. EV-TRACK

Transparent Reporting and Centralizing Knowledge in Extracellular Vesicle Research (EV-TRACK) is an online crowdsourcing knowledgebase (<http://evtrack.org>, accessed on 2 February 2021) that centralizes EV biology and methodology intending to stimulate the authors, reviewers, editors, and funders to put experimental guidelines into practice. After uploading of the requested experimental parameters on the EV-TRACK platform, an EV-TRACK ID is assigned and an EV-metric is calculated. It is a feature designed to reflect the level of check-up in validation experiments and reporting of experimental parameters. It is presented as a percentage of fulfilled components from a list of nine, which were argued by the EV-TRACK consortium to be indispensable for unambiguous interpretation and independent replication of EV experiments [16,17].

We have submitted all relevant data of our experiments to the EV-TRACK knowledge base (EV-TRACK ID: EV200181). Our EV-metric is up to 63% for plasma and 67% for BALF-EVs of NSCLC patients.

## 3. Results

### 3.1. Characterization of Plasma/BALF EVs from NSCLC Patients

The process of selecting isolation methods and their detailed descriptions is described in the Materials and Methods section.

After the separation of EVs from plasma and BALF, we performed characterization experiments of the obtained EVs following MISEV guidelines [12].

Figure 2 shows that the separation of EVs from both sources was effective. In Figure 2a, we can see that the exosomal markers Tsg101, CD9, CD81, and syntenin were detectable in both plasma-EVs and BALF-EVs. The non-EV marker calnexin is visible only in the cell lysate, which proves a good EV separation process and the lack of contaminating ER components. We checked the morphology of the separated EVs by cryo-TEM imaging (Figure 2b). In both BALF-EV samples, we found single round structures, comparing a clearly visible double-layer membrane with a thickness of 4 nm. The morphology and membrane thickness corresponded to the structures known as small EVs. Only a few such vesicles of 150 to 200 nm in size were visible per field, and only occasional clusters of EVs were seen. Most of the observed EVs were single EVs of a spherical shape. However, multi-vesicular particles with smaller double-membrane vesicles inside a bigger vesicle could also be observed such as in the presented cBALF-EV sample (Figure 2b). The much smaller, visible single-membrane dark irregular vesicles were not true vesicles, but frozen ethane as the solvent. In contrast, in the plasma-EV sample, there were many vesicles visible per

field. However, only very few presented the typical size and double-membrane of true EVs. Most of the visible particles were single-layered, electron-dense, and had a smaller size than EVs (<50 nm). They mostly appeared in aggregates, and many of them displayed a typical striped inside structure. Based on previously reported cryo-TEM analyses of EV preparations, we concluded that these particles are lipoproteins and protein aggregates (especially the striped structures, typical for lipoproteins; see also the cryo-TEM picture at smaller magnification in Figure S7b). Bead-assisted flow cytometry analysis of the presence of tetraspanin at the EV surface confirmed the results obtained by western blotting. BALF EVs captured by tetraspanin beads showed a higher percentage for all three exosomal markers (97.2% CD63, 61.4% CD9, and 26.3% CD81 positive particles) than plasma EVs (39.2% CD63, 40.7% CD9, and 1.7% CD81 positive particles). The supplementary data for gating strategy and flow cytometry analysis of the single bead type with BALF EVs are shown in Figure S2.

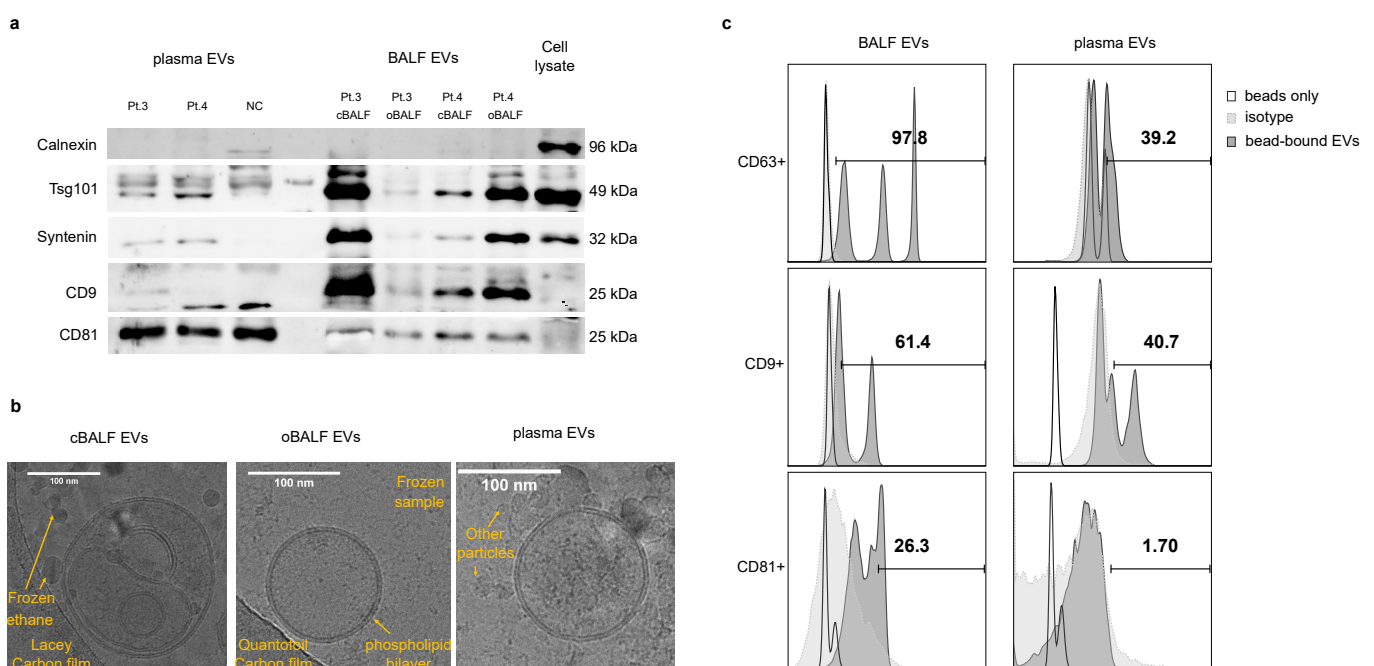


**Figure 2.** Characterization of plasma/BALF EVs from NSCLC patients. **(a)** Immunoblot analysis of EVs from plasma and BALF of two NSCLC patients (Pt.3, Pt.4), a normal donor (NC), and a cell lysate. The loaded EV amounts correspond to 100  $\mu$ L of the patients' plasma or 4 mL of the patients' BALF, respectively. As a control, 10  $\mu$ g of a cell lysate from the SEMK2 cell line was loaded. Full blots from **(a,b)** are provided in the Supplementary Materials. **(b)** Cryo-TEM imaging of EVs from cBALF, oBALF, and plasma from a NSCLC patient. **(c)** Flow cytometry of EVs from BALF and plasma attached to a mix of anti-CD63, anti-CD9, and anti-CD81 magnetic beads and then labeled with fluorescent anti-CD63, anti-CD9, and anti-CD81 antibodies, respectively.

### 3.2. NTA of Plasma and BALF EVs in Scatter Mode

Our NTA-analysis in scatter mode of EVs separated from plasma and BALF showed a different particle distribution of both EV types. A representative particle size distribution of plasma and BALF EVs from one patient is shown in Figure 3a. The BALF-EVs present a broader size distribution and are less numerous than plasma EVs from the same patients. The pairwise comparison of EVs isolated from all analyzed patients revealed that the concentration of plasma-EVs (mean  $\pm$  SD:  $2.44 \times 10^{11} \pm 4.71 \times 10^{11}$  particles/mL of plasma) was significantly higher than the concentration of BALF EVs (mean  $\pm$  SD: cBALF:  $8.85 \times 10^8 \pm 1.30 \times 10^9$ ; oBALF  $1.22 \times 10^9 \pm 1.68 \times 10^9$  particles/mL of BALF) for all patients (Figure 3b). Our identified mean total particle numbers in plasma corresponded very well to the mean particle amounts detected by Mork et al. directly in platelet-free

plasma (PFP) of fasting NC by NTA (Nanosight LM10 instrument), with a comparable broad intra-individual variation (observed range  $8.9 \times 10^{10}$ – $1.0 \times 10^{12}$ , 95% reference interval  $1.4 \times 10^{11}$ – $1.2 \times 10^{12}$ , Mork 2017). There was no significant difference between the concentration of EVs in cBALF and oBALF. The mode size of EVs from plasma (mean  $\pm$  SD:  $98.43 \pm 10.13$  nm) was bigger than the detected particle mean size in PFP (62 nm) by Mork et al., but comparable to the particle mean size of postprandial samples (93 nm) [18]. Our detected mode size of plasma particles was significantly smaller than the mode size of BALF-EVs (mean  $\pm$  SD: cBALF:  $171.95 \pm 23.72$  nm; oBALF  $166.60 \pm 13.82$  nm) for all patients (Figure 3c). There was no significant difference between the mode size of EVs in cBALF and oBALF.

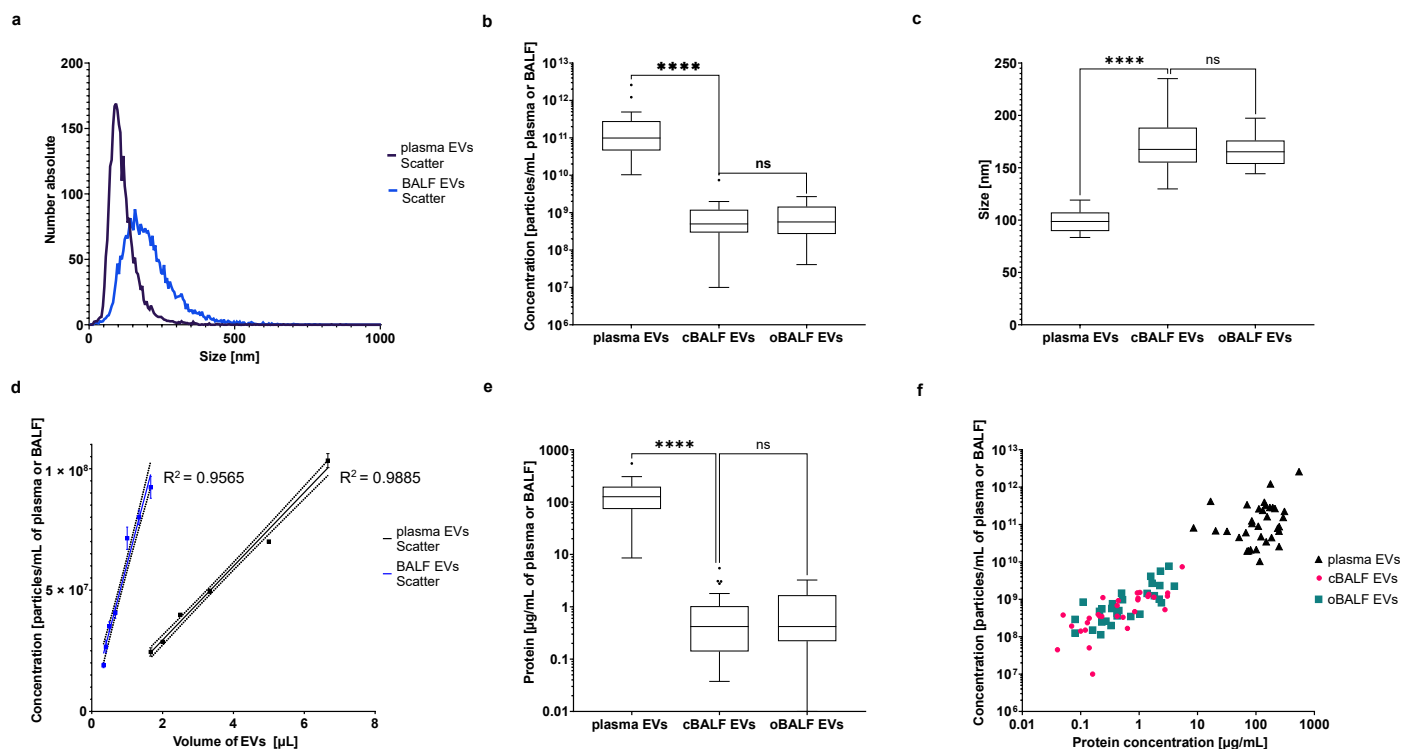


**Figure 3.** NTA of plasma and BALF EVs in scatter mode. (a) Distribution of number and size of detected particles in scatter mode of plasma and BALF-EVs. A representative NTA histogram of one patient is shown. (b) Mean concentration of EVs from plasma, cBALF, and oBALF for all patients. (c) Mode size of EVs from plasma, cBALF, and oBALF for all patients. (d) The concentration of particles measured in scatter mode depend on the volume of EV sample taken for the measurement. A line from simple linear regression with CI and  $R^2$  was plotted for both types of EVs. (e) Protein concentration calculated for one mL of plasma or BALF. (f) Correlation between the concentration of particles and protein concentration for plasma and BALF-EVs. Graphs (b,c,e) present a Tukey plot for all patients. \*\*\*\* refers to  $p$  value  $\leq 0.0001$ , ns refers to  $p$  value  $> 0.05$  from the Wilcoxon test-paired comparison (b,e) and  $t$ -test-paired comparison (c).

To check the NTA-measurement linearity in scatter mode, we performed measurements of different EV amounts. The results (Figure 3d) showed that there was a linear correlation ( $R^2$  for BALF EVs was 0.9565 and for plasma EVs 0.9885) between the EV amount and NTA-signal in scatter mode. Protein concentration of plasma EVs (mean  $\pm$  SD:  $147.45 \pm 105.99$   $\mu\text{g}/\text{mL}$  of plasma) was significantly higher than the concentration of BALF-EVs (mean  $\pm$  SD: cBALF:  $0.91 \pm 1.21$ ; oBALF  $0.99 \pm 1.06$   $\mu\text{g}/\text{mL}$  of BALF) for all patients (Figure 3e) and was comparable to EV-protein concentrations obtained by other researchers using the same isolation methods (e.g., by Dong et al., who reported a concentration of  $160.27 \pm 14.81$   $\mu\text{g}/\text{mL}$  [19]). Our obtained BALF-EV protein concentrations were in a similar range as concentrations for EVs obtained by ultracentrifugation from cell culture or urine by Dong et al., but significantly lower than for BALF-EVs isolated from cystic fibrosis, asthmatic, and primary ciliary dyskinesia patients by Rollet-Cohen et al. [20].

In this case, the authors obtained EV protein concentrations from around 43  $\mu\text{g}/\text{mL}$  for asthma to around 158  $\mu\text{g}/\text{mL}$ . However, the difference may be due to differences in pre-analytical handling, isolation method (no wash-step after EV pelleting like in our case), and a different patient cohort. In our study, there was no significant difference between the protein concentration of EVs in cBALF and oBALF. For both BALF EV types, there was a meaningful correlation between the concentration of particles on NTA and protein concentration (Spearman correlation  $r_s = 0.82$  for cBALF EVs and  $r_s = 0.77$  for oBALF EVs,  $p < 0.0001$ ) (Figure 3f). In plasma EVs, a similar correlation between those two factors was lacking (Spearman correlation  $r_s = 0.26$  for plasma EVs,  $p > 0.05$ ).

### 3.3. Membrane Labeling of Plasma and BALF EVs

The size distribution of particles after CMDR labeling (final concentration during NTA measurement 4 ng/mL CMDR, see Supplementary Figure S4) for both EV types (plasma and BALF) in FL-NTA was similar to scatter mode and is represented in Figure 4a. Concentration measurements of different EV volumes after CMDR labeling in fluorescent mode (640 nm) also showed linear dependency as it was in scatter (Figure 4b).  $R^2$  for BALF-EVs in CMDR was 0.9387 and for plasma EVs 0.9610. Labeling of EV samples with CMDR revealed that BALF-EVs had a significantly higher percent of particles positive for CMDR (cBALF 50.9% and oBALF 49.3%) than plasma EVs (30.9%) (Figure 4c). There was no meaningful difference between the percent of CMDR positive particles in cBALF-EVs and oBALF-EVs. The mode size of EVs positive for CMDR was significantly higher than in scatter mode for all EV types (Figure 4d). However, plasma-EVs were still significantly smaller (mean  $\pm$  SD: 117.32  $\pm$  17.93 nm) than both BALF-EV types (mean  $\pm$  SD: cBALF: 183.23  $\pm$  32.70 nm; oBALF 175.80  $\pm$  17.01 nm), and interestingly, cBALF-EVs were meaningfully larger than oBALF-EVs in the CMDR staining (Figure 4e). Similar to the scatter mode measurement, for both BALF-EV types, there was a correlation between the concentration of particles and protein concentration in FL-NTA at 640 nm (Spearman correlation  $r_s = 0.74$  for cBALF-EVs and  $r_s = 0.72$  for oBALF-EVs,  $p < 0.0001$ ) (Figure 4f). There was no significant correlation between these two factors (Spearman correlation  $r_s = 0.23$ ,  $p > 0.05$ ) in plasma-EVs.

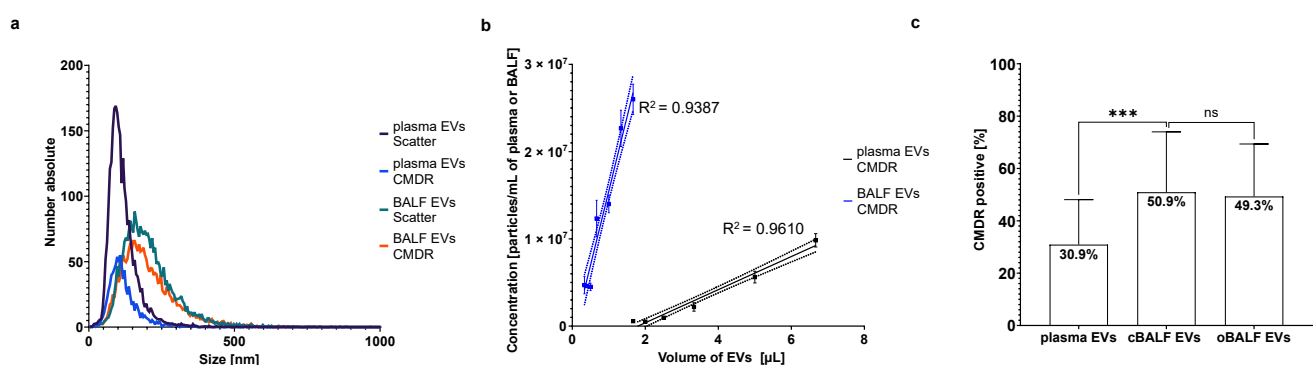
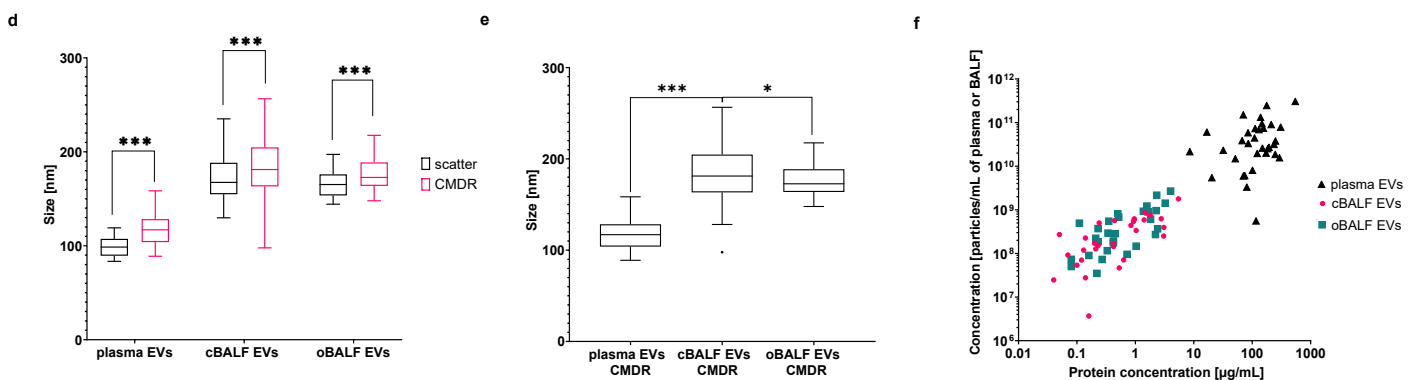


Figure 4. Cont.





**Figure 4.** CMDR labeling of EVs. (a) Distribution of particles in scatter and fluorescent mode (640 nm) for EVs from plasma and cBALF. A representative NTA histogram of one patient is shown. (b) Concentration of particles measured in fluorescent mode (640 nm) depending on the volume of the EV sample taken to measure the BALF and plasma EVs of one patient. A line from simple linear regression with CI and  $R^2$  was plotted for both types of EVs. (c) The percent of CMDR-positive particles in comparison to all particles visible in scatter mode for all analyzed EV types. (d) Comparison of EV mode sizes measured in scatter and after CMDR labeling within the three analyzed EV types. (e) Comparison of the mode sizes measured after CMDR labeling of the three analyzed EV types. (f) Correlation between the concentration of particles and protein concentration for plasma and BALF-EVs after CMDR staining. Graph (c) presents mean and SD for all patients. Graphs (d,e) presents a Tukey plot for all patients. \*\*\* refers to  $p$  value  $\leq 0.0002$ , \* refers to  $p$  value  $\leq 0.05$ , ns refers to  $p$  value  $> 0.05$  from  $t$ -test-paired comparison.

### 3.4. Antibody Labeling of Plasma, BALF, and NSCLC Cell Line EVs

After fluorescence staining against typical exosomal tetraspanins (CD63, CD9, CD81), the plasma-derived EVs showed a very different profile in FL-NTA in comparison to BALF-EVs and cell line-derived EVs (cl-EVs), which were more similar to each other (Figure 5). The measured signal from the exosomal markers CD63, CD81, and CD9 was very weak and mostly below the detection limit for plasma-EVs. Only in a few plasma-EVs samples (three out of 34), the signal from CD9 was detectable, but much lower than in scatter or CMDR (Figure 5a). In BALF-EVs, in most cases, all tetraspanin-positive EVs were well detectable, though their distribution explicitly shifted toward smaller sizes (Figure 5b). Antibody labeling against tetraspanins of commercially available standard EVs derived from the NSCLC cell line (cl-EVs) showed similar results, albeit the particle size distribution was slightly narrower (Figure 5c). A closer analysis of the size distributions after dividing the particles into six size fractions provided more differences between the three analyzed EV types (Figure 5d–f and Supplementary Table S4). The size distribution of the CMDR+ particles closely corresponded to the size distribution of all particles measured in scatter mode within every EV type. After the fluorescent staining for tetraspanins and FL-NTA analysis, the size distribution of tetraspanin-positive EVs shifted for all EV types, as already previously mentioned, clearly to the left toward smaller particle sizes. In plasma-EVs, around half of all CD9 positive particles (52.17%) lie within the size range of typical exosomes between 50–100 nm. In the case of BALF- and cl-EVs, this percentage was a little lower and was around 40–45%. For all EV types, the fluorescence staining for tetraspanins exposed a fraction of very small EVs under 50 nm that was not previously visible in scatter mode and after membrane staining. In the case of plasma-EVs, this population accounted for almost 20% of all CD9+ particles. In the case of BALF- and cl-EVs, this fraction was around 10–15%. The size distributions of BALF- and cl-EVs of all particles as well as CMDR+ and tetraspanin-positive particles corresponded largely to each other. Additionally, the size distributions of CD9, CD63, and CD81 positive particles of BALF- and cl-EVs were very similar. The exact percentages of all particle fractions are listed in Supplementary Table S4.

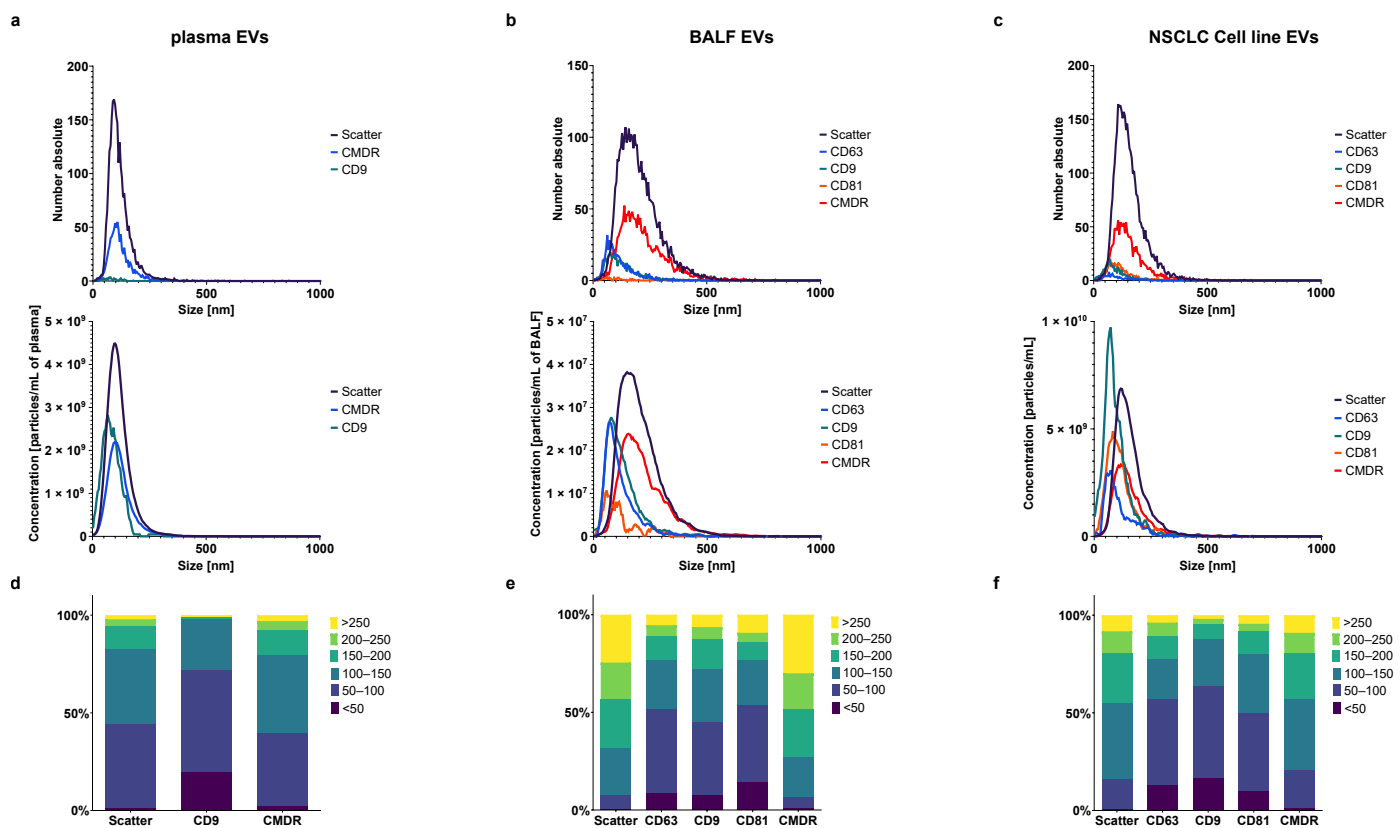


**Figure 5.** Size distributions from FL-NTA of particles in scatter and fluorescence mode (488, 640 nm) after immunolabeling of EVs against EV specific markers CD63, CD81, and CD9 and membrane marker CMDR. (a–c) Representative distributions measured in scatter and fluorescence mode of EVs from plasma (a), oBALF (b), and NSCLC cell line (c). The upper graphs present absolute numbers of particles measured by NTA, and the lower present the concentration of particles per one mL of plasma/BALF/NSCLC cell line EVs. The concentration of particles per one mL of each biological fluid is calculated by Particle Matrix software as  $\text{Concentration} = \text{Number} / (\text{Area} \times \text{depth})$ . The component “Area  $\times$  depth” differs between measures and is constant in the single measurement. Its value depends on outliers during each measurement. This “measured volume” effect leads to a different curve profile between the number absolute graphs and concentration graphs. (d–f) Concentration of particles—fraction of all particles [%] in six size fractions (<50 nm, 50–100 nm, 100–150 nm, 150–200 nm, 200–250 nm, >250 nm) for plasma (d), BALF (e) and cell line EVs (f). For all exact percent values, see Supplementary Table S4.

### 3.5. FL-NTA Characterization of BALF EVs

The fluorescent staining of BALF-EVs and their FL-NTA analysis showed linearity with particle concentrations for all analyzed tetraspanins (Figure 6a).  $R^2$  from linear regression for particles positive for CD63 was 0.9868, for CD9 0.9357, and for CD81 0.9611. Comparison of concentrations of particles per one mL of BALF for cBALF and oBALF showed no significant differences for all markers between these two groups (Figure 6b). No significant differences were also detected in the percent of fluorescent particles in these two groups (Supplementary Figure S5a). The representative percentages of fluorescent particles of cBALF-EVs are presented in Figure 6c. The percent of fluorescent particles in comparison to all particles visible in scatter was high in CMDR (50.9%) and CD9 (56.0%), lower in CD63 (35.5%), and the lowest in CD81 (8.2%). According to measured particle sizes, most detected differences between cBALF and oBALF were not meaningful. Only in the case of CMDR labeled particles did cBALF-EVs turn out to be slightly bigger than oBALF-EVs (Supplementary Figure S5b).



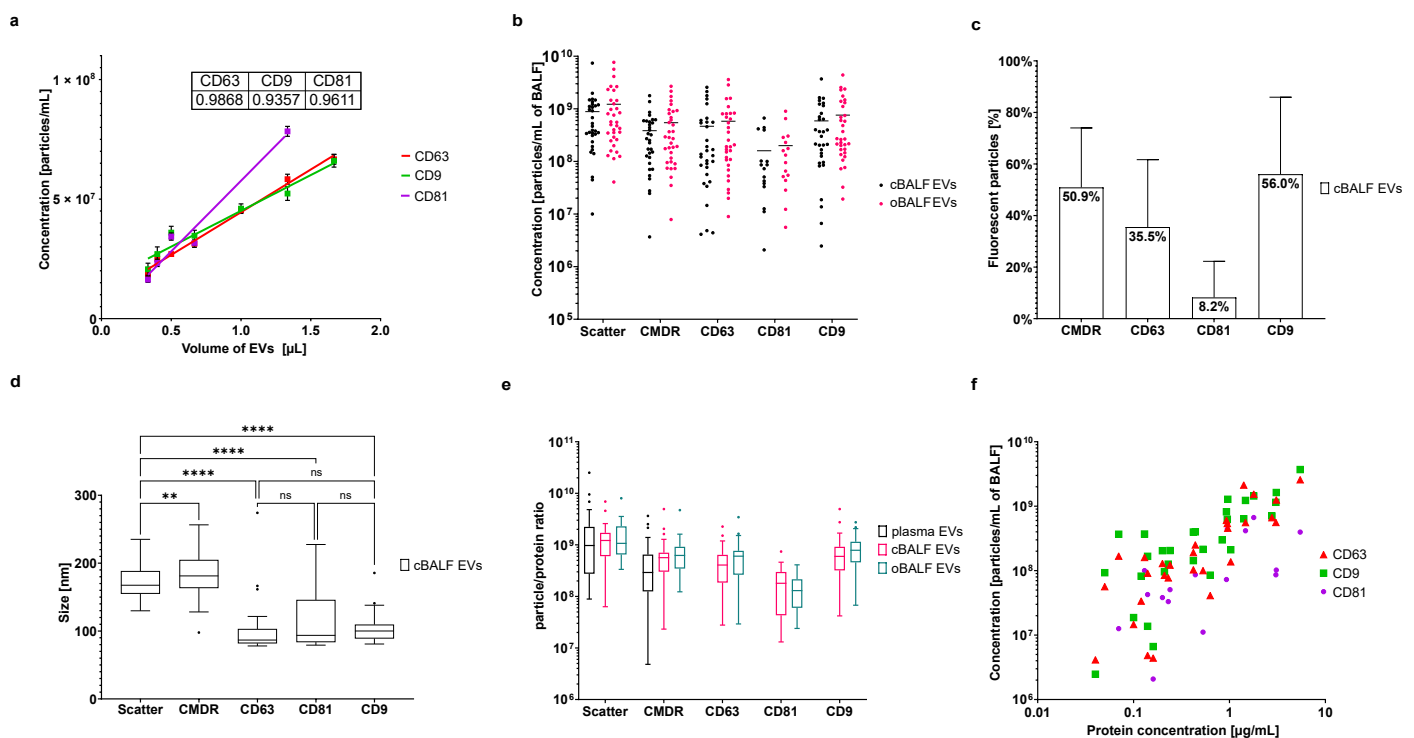


**Figure 6.** FL-NTA characterization of BALF EVs. (a) Concentration of BALF-derived particles measured in fluorescent mode (488 nm) after labeling with tetraspanin markers depending on the EV sample volume taken for the measurement. A line from simple linear regression was plotted and  $R^2$  was placed in the table for each tetraspanin marker. (b) Concentration of particles calculated per one mL BALF for cBALF-EVs and oBALF-EVs for all patients in FL-NTA. (c) The percent of fluorescent particles in comparison to all particles visible in scatter mode for cBALF EVs for all patients. (d) Measured mode sizes of particles in the scatter and fluorescent mode (488, 640 nm) for cBALF EVs for all patients. (e) Particle/protein ratio of plasma and BALF-EVs in the scatter and fluorescent mode. (f) Correlation between the concentration of particles and protein concentration of tetraspanin-positive cBALF-EVs. Graph (c) presents the mean and SD for all patients. Graphs (d,e) present the Tukey plot for all patients. \*\*\*\* refers to  $p$  value  $\leq 0.0001$ , \*\* refers to  $p$  value  $\leq 0.0021$ , ns refers to  $p$  value  $> 0.05$  from  $t$ -test-paired comparison (d) and Wilcoxon test-paired comparison (e).

However, the particle sizes differed significantly depending on the type of fluorescent marker. The CMDR-positive EVs in cBALF EVs were detected as being meaningfully larger (mean  $\pm$  SD:  $183.23 \pm 32.70$  nm) than particles detected in scatter (mean  $\pm$  SD:  $171.95 \pm 23.72$  nm). In contrast, all the particles positive for CD63, CD9, and CD81 showed much lower sizes (mean  $\pm$  SD: CD63:  $100.76 \pm 38.62$  nm; CD9:  $104.21 \pm 22.11$  nm; CD81:  $115.81 \pm 46.01$  nm) than those detected in scatter (Figure 6d). The particles positive for CD63, CD81, and CD9 were all similar in size. The individual size for all measured plasma and BALF EV samples are listed in Supplementary Table S3. Based on the measured protein concentrations of the EV samples (see Supplementary Table S5), the particle/protein ratio for all EV types in scatter and after fluorescent labeling was calculated. The obtained particle/protein ratios were 100 times higher for plasma than the ratio reported by Dong et al. and 10 times higher for BALF-EVs than ratios obtained for cell culture or urine EVs [19]. Our ratios showed no significant differences between all EV types (Figure 6e). Nonetheless, there was a strong positive correlation between tetraspanin-positive particle concentration and protein concentration for BALF-EVs (Figure 6f). For cBALF, the Spearman correlation was  $r_s = 0.81$ ,  $p < 0.0001$  for CD63 EVs,  $r_s = 0.65$ ,  $p < 0.0001$  for CD9 EVs, and  $r_s = 0.81$ ,  $p = 0.0074$  for CD81 EVs. For oBALF, the Spearman correlation was  $r_s = 0.69$ ,  $p < 0.0001$  for CD63 EVs,  $r_s = 0.71$ ,  $p < 0.0001$  for CD9 EVs, and  $r_s = 0.75$ ,  $p = 0.0007$  for CD81 EVs.

### 3.6. Control-Experiments for FL-NTA

#### 3.6.1. RIPA Lysis of EVs

In order to ensure that our fluorescent staining of the EV membrane and tetraspanins identified true EVs during FL-NTA measurements, we applied differential detergent lysis [21] with RIPA of a representative standard EV sample (commercially available, lyophilized EVs derived from the NSCLC cell line, with confirmed presence of exosomal markers), expecting that fluorescent signals connected to true EVs should disappear after detergent lysis [22]. Additionally, the scatter signal should either shift left toward smaller sizes (disruption of whole EVs into smaller fragments) or decrease when the fragmented EVs fall under the instrument's detection limit. Our goal was to confirm that NTA properly detect EVs in our samples and our labeling methods are specific.

Indeed, the mean particle concentration decreased in scatter mode from  $1.73 \times 10^{11} \pm 1.75 \times 10^{10}$  particles/mL before treatment to  $5.24 \times 10^{10} \pm 9.90 \times 10^9$  particles/mL in RIPA treated samples. Overall, there was a 65–73% decrease in the particle concentration in scatter mode after the treatment depending on labeling type (Figure 7a). The fact that the particles were still detectable after RIPA lysis could be caused by a too low concentration of RIPA or by a too-short time of lysis. In the fluorescent mode, the decrease in detected particles was so pronounced that the number of fluorescent particles after treatment dropped down below the NTA detection limit. Before the treatment, the percent of fluorescent particles compared to all particles visible in scatter mode fluctuated depending on the marker (CMDR  $55.92 \pm 1.66\%$ , CD63  $36.54 \pm 5.29\%$ , CD81  $34.60 \pm 1.15\%$ , and CD9  $88.46 \pm 0.38\%$ ), and after the treatment, there was no detectable fluorescence (Figure 7b).

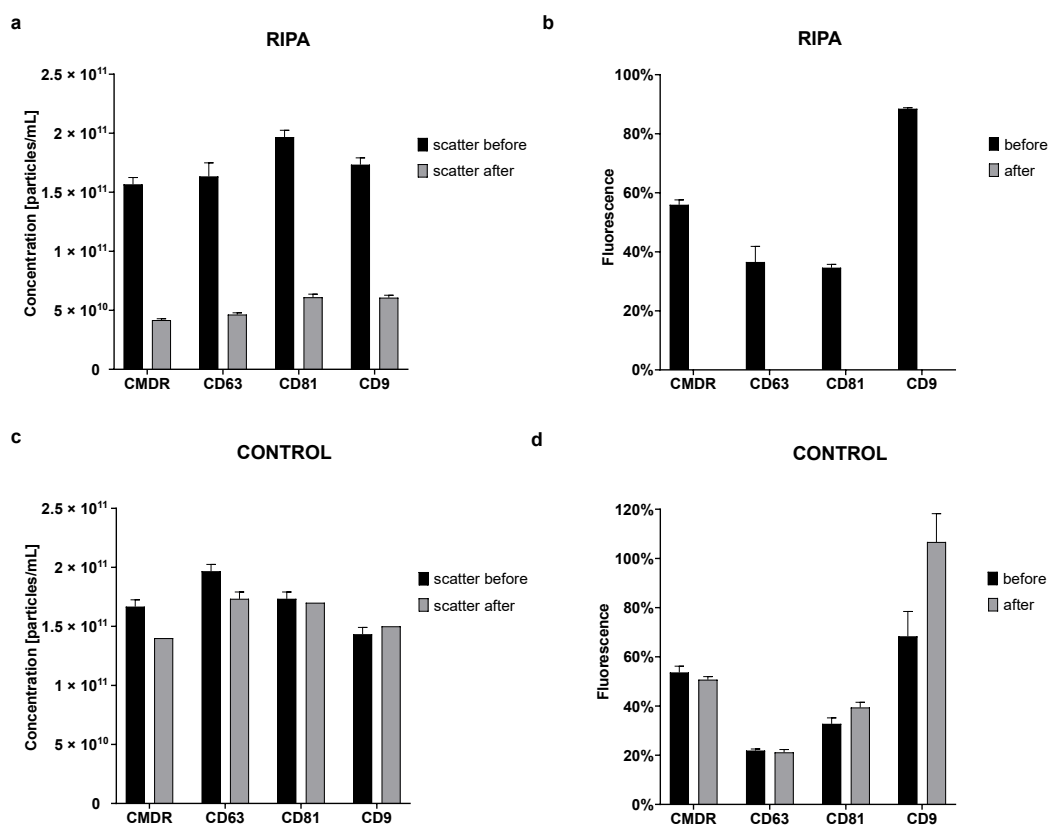


**Figure 7.** RIPA lysis of standard EVs derived from the NSCLC cell line. (a) The concentration of particles measured in scatter mode after labeling with CMDR and fluorescent antibodies against tetraspanin markers before and after incubation with RIPA lysis buffer. (b) The percent of fluorescent particles in comparison to all particles visible in scatter mode before and after incubation with RIPA lysis buffer. (c) The concentration of particles measured in scatter mode after labeling before and after incubation with PBS (control). (d) The percent of fluorescent particles in comparison to all particles visible in scatter mode before and after incubation with PBS as the control. Graphs (a–d) present the mean and SD from three replicates.

In contrast, for samples treated with PBS instead of RIPA (control), there was only a slight decrease after the treatment in scatter mode (the mean concentration in scatter mode before the treatment was  $1.70 \times 10^{11} \pm 2.19 \times 10^{10}$  particles/mL and after the treatment  $1.58 \times 10^{11} \pm 1.60 \times 10^{10}$  particles/mL) (Figure 7c). Control samples also remained fluorescent after the treatment. The overall difference in fluorescence for the control samples was only 2.94% for CMDR, 0.72% for CD63, and 6.67% for CD81. For unknown reasons, the fluorescence for CD9 increased by 38.33% after the treatment (Figure 7d). The sizes of the particles in both RIPA and the control samples remained the same before and after the treatment (Figure S6).

This experiment confirmed that our labeling methods really stained exosomal markers and that we measured true EVs.

### 3.6.2. FL-NTA Measurements of Tetraspanin-Labeled EVs after Immunomagnetic Removal of EV Subpopulations

To further prove the correctness of the performed tetraspanin-specific FL-NTA measurements of our EV samples, we investigated whether the removal of selected tetraspanin-positive EV subpopulations from the analyzed sample would be reflected by a decrease in the corresponding fluorescent signal in FL-NTA. For this experiment, we chose an oBALF-EV sample with a relatively high expression of CD63 and CD9 (we omitted CD81 due to the relatively low expression in BALF-EV samples). We removed either CD63 positive or CD9 positive EVs using magnetic beads coated with anti-CD63 or anti-CD9 antibodies, respectively. Next, we performed fluorescent labeling against CD63, CD9, and membrane labeling with CMDR.

The fluorescent staining and subsequent FL-NTA analysis of the CD63+ EV-depleted fraction revealed a decrease in detected CD63 positive particles (in comparison to all particles measured in scatter mode). Fluorescence dropped from 92% to 68% after depletion. There was also a slight decrease in the number of CD9 positive particles from 63% to 50% (Figure 8a). Accordingly, the depletion of CD9+ EVs resulted in a higher decrease in detected CD9 positive particles and a smaller decrease in CD63 particles. The number of CD63 and CD9 positive EVs dropped to 80% and 31%, respectively. For unknown reasons, we observed an increase in the relative percentage and absolute numbers (data not shown) of CMDR positive particles.

Measurements of the negative control samples with PBS instead of EVs resulted in no signal in both scatter and fluorescence mode (data not shown). We also eluted the bead-bound EVs using a commercial elution buffer and stained them accordingly with CMDR and tetraspanins. We could measure the eluted beads in scatter mode, whereas the measurements in fluorescence mode detected no or only low and not reproducible percentages of fluorescence-positive particles (both for tetraspanins and CMDR—data not shown). This could be due to several reasons. First, the relatively low number of captured EVs imposed a low end-dilution of the sample for the NTA-measurement. It caused a higher than usual dilution of the fluorescent antibodies or CMDR at the time of staining, which could decrease the staining efficiency. Additionally, we suspected that the used elution buffer negatively impacts the CMDR and tetraspanin staining since we observed a decrease in the fluorescent signals after EV staining in the presence of the elution buffer only (data not shown).

Interestingly, comparing the size of the particles detected in scatter mode of the bead depleted EV-fractions with the corresponding CD63+ or CD9+ eluted EV-fractions, we once again obtained a confirmation of the smaller size of tetraspanin-positive EVs. The mode size of the particles remaining after bead depletions measured in scatter mode was only slightly larger than the control ( $168.9 \pm 4.6$  nm for the CD63 unbound and  $170.2 \pm 5.0$  nm for the CD9 unbound population vs.  $166.8 \pm 3.7$  nm for the control). The captured EVs' mode size was significantly smaller ( $135.8 \pm 2.3$  nm for the eluted CD63+ and  $136.4 \pm 1.8$  nm for the eluted CD9+ population; see Figure 8b). The determination of the captured EVs' mode size in fluorescent mode was hindered by the low particle number and therefore not statistically assured for all measured samples. However, the measured mode sizes between 80–120 nm

in single samples of the captured CD63+ and CD9+ EVs (data not shown) corresponded to the size of previously detected tetraspanin-positive particles in whole EV preparations, as described above.

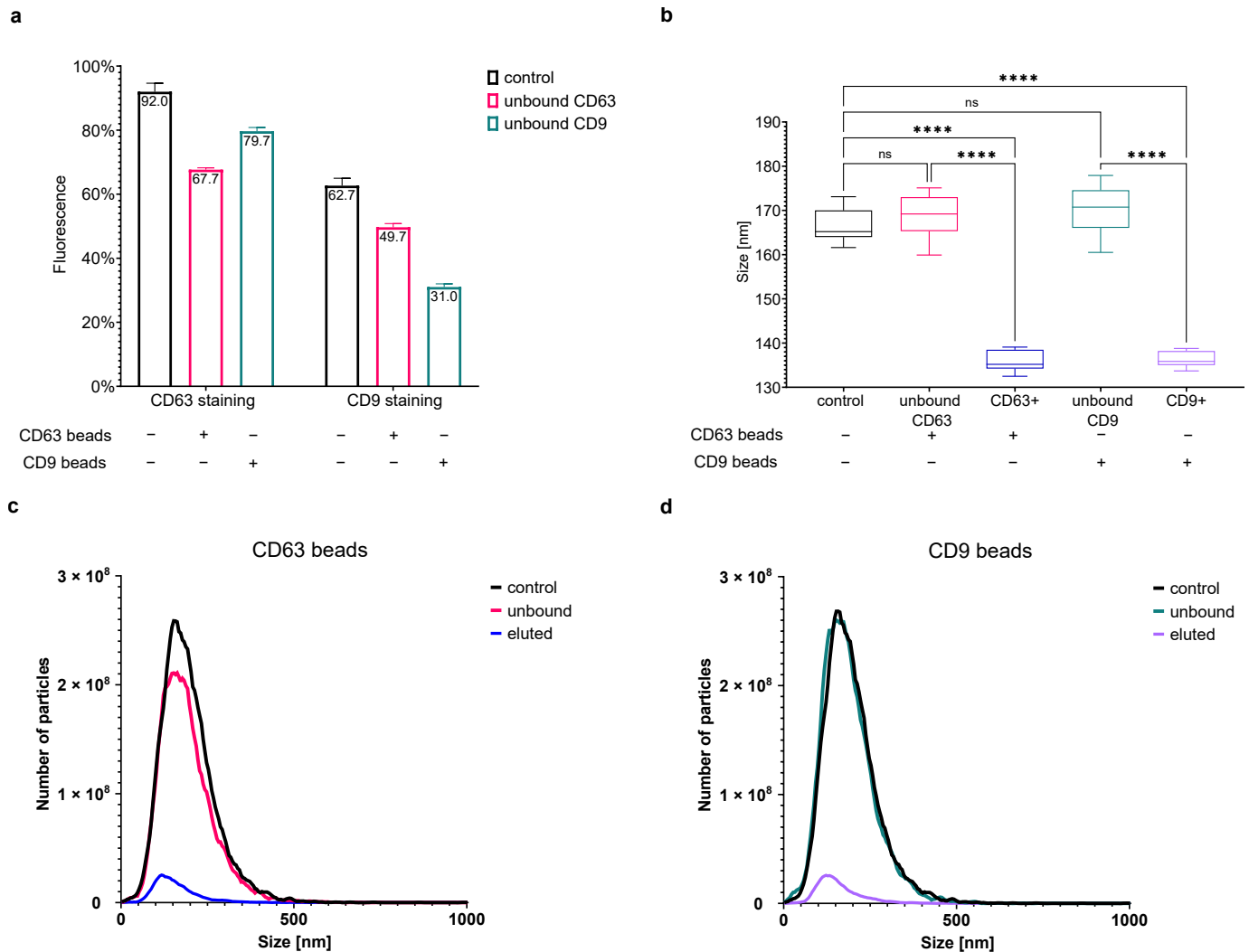


**Figure 8.** Depletion of EV-subpopulations by immune-magnetic bead separation. (a) The percent of fluorescent particles in comparison to all particles visible in scatter mode for oBALF-EVs of one patient. The first three bars represent the percentage CD63 positive particles, and bars 4–6 represent the percentage of CD9 positive particles relative to particles in scatter. (b) Measured mode sizes of particles in scatter mode of oBALF-EVs of one patient. (c,d) Distribution of number and size of detected particles in scatter mode of oBALF-EVs of one patient for the CD63 beads (c) and CD9 beads (d) experiment. For graphs (a–d), the colors stand for the following sample types: control sample (black), fraction unbound to CD63 beads (pink), fraction eluted from CD63 beads (blue), fraction unbound to CD9 beads (green), and fraction eluted from CD9 beads (violet). Graph (a) presents the mean and SD from three repetitions. Graph (b) presents the mean and SD from twelve repetitions. Graphs (c,d) present the mean from three repetitions. \*\*\*\* refers to  $p$  value  $\leq 0.0001$ , ns refers to  $p$  value  $> 0.05$ , from  $t$ -test-paired comparison.

Admittedly, the number of captured EVs was relatively low, looking at the measured concentrations in scatter (Figure 8c,d) and the still high percentage of tetraspanin-positive particles in the unbound-fraction. Obviously, further optimization of the method would be required to obtain better results. A longer incubation time or different bead–EV ratio could increase the captured EV number. However, since this experiment was intended only as a proof-of-concept and was not designed to provide exact values, we did not aim for complete removal of all CD63 or CD9 positive EVs or exactly checked the effi-

ciency of EV removal. In summary, this proof-of-concept experiment verified our FL-NTA immunolabeling technique for the detection of tetraspanin-positive EVs.

### 3.6.3. Impact of Plasma Lipoproteins on FL-NTA Measurements

To verify our assumption that the high lipoprotein content in our plasma EV-isolates interferes with CMDR labeling and prevents the detection of tetraspanin-positive EVs in FL-NTA, we removed lipoproteins from plasma prior to EV isolation. After lipoprotein removal (-LP) and EV isolation by SEC, we did not observe a change in total particle concentration or size of the particles in scatter mode compared to the control (CTRL), where there was no lipoprotein removal step before the isolation. Mean concentration in -LP was  $4.10 \times 10^{10} \pm 2.19 \times 10^9$  particles/mL and in CTRL it was  $4.08 \times 10^{10} \pm 3.40 \times 10^9$  particles/mL. However, we observed a significant increase in CMDR-positive particle concentration (Figure 9a,b). The mean concentration of CMDR+ particles in -LP was  $3.83 \times 10^{10} \pm 2.50 \times 10^9$  particles/mL and in CTRL  $2.58 \times 10^{10} \pm 2.77 \times 10^9$  particles/mL. Measurement of the content of CMDR+ particles by FL-NTA of EVs separated from plasma of four different patients after removing lipoproteins showed a significant increase in CMDR positive particles in comparison to the control samples in three patients (Figure 9c). In the case of the staining for tetraspanins, we unfortunately obtained non-reproducible results (data not shown). For the plasma-EV samples for which no tetraspanins could previously be detected by NTA, lipoprotein removal did not improve the detection. For other EV samples where CD9 positive EVs could be initially detected, the percentage of CD9+ EVs increased in the -LP sample. However, this result was not explicitly reproducible for all tested samples.

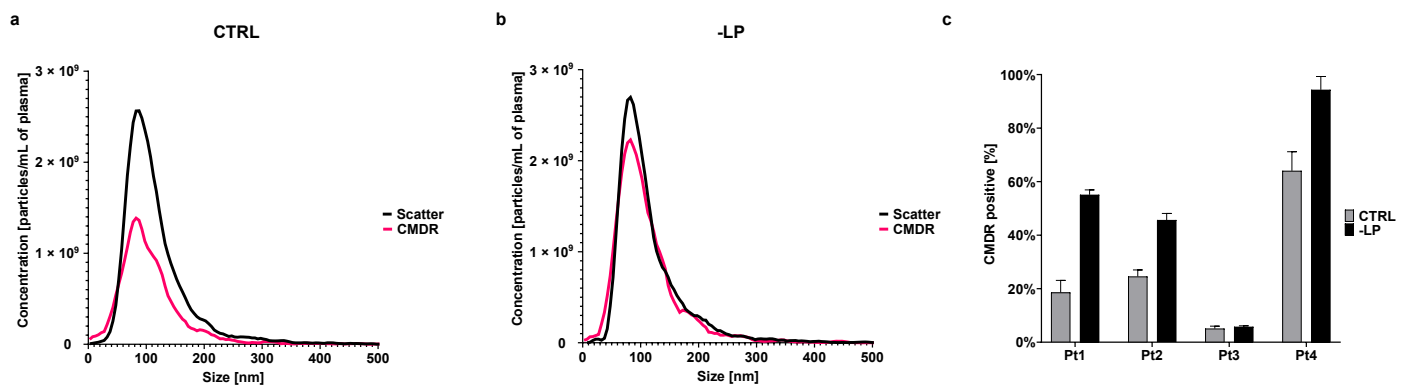


**Figure 9.** Lipoprotein removal from plasma EVs. (a) Distribution of particles in the scatter and fluorescent mode (640 nm) for plasma EVs of a representative patient during NTA measurement (CTRL). (b) Distribution of particles in the scatter and fluorescent mode (640 nm) for plasma EVs of a representative patient during NTA measurement after lipoprotein removal (-LP). (c) The percent of CMDR positive particles in comparison to all particles visible in the scatter mode of plasma EVs before and after lipoprotein removal. Graphs (a,b) present the mean from four replicates. Graph (c) presents the mean and SD from three (Pt1) to six (Pt2–4) replicates.

### 3.7. Correlation of BALF or Plasma-EVs Characteristics with NSCLC Patient Diagnosis

Given that within our small patient cohort, six patients during the diagnosis process turned out to have a lung lesion other than NSCLC, and in three patients the lung tumor could not be unequivocally confirmed, we decided to look at the potential of any of the investigated EV-related markers to differentiate between NSCLC patients and patients with other lung lesions. However, for none of the investigated parameters of both plasma and BALF-EVs (total particle number, particle size, CMDR+ particle number, tetraspanin-positive EV number, etc.), was a significant difference observed. We also could not find a correlation of the investigated EV-metrics with any of the clinical parameters (data not shown). One reason could be the small size of the patient cohort, which did not allow statistical significance to be reached. Another reason is that plasma and BALF-derived

EVs from patients contain both cancer-derived as well as normal EVs, so that general EV-markers may not be powerful enough to diagnose NSCLC patients.

#### 4. Discussion

##### 4.1. Selection of Isolation Methods for Plasma- and BALF-EVs

In the last several years, EVs have emerged as a promising new version of a liquid biopsy in cancer treatment. Playing a fundamental role in cell communication within the tumor microenvironment and mediating immunoinhibitory and pro-tumorigenic signals, they are under intensive research as potential biomarkers in diagnosis, prognosis, and treatment response or as therapeutic drug carriers.

It seems that plasma or serum-derived EVs are the easiest accessible sources of EV-based biomarkers. Unfortunately, their molecular characterization and translation into the clinic have been impeded by challenges to isolate EVs with sufficient yield and purity. This is because plasma contains a high concentration of proteins (mostly albumin, 35–55 mg/mL) and several orders of magnitude more lipoproteins ( $\sim 10^{16}$ /mL) than EVs ( $\sim 10^7$ – $10^9$ /mL) [23]. Several methods have been described for the separation of EVs, which vary in purity and yield of the received EV isolate. SEC is the most common method for EV enrichment from plasma since it removes the most contaminating proteins and allows for the purification of EV-enriched fractions from LDLs and HDLs. The method results in relatively pure and intact EVs, are broadly described in the literature, and are already well established in our laboratory, in contrast to differential ultracentrifugation (UC), which is not recommended for isolating EVs from plasma [24,25]. Therefore, we used centrifugation and homemade SEC columns for plasma EVs.

Another promising source of tumor derived EVs in lung cancer patients seems to be BALF. Unfortunately, BALF and plasma have a completely different composition and volume, and therefore each requires a unique approach for EV separation. Because BALF does not contain lipoproteins or high amounts of protein, we did not expect high contaminations. At the time of method development, there was no available SEC method for large volumes of fluid and our attempts to concentrate it were unsuccessful because of its high viscosity. Since the literature suggests UC as a good isolation method for BALF, we decided to use it [26]. During method optimization, we also performed an additional SEC purification step of the resuspended BALF-EV pellet after UC and compared it to EVs isolated only by UC. We found no differences in the EV profile measured by NTA (size), but noticed a substantial drop in EV recovery, which would leave not enough material for all planned analyses (data not shown). For these reasons, we decided to omit this step.

##### 4.2. Characterization of EVs in the Context of Standardization and Previous Reports

The importance of standardization and parameter monitoring was strongly emphasized by Vestad et al. [27]. Even small changes can lead to different measured concentrations and sizes of particles. Mørk et al. [28] noticed in their paper the loss of quality when one analyzed EV-enriched particle fractions after a freeze–thaw cycle. We performed our NTA experiments on freshly isolated EV preparations from frozen plasma. However, in the case of BALF, NTA experiments were performed on previously isolated and frozen EV samples for technical reasons. However, our cryo-TEM pictures of thawed EVs from BALF proved that the phospholipid bilayer remained intact, and the EVs kept their usual shape and integrity (Figure S7a).

Using MISEV-recommended “classical” EV characterization methods, we showed that our EV separation methods were effective. We managed to detect classical transmembrane (CD9, CD81) and cytosolic (Tsg101, syntenin) EV-markers in both plasma and BAL-EVs and excluded secretory pathway contaminants (calnexin). Our NTA analysis in the scatter mode of both EV types suggested that plasma may be a better source of EVs in lung cancer patients since in comparison to BALF, it contained approximately 500 to 250 times more particles per mL of more homogenous size and around 3.5 times more exosomal proteins. Rodriguez et al. [29] similarly noticed higher particle numbers in BALF than in plasma,



however, there, the obtained particle number was 5–10 times lower in BALF and 1000 times lower in plasma compared to our results. This could be explained by the different isolation methods and pooled samples used by Rodriguez. In contrast, we performed all of our analyses pairwise, comparing plasma, oBALF, and cBALF EVs separately for every patient. The lower EV numbers in BALF were expected since BALF is not a “true” biological fluid, but is obtained by diluting some original biological material with saline solution and contains much fewer EV donor-cells.

#### 4.3. Membrane Labeling Reveals EV Sample Purity

Our further NTA-based identification of “true” EVs based on CMDR membrane staining and tetraspanin detection showed that a substantial proportion of the particles measured by NTA in scatter mode, especially in the case of plasma, were of non-vesicular origin and rather represented protein aggregates and lipoproteins than EVs. Membrane labeling revealed that BALF contained a higher proportion of true EVs than plasma, with around 50% of CMDR-positive particles in BALF in comparison to only 30% in plasma. Indeed, our cryo-TEM analysis already showed significantly higher contamination of the plasma-derived EV-sample with protein aggregates and single-membrane vesicles in comparison to the BALF sample; although rare per field, only double-membrane bona-fide EVs were visible.

Additionally, we noticed that the EV mode size increased after labeling with CMDR by around 10–20 nm in all of our EV sample types, which is in line with the observations after EV labeling with PKH [30] or the FM dye [31]. An explanation for this observation may be the intercalation of CMDR molecules into the EV membrane, causing an increase in size. In addition, particularly smaller particles probably representing protein aggregates that are not stained with CMDR, contribute to a smaller mode size in scatter mode and are eliminated in the fluorescence measurement. Furthermore, our preliminary experiments optimizing the dye concentrations showed a strong particle size increase at very high CMDR concentrations. This points to the possibility of the aggregation of CMDR particles that are then detected by the NTA, causing a shift in the particle size distribution toward bigger sizes, as also observed by Wu Y et al. [32].

#### 4.4. Lipoprotein Influence on EV-Membrane Labeling and NTA-Analysis

The results discussed above point to the possibility that our SEC method does not provide a full separation of plasma EVs from lipoproteins due to the overlap in size, which was already previously observed [33–35]. The lipoproteins in plasma are composed of very-low-density lipoproteins (VLDLs), intermediate and low-density lipoproteins (IDLs and LDLs), high-density lipoproteins (HDLs), and chylomicrons, which all interfere with the characterization of EV preparations from this source including NTA measurements [23]. Measuring particles directly in plasma by NTA, Gardiner et al. shown that lipoproteins may account for more than 98% of particles [10].

SEC-isolation of EV fractions removes contaminating HDLs and LDLs due to their small size below 30 nm. However, bigger VLDLs and chylomicrons may still be present, as evident by their triglyceride or Apo-B content [36]. To address this issue, we performed additional western blot analysis of our EV isolates for the presence of lipoprotein marker Apo-B. We managed to detect it in our plasma EV samples, but not in the BALF EVs or cell lysate (Supplementary Figure S8).

Although staining with membrane dyes may help exclude some impurities mimicking EVs from analysis, it will not fully differentiate between true EVs and lipoproteins or even protein aggregates. Recently, it has been discovered that fluorescent lipophilic membrane dyes such as PKHs, DiD, or Cell Mask dyes, which are commonly used to identify true EVs, are not specific to the vesicular membrane and can be incorporated into any lipid structure including lipoproteins and also bind to free proteins [37]. Takov et al. showed that fluorescent dye transfers to the target cell after staining of the small EVs (sEVs) obtained from plasma by SEC did not correlate with sEV content. The authors observed a

similar or even higher fluorescent uptake of vesicle-poor but protein-rich SEC fractions. They concluded that lipoproteins and free proteins unavoidably co-isolated with sEVs significantly contribute to the fluorescent membrane dye's transfer and uptake by target cells [35].

So far, no studies have investigated the impact of lipoproteins on NTA measurements after membrane dye staining. In our case, we observed a lower percentage of CMDR-positive particles in plasma-EV samples in comparison to the BALF-EV samples. We suspected that the lipoproteins present in our plasma EV samples interfered here with the staining and NTA-measurement. They may compete with true EVs for dye binding, interfere with EV labeling, and contribute in an undefined way to the CMDR+ particle count detected by NTA. Furthermore, some of the remaining LDLs and HDLs not removed by SEC could also incorporate the dye, reducing the available dye amount for EV staining. However, due to their small size, they would be under the ZetaView instrument's detection limit. Based on the previous reports and our results, we concluded that lipophilic dyes might not be reliable for labeling small EVs from plasma unless an entirely pure population without proteins and lipoproteins of EVs is obtained, which given the currently available isolation methods has not been achieved thus far.

Attempts to increase the purity of EV preparations from plasma by including additional gradient separation or differential UC have only been partially successful [38]. This also has some implications for sample collection since EV-enriched plasma samples collected in the postprandial state demonstrated an increase in total particle numbers in NTA [28,39–41]. On one hand, which exposes the possible strong interference of lipoproteins with NTA-measurements and, on the other hand, the need to analyze plasma EV samples in the fasting state. In our case, food intake before blood draw was not a strict exclusion criterion in our patients' group, however, most of the blood samples were routinely drawn in the fasting state. The strong interference of lipoproteins with NTA-measurements also implies that direct measurements of EVs in unpurified plasma by NTA in scatter mode, even though it is technically possible and has already been performed by several researchers [10,18,22], may lead to a high overestimation of the actual EV numbers and have to be interpreted with caution. To further complicate the issue, recently, an in vitro association of LDLs with EVs and their interference with vesicle analysis has been observed [22].

#### 4.5. Antibody Labeling Show Significant Differences between Plasma and BALF EVs

Given the CMDR-labeling inaccuracy in EV number evaluation, we performed staining of our EV samples with fluorescent antibodies directed against tetraspanins as classical small EV or exosomes markers. We detected expression of all tested tetraspanins on BALF-derived EVs, with the amount of detected CD9-positive particles being the highest and corresponding to the amount of detected CMDR+ vesicles and the amount of CD81 positive particles being the lowest. Interestingly, all tetraspanin-labeled samples detected in fluorescent mode showed a decreased mean size in comparison to the whole vesicle population in scatter mode or the CMDR+ population. On one hand, this was expected since tetraspanins are regarded to be predominantly markers of smaller EVs of endosomal origin, named exosomes. It seems that in our BALF-EV population, preferably the smaller exosomal EVs around 100 nm express tetraspanins, and their presence is becoming less common the larger the EVs. On the other hand, we were surprised to note that the detected tetraspanin-positive particle size distribution curve did not fully overlap with the scatter or the CMDR+ distribution curves and shifted toward smaller sizes. Understandably, the smallest tetraspanin-positive EVs were not detected in the scatter mode or after CMDR staining. One explanation for this phenomenon could be the technical limitation of the NTA instrument. In highly polydispersed samples such as EV preparations from biological fluids, large and therefore strongly light-scattering particles overshadow the smaller particles and exhibit halo effects in scatter mode. Additionally, in comparison to polystyrene beads, EVs have a very low refractive index. Thus, they may lie under the ZetaView instrument's



detection limit in scatter mode and may also be too small to incorporate enough CMDR dye to be detected in the fluorescent mode. After labeling with tetraspanin-specific fluorescent antibodies, bigger tetraspanin-negative particles become invisible, whereas the smaller tetraspanin-positive EVs become traceable in the fluorescent mode. Similar observations were made by other researchers. Oesterreicher et al. detected higher EV-specific CD63 and CD81 marker expression in the small vesicle range (<200 nm) than in the intermediate and large ranges [42]. Staining with quantum dots for CD9 of canine MSC-derived EVs resulted in the detection of small particles ranging in size from 30–100 nm, which were significantly less numerous in scatter mode [43]. The authors concluded that these smaller fluorescent particles could be CD9 positive small EVs not visible in scatter or free quantum dots and quantum dots aggregates. Here, by evaluating the fluorescence background of the control samples (fluorescent antibodies only) and adjusting the instrument settings accordingly, we could largely exclude the detection of free antibodies or antibody aggregates. In our study, the peak shift in fluorescent mode can be attributed to tetraspanin-bearing small EVs not detectable in scatter mode (which also explains the over 100% scatter/fluorescent mode particle ratios of some samples). Our control NTA-measurement of CD63 and CD9 labeled BALF-EVs after EV-depletion by CD63- or CD9-specific magnetic beads confirmed that we detected true CD63 or CD9 positive EVs in fluorescence NTA since EV-depletion markedly reduced the tetraspanin-specific fluorescence.

In contrast, we could not detect any tetraspanins in our plasma EV samples at the same staining conditions except only single samples. We believe that the reason lies in the high concentration of contaminating lipoproteins, which do not express tetraspanins, but are detected in the scatter mode of the instrument. Since we have to adjust the dilution of the sample for measurement based on the particle count in scatter mode, the lipoprotein contamination of the plasma-EVs impose a high sample dilution factor to stay within the optimal measurement range of the instrument. This dilution is then too high to detect the low abundant tetraspanin-positive EVs in fluorescent mode. However, biological reasons may also be possible (e.g., plasma EVs may have less tetraspanin-epitopes on their EV surface than BALF-EVs and may therefore be less detected by the instrument. Indeed, direct phenotyping of plasma-derived EVs by nano flow cytometry revealed a very low percentage of tetraspanin-positive EVs, which barely exceeded 4% [19]. Furthermore, only ultracentrifugation and SEC with ultrafiltration as EV-isolation methods resulted in detectable numbers of tetraspanin-positive EVs. In contrast, EVs from the cell culture supernatant or urine showed significantly higher tetraspanin expression rates between 25–40%, which is comparable to our results obtained from BALF. An increase in sample input for the measurement to reach the detection level is not feasible for NTA since a too concentrated sample will fall out of the instrument's linear range.

Sodar et al. showed that even after applying the most efficient and purifying EV isolation methods currently available, the obtained EV samples still contained at least one order of magnitude less "true" EVs in comparison to the contaminating lipoproteins and protein aggregates [22]. Therefore, we decided to remove lipoproteins from the plasma sample prior to our standard EV isolation using a commercially available kit. We observed an increase in the % of detectable CMDR-positive particles in most cases, indicating that the presence of lipoproteins in the EV isolates indeed interfered somehow with EV membrane staining. Unfortunately, the staining against tetraspanins after lipoprotein removal provided somewhat contradictory results (in some samples an increase, in others no change—data not shown). Right now, we do not know exactly what the mechanism of lipoprotein interference during EV labeling and FL-NTA detection is, but our experiment confirms that it has an impact on the results. Mork et al. performed a similar experiment, but the NTA-measurements were performed directly in platelet-free plasma (PFP) without EV-isolation and only in scatter mode. Lipoprotein removal resulted in a median reduction of 62% of the measured particle concentration, once again emphasizing the fact that scatter NTA-measurements do not only detect true EVs [18].

#### 4.6. NSCLC Patients Differentiation

None of the investigated general EV-parameters could differentiate between NSCLC patients and non-NSCLC patients or correlated to any clinical parameter. Although several studies have already shown a correlation between total EV levels in plasma and disease activity and progression [44], recently the EV research has moved toward the investigation of more specific EV-cargo as a diagnostic or prognostic marker (e.g., the presence of immunosuppressive factors, cancer-specific molecules or miRNAs). In our ongoing studies, we plan to further characterize the molecular cargo of BALF-EVs in the context of EV-mediated immunosuppression in the lung TME in a much larger cohort of NSCLC patients. We are convinced that a comprehensive examination of the molecular composition of BALF-EVs might provide specific EV-cargo signatures that will be more accurate and reliable diagnostic or prognostic biomarkers than any single soluble BALF or plasma biomarker.

#### 4.7. Conclusions

In summary, in this study, we presented the first comprehensive phenotyping of BALF-derived EVs from lung cancer patients using classical EV-characterization methods as well as the relatively new FL-NTA method. In addition, we have shown that EV immunolabeling for specific EV markers combined with the differential use of the scatter mode and fluorescent mode NTA analysis can provide the concentration, size, distribution, and surface phenotype of bona fide EVs in a heterogeneous solution. By performing FL-NTA analysis of BALF-derived EVs in comparison to plasma-derived EVs, we have revealed that this method is suitable only for relatively pure EV isolates such as BALF or CCM. In particular, EV preparations from plasma or serum, with very low EV levels in comparison to contaminating lipoproteins, are less suitable for FL-NTA phenotyping, and even membrane-specific labeling might strongly overestimate EV numbers. The different composition of BALF-EV versus plasma EV samples and its impact on NTA analysis are summarized in Figure 10. Development of applicable purification methods for these EV preparations to remove lipoproteins, as has recently been attempted by Onodi et al. [45], and further refinement of the immunolabeling process and optimization of the FL-NTA settings are needed for the analysis of such polydispersed EV preparations. Further development of FL-NTA based EV-phenotyping toward the detection of more specific cargo such as cancer-biomarkers will advance our understanding of the composition and quality of different EV preparations. This is indispensable before a conclusive statement about their biological function and clinical significance can be made.

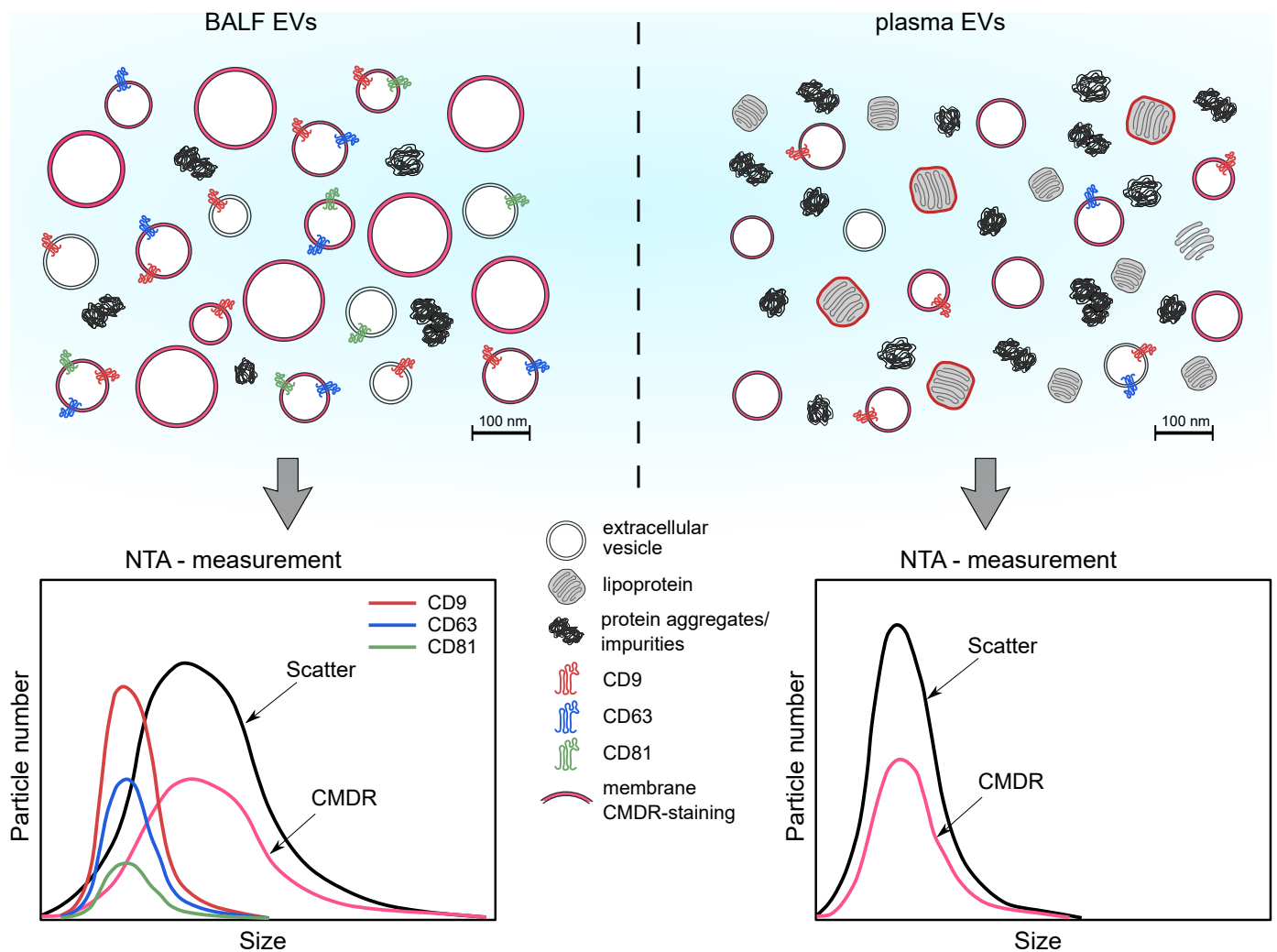


Figure 10. BALF and plasma EV characterization summary.

**Supplementary Materials:** The following are available online at <https://www.mdpi.com/article/10.3390/cells10123473/s1>, Supplementary Table S1: Fluorescent label, antibodies, isotype controls, and secondary antibody used for NTA, flow cytometry, and western blot analysis; Supplementary Table S2: Concentration of particles for 1 mL of plasma/BALF in scatter, membrane, and tetraspanin labeling; Supplementary Table S3: Size of particles for 1 mL of plasma/BALF in scatter, membrane, and tetraspanin labeling; Supplementary Table S4: The concentration of particles—the fraction of all particles [%] in six size fractions (<50 nm, 50–100 nm, 100–150 nm, 150–200 nm, 200–250 nm, >250 nm) for plasma, BALF, and cell line EVs; Supplementary Table S5: Concentration of protein for 1 mL of plasma/BALF; Figure S1: EVs separation from plasma on SEC—particle/protein ratio; Figure S2: Flow cytometry analysis of oBALF-EVs bound to magnetic Dynabeads coated with antibodies against tetraspanins; Figure S3: Variability of the measured size and concentration of standard beads on NTA; Figure S4: Optimization of CMDR concentration; Figure S5: Antibody labeling of cBALF and oBALF EVs; Figure S6: RIPA lysis of EVs—size; Figure S7: Cryo-TEM images of thawed cBALF EVs; full blots from Figure S2a; Figure S8: Lipoprotein marker Apo-B; raw pictures from Cryo-TEM from Figure S2b.

**Author Contributions:** Conceptualization, M.C.-K.; Methodology, M.D. and M.C.-K.; Software, M.D.; Validation, M.D.; Formal analysis, M.D.; Investigation, M.D., J.S., L.Z., and Z.H.; Resources, M.C.-K.; Data curation, M.D.; Writing—original draft preparation, M.D. and M.C.-K.; Writing—review and editing, M.D. and M.C.-K.; Visualization, M.D. (Figures 2–9) and J.S. (Figures 1 and 10); Supervision, M.C.-K.; Project administration, M.C.-K.; Funding acquisition, M.C.-K.; Patient recruitment, M.P.-K.

and J.D.-K.; BAL-procedure, M.P.-K. All authors have read and agreed to the published version of the manuscript.

**Funding:** This research was funded by the National Science Centre under grant OPUS 14 2017/27/B/NZ6/01990; and NAWA under grant PPI/APM/2019/1/00051/V/00001.

**Institutional Review Board Statement:** The study was conducted according to the guidelines of the Declaration of Helsinki and approved by the Institutional Bioethical Review Board of the Medical University of Warsaw (approval no. KB/183/2018, 8 October 2018).

**Informed Consent Statement:** Informed consent was obtained from all patients involved in the study.

**Data Availability Statement:** Additional supporting information may be found online in the Supplementary Materials or are available from the corresponding author upon reasonable request.

**Acknowledgments:** We thank Iwona Kwiecien from the Laboratory of Hematology and Flow Cytometry, Department of Internal Medicine and Hematology, Military Institute of Medicine, Warsaw, Poland for the pre-clearing of the BALF-samples. We also thank Tomasz Goral from the Transmission Electron Microscopy Core Facility in Center of New Technologies University of Warsaw, Poland for taking the Cryo-TEM images.

**Conflicts of Interest:** The authors declare no conflict of interest.

## References

1. Czystowska-Kuzmicz, M.; Whiteside, T.L. The potential role of tumor-derived exosomes in diagnosis, prognosis, and response to therapy in cancer. *Expert Opin. Biol. Ther.* **2021**, *21*, 241–258. [[CrossRef](#)] [[PubMed](#)]
2. Domagala-Kulawik, J. The relevance of bronchoalveolar lavage fluid analysis for lung cancer patients. *Expert Rev. Respir. Med.* **2020**, *14*, 329–337. [[CrossRef](#)]
3. Li, J.; Hu, Y.M.; Wang, Y.; Tang, X.P.; Shi, W.L.; Du, Y.J. Gene mutation analysis in non-small cell lung cancer patients using bronchoalveolar lavage fluid and tumor tissue as diagnostic markers. *Int. J. Biol. Markers* **2014**, *29*, 328–336. [[CrossRef](#)] [[PubMed](#)]
4. Uribarri, M.; Hormaeche, I.; Zalacain, R.; Lopez-Vivanco, G.; Martinez, A.; Nagore, D.; Ruiz-Arguello, M.B. A new biomarker panel in bronchoalveolar lavage for an improved lung cancer diagnosis. *J. Thorac. Oncol.* **2014**, *9*, 1504–1512. [[CrossRef](#)]
5. Siedentopf, H.; Zsigmondy, R. Über Sichtbarmachung und Größenbestimmung ultramikroskopischer Teilchen, mit besonderer Anwendung auf Goldrubingläser. *Ann. Der Phys.* **1902**, *315*, 1–39. [[CrossRef](#)]
6. Carpenter, D.K. Dynamic light scattering with applications to chemistry, biology, and physics (Berne, Bruce J.; Pecora, Robert). *J. Chem. Educ.* **1977**, *54*, A430. [[CrossRef](#)]
7. Filipe, V.; Hawe, A.; Jiskoot, W. Critical evaluation of Nanoparticle Tracking Analysis (NTA) by NanoSight for the measurement of nanoparticles and protein aggregates. *Pharm. Res.* **2010**, *27*, 796–810. [[CrossRef](#)]
8. Giebel, B.; Helmbrecht, C. Methods to analyze EVs. In *Exosomes and Microvesicles: Methods and Protocols*; Hill, A.F., Ed.; Springer: New York, NY, USA, 2017; pp. 1–20.
9. Dragovic, R.A.; Gardiner, C.; Brooks, A.S.; Tannetta, D.S.; Ferguson, D.J.P.; Hole, P.; Carr, B.; Redman, C.W.G.; Harris, A.L.; Dobson, P.J.; et al. Sizing and phenotyping of cellular vesicles using nanoparticle tracking analysis. *Nanomed. Nanotechnol. Biol. Med.* **2011**, *7*, 780–788. [[CrossRef](#)] [[PubMed](#)]
10. Gardiner, C.; Ferreira, Y.J.; Dragovic, R.A.; Redman, C.W.; Sargent, I.L. Extracellular vesicle sizing and enumeration by nanoparticle tracking analysis. *J. Extracell. Vesicles* **2013**, *2*, 19671. [[CrossRef](#)]
11. Carnell-Morris, P.; Tannetta, D.; Siupa, A.; Hole, P.; Dragovic, R. Analysis of extracellular vesicles using fluorescence nanoparticle tracking analysis. In *Extracellular Vesicles: Methods and Protocols*; Kuo, W.P., Jia, S., Eds.; Springer: New York, NY, USA, 2017; pp. 153–173.
12. Thery, C.; Witwer, K.W.; Aikawa, E.; Alcaraz, M.J.; Anderson, J.D.; Andriantsitohaina, R.; Antoniou, A.; Arab, T.; Archer, F.; Atkin-Smith, G.K.; et al. Minimal information for studies of extracellular vesicles 2018 (MISEV2018): A position statement of the international society for extracellular vesicles and update of the MISEV2014 guidelines. *J. Extracell. Vesicles* **2018**, *7*, 1535750. [[CrossRef](#)]
13. Chcialowski, A.; Chorostowska-Wynimko, J.; Fal, A.; Pawlowicz, R.; Domagala-Kulawik, J. Recommendation of the Polish respiratory society for bronchoalveolar lavage (BAL) sampling, processing and analysis methods. *Pneumonol. Alergol. Pol.* **2011**, *79*, 75–89. [[PubMed](#)]
14. Czystowska-Kuzmicz, M.; Sosnowska, A.; Nowis, D.; Ramji, K.; Szajnik, M.; Chlebowska-Tuz, J.; Wolinska, E.; Gaj, P.; Grazul, M.; Pilch, Z.; et al. Small extracellular vesicles containing arginase-1 suppress T-cell responses and promote tumor growth in ovarian carcinoma. *Nat. Commun.* **2019**, *10*, 3000. [[CrossRef](#)]
15. Ludwig, N.; Hong, C.S.; Ludwig, S.; Azambuja, J.H.; Sharma, P.; Theodoraki, M.N.; Whiteside, T.L. Isolation and analysis of tumor-derived exosomes. *Curr. Protoc. Immunol.* **2019**, *127*, e91. [[CrossRef](#)] [[PubMed](#)]

16. Consortium, E.-T.; Van Deun, J.; Mestdagh, P.; Agostinis, P.; Akay, O.; Anand, S.; Anckaert, J.; Martinez, Z.A.; Baetens, T.; Beghein, E.; et al. EV-TRACK: Transparent reporting and centralizing knowledge in extracellular vesicle research. *Nat. Methods* **2017**, *14*, 228–232. [[CrossRef](#)]
17. Roux, Q.; Van Deun, J.; Dedeyne, S.; Hendrix, A. The EV-TRACK summary add-on: Integration of experimental information in databases to ensure comprehensive interpretation of biological knowledge on extracellular vesicles. *J. Extracell. Vesicles* **2020**, *9*, 1699367. [[CrossRef](#)]
18. Mork, M.; Handberg, A.; Pedersen, S.; Jorgensen, M.M.; Baek, R.; Nielsen, M.K.; Kristensen, S.R. Prospects and limitations of antibody-mediated clearing of lipoproteins from blood plasma prior to nanoparticle tracking analysis of extracellular vesicles. *J. Extracell. Vesicles* **2017**, *6*, 1308779. [[CrossRef](#)] [[PubMed](#)]
19. Dong, L.; Zieren, R.C.; Horie, K.; Kim, C.J.; Mallick, E.; Jing, Y.; Feng, M.; Kuczler, M.D.; Green, J.; Amend, S.R.; et al. Comprehensive evaluation of methods for small extracellular vesicles separation from human plasma, urine and cell culture medium. *J. Extracell. Vesicles* **2020**, *10*, e12044. [[CrossRef](#)] [[PubMed](#)]
20. Rollet-Cohen, V.; Bourderioux, M.; Lipecka, J.; Chhuon, C.; Jung, V.A.; Mesbahi, M.; Nguyen-Khoa, T.; Guerin-Pfyffer, S.; Schmitt, A.; Edelman, A.; et al. Comparative proteomics of respiratory exosomes in cystic fibrosis, primary ciliary dyskinesia and asthma. *J. Proteom.* **2018**, *185*, 1–7. [[CrossRef](#)]
21. Osteikoetxea, X.; Sodar, B.; Nemeth, A.; Szabo-Taylor, K.; Paloczi, K.; Vukman, K.V.; Tamasi, V.; Balogh, A.; Kittel, A.; Pallinger, E.; et al. Differential detergent sensitivity of extracellular vesicle subpopulations. *Org. Biomol. Chem.* **2015**, *13*, 9775–9782. [[CrossRef](#)]
22. Sodar, B.W.; Kittel, A.; Paloczi, K.; Vukman, K.V.; Osteikoetxea, X.; Szabo-Taylor, K.; Nemeth, A.; Sperlagh, B.; Baranyai, T.; Giricz, Z.; et al. Low-density lipoprotein mimics blood plasma-derived exosomes and microvesicles during isolation and detection. *Sci. Rep.* **2016**, *6*, 24316. [[CrossRef](#)]
23. Simonsen, J.B. What are we looking at? Extracellular vesicles, lipoproteins, or both? *Circ. Res.* **2017**, *121*, 920–922. [[CrossRef](#)]
24. Hong, C.S.; Funk, S.; Whiteside, T.L. Isolation of biologically active exosomes from plasma of patients with cancer. *Methods Mol. Biol.* **2017**, *1633*, 257–265. [[CrossRef](#)]
25. Carnino, J.M.; Lee, H.; Jin, Y. Isolation and characterization of extracellular vesicles from Broncho-alveolar lavage fluid: A review and comparison of different methods. *Respir. Res.* **2019**, *20*, 240. [[CrossRef](#)] [[PubMed](#)]
26. Muller, L.; Hong, C.S.; Stolz, D.B.; Watkins, S.C.; Whiteside, T.L. Isolation of biologically-active exosomes from human plasma. *J. Immunol. Methods* **2014**, *411*, 55–65. [[CrossRef](#)] [[PubMed](#)]
27. Vestad, B.; Llorente, A.; Neurauter, A.; Phuyal, S.; Kierulf, B.; Kierulf, P.; Skotland, T.; Sandvig, K.; Haug, K.B.F.; Ovstebo, R. Size and concentration analyses of extracellular vesicles by nanoparticle tracking analysis: A variation study. *J. Extracell. Vesicles* **2017**, *6*, 1344087. [[CrossRef](#)] [[PubMed](#)]
28. Mork, M.; Pedersen, S.; Botha, J.; Lund, S.M.; Kristensen, S.R. Preanalytical, analytical, and biological variation of blood plasma submicron particle levels measured with nanoparticle tracking analysis and tunable resistive pulse sensing. *Scand. J. Clin. Lab. Investig.* **2016**, *76*, 349–360. [[CrossRef](#)]
29. Rodriguez, M.; Silva, J.; Lopez-Alfonso, A.; Lopez-Muniz, M.B.; Pena, C.; Dominguez, G.; Garcia, J.M.; Lopez-Gonzalez, A.; Mendez, M.; Provencio, M.; et al. Different exosome cargo from plasma/bronchoalveolar lavage in non-small-cell lung cancer. *Genes Chromosomes Cancer* **2014**, *53*, 713–724. [[CrossRef](#)]
30. Dehghani, M.; Gulvin, S.M.; Flax, J.; Gaborski, T.R. Systematic evaluation of PKH labelling on extracellular vesicle size by nanoparticle tracking analysis. *Sci. Rep.* **2020**, *10*, 9533. [[CrossRef](#)] [[PubMed](#)]
31. Pospichalova, V.; Svoboda, J.; Dave, Z.; Kotrbova, A.; Kaiser, K.; Klemova, D.; Ilkovic, L.; Hampl, A.; Crha, I.; Jandakova, E.; et al. Simplified protocol for flow cytometry analysis of fluorescently labeled exosomes and microvesicles using dedicated flow cytometer. *J. Extracell. Vesicles* **2015**, *4*, 25530. [[CrossRef](#)] [[PubMed](#)]
32. Wu, Y.; Deng, W.; Klinke, D.J., 2nd. Exosomes: Improved methods to characterize their morphology, RNA content, and surface protein biomarkers. *Analyst* **2015**, *140*, 6631–6642. [[CrossRef](#)]
33. Boing, A.N.; van der Pol, E.; Grootemaat, A.E.; Coumans, F.A.; Sturk, A.; Nieuwland, R. Single-step isolation of extracellular vesicles by size-exclusion chromatography. *J. Extracell. Vesicles* **2014**, *3*, 23430. [[CrossRef](#)] [[PubMed](#)]
34. Welton, J.L.; Webber, J.P.; Botos, L.A.; Jones, M.; Clayton, A. Ready-made chromatography columns for extracellular vesicle isolation from plasma. *J. Extracell. Vesicles* **2015**, *4*, 27269. [[CrossRef](#)] [[PubMed](#)]
35. Takov, K.; Yellon, D.M.; Davidson, S.M. Confounding factors in vesicle uptake studies using fluorescent lipophilic membrane dyes. *J. Extracell. Vesicles* **2017**, *6*, 1388731. [[CrossRef](#)] [[PubMed](#)]
36. Pang, B.; Zhu, Y.; Ni, J.; Ruan, J.; Thompson, J.; Malouf, D.; Bucci, J.; Graham, P.; Li, Y. Quality assessment and comparison of plasma-derived extracellular vesicles separated by three commercial kits for prostate cancer diagnosis. *Int. J. Nanomed.* **2020**, *15*, 10241–10256. [[CrossRef](#)] [[PubMed](#)]
37. Lai, C.P.; Kim, E.Y.; Badr, C.E.; Weissleder, R.; Mempel, T.R.; Tannous, B.A.; Breakefield, X.O. Visualization and tracking of tumour extracellular vesicle delivery and RNA translation using multiplexed reporters. *Nat. Commun.* **2015**, *6*, 7029. [[CrossRef](#)] [[PubMed](#)]
38. Karimi, N.; Cvjetkovic, A.; Jang, S.C.; Crescitelli, R.; Hosseinpour Feizi, M.A.; Nieuwland, R.; Lotvall, J.; Lasser, C. Detailed analysis of the plasma extracellular vesicle proteome after separation from lipoproteins. *Cell. Mol. Life Sci.* **2018**, *75*, 2873–2886. [[CrossRef](#)]



39. Tushuizen, M.E.; Diamant, M.; Peypers, E.G.; Hoek, F.J.; Heine, R.J.; Sturk, A.; Nieuwland, R. Postprandial changes in the phospholipid composition of circulating microparticles are not associated with coagulation activation. *Thromb. Res.* **2012**, *130*, 115–121. [[CrossRef](#)]
40. Tushuizen, M.E.; Nieuwland, R.; Scheffer, P.G.; Sturk, A.; Heine, R.J.; Diamant, M. Two consecutive high-fat meals affect endothelial-dependent vasodilation, oxidative stress and cellular microparticles in healthy men. *J. Thromb. Haemost.* **2006**, *4*, 1003–1010. [[CrossRef](#)]
41. Ferreira, A.C.; Peter, A.A.; Mendez, A.J.; Jimenez, J.J.; Mauro, L.M.; Chirinos, J.A.; Ghany, R.; Virani, S.; Garcia, S.; Horstman, L.L.; et al. Postprandial hypertriglyceridemia increases circulating levels of endothelial cell microparticles. *Circulation* **2004**, *110*, 3599–3603. [[CrossRef](#)]
42. Oesterreicher, J.; Pultar, M.; Schneider, J.; Muhleder, S.; Zipperle, J.; Grillari, J.; Holnthoner, W. Fluorescence-based nanoparticle tracking analysis and flow cytometry for characterization of endothelial extracellular vesicle release. *Int. J. Mol. Sci.* **2020**, *21*, 9278. [[CrossRef](#)] [[PubMed](#)]
43. Thane, K.E.; Davis, A.M.; Hoffman, A.M. Improved methods for fluorescent labeling and detection of single extracellular vesicles using nanoparticle tracking analysis. *Sci. Rep.* **2019**, *9*, 12295. [[CrossRef](#)] [[PubMed](#)]
44. Whiteside, T.L. The emerging role of plasma exosomes in diagnosis, prognosis and therapies of patients with cancer. *Contemp. Oncol.* **2018**, *22*, 38–40. [[CrossRef](#)] [[PubMed](#)]
45. Onodi, Z.; Pelyhe, C.; Terezia Nagy, C.; Brenner, G.B.; Almasi, L.; Kittel, A.; Mancek-Keber, M.; Ferdinandy, P.; Buzas, E.I.; Giricz, Z. Isolation of high-purity extracellular vesicles by the combination of iodixanol density gradient ultracentrifugation and bind-elute chromatography from blood plasma. *Front. Physiol.* **2018**, *9*, 1479. [[CrossRef](#)] [[PubMed](#)]

**Supplementary data:**

**Supplementary Table S1. Fluorescent label, antibodies, isotype controls, and secondary antibody used for NTA, flow cytometry, and Western blot analysis**

Antibody/dye	Source, Catalog number:	Antigen	Dilution	Application
CellMask™ Deep Red plasma membrane stain	Invitrogen™ Thermo Fisher Scientific, C10046	Membrane Stain	1:1250000	NTA
PE	Invitrogen™ Thermo Fisher Scientific, MA1-19650	CD63	1:5000	NTA
PE	Biolegend, 349506	CD81	1:40000	NTA
PE	Biolegend, 312106	CD9	1:6000	NTA
FITC	Beckman Coulter, IM1755U	CD9	1:20	Flow cytometry
PE	BD Pharmingen™, 556020	CD63	1:20	Flow cytometry
APC	Beckman Coulter, A87789	CD81	1:20	Flow cytometry
Mouse IgG1 κ Isotype Control -PE	eBioscience™, 12-4714-82	Isotype Control PE	1:10	Flow cytometry
Mouse IgG2b κ Isotype Control -APC	eBioscience™, 17-4732-81	Isotype Control APC	1:10	Flow cytometry
Mouse IgG2b κ Isotype Control-FITC	eBioscience™, 11-4732-81	Isotype Control FITC	1:10	Flow cytometry
Anti-ALIX	abcam, ab117600	ALIX	1:1000	WB
Anti-Calnexin	abcam, ab13504	Calnexin	1:2000	WB
Anti-CD9	Invitrogen™ Thermo Fisher Scientific, 10626D	CD9	1:500	WB
Anti-CD81	Invitrogen™ Thermo Fisher Scientific, 10630D	CD81	1:1000	WB
Anti-NY-ESO-1	Santa Cruz Biotechnology, Sc-53869	NY-ESO-1	1:200	WB
Anti-Synthenin	abcam, ab19903	Synthenin	1:1000	WB
Anti-Tsg-101	abcam, ab30871	TSG-101	1:1000	WB
Biotin Anti-Aliipoprotein B	Abcam, ab20898	Apo-B	1:1000	WB
HRP	Thermo Fisher Scientific, A16078	mouse antibodies	1:10000	WB
HRP	Thermo Fisher Scientific, A16110	rabbit antibodies	1:10000	WB
HRP	Santa Cruz Biotechnology, Sc-2020	donkey anti-goat antibodies	1:10000	WB

**Supplementary Table S2. Concentration of particles for 1 mL of plasma/BALF in scatter, membrane, and tetraspanin labeling**

Pt	Plasma EVs			cBALF EVs					oBALF EVs				
	Scatter [particles x10 <sup>-7</sup> /mL plasma]	CMDR [particles x10 <sup>-7</sup> /mL plasma]	CD9 [particles x10 <sup>-7</sup> /mL plasma]	Scatter [particles x10 <sup>-7</sup> /mL BALF]	CMDR [particles x10 <sup>-7</sup> /mL BALF]	CD63 [particles x10 <sup>-7</sup> /mL BALF]	CD81 [particles x10 <sup>-7</sup> /mL BALF]	CD9 [particles x10 <sup>-7</sup> /mL BALF]	Scatter [particles x10 <sup>-7</sup> /mL BALF]	CMDR [particles x10 <sup>-7</sup> /mL BALF]	CD63 [particles x10 <sup>-7</sup> /mL BALF]	CD81 [particles x10 <sup>-7</sup> /mL BALF]	CD9 [particles x10 <sup>-7</sup> /mL BALF]
1	6600.0	2333.3	2533.3	136.0	86.0	55.7	41.6	123.0	101.3	27.2	80.8	28.7	147.7
2	4733.3	1966.7		68.0	17.1	10.3		39.7	29.0	7.3	6.9		10.6
3	3466.7	2600.0		1.0	0.4	0.4	0.2	0.7	40.0	14.7	64.1	5.5	48.0
4	41866.7	6080.0		4.5	2.5	0.4		0.2	143.6	92.8	54.2	17.6	69.1
5	6666.7	1873.3		153.3	33.7	13.7		21.1	97.5	68.1	36.0	13.2	20.8
6	24000.0	6933.3		91.8	56.5	25.1	8.6	40.0	55.6	37.1	80.4	5.2	22.8
7	22533.3	7866.7		5.0	2.8	0.5		1.4	42.6	19.3	10.7		26.2
8	1033.3	56.0		34.7	15.1	7.7	3.3	12.6	56.7	29.3	8.5		74.7
9	4533.3	1493.3		106.7	62.1	45.7		127.8	12.5	5.0	2.0		7.3
10	9066.7	4466.7	3600.0	52.8	62.4	66.4		70.4	225.3	269.3	69.3		110.7
11	8000.0	3166.7		96.7	59.3	54.0	44.0	62.7	125.2	61.3	5.3	4.4	12.3
12	28666.7	2000.0		118.8	58.6	212.7		63.7	47.6	22.3	15.1		13.5
13	122000.0	24666.7							4.1	0.8	0.9		1.9
14	26796.0	9034.7		23.6	11.9	16.0	10.0	37.0	24.7	18.6	16.9	9.5	27.1
15	6066.7	3866.7		19.2	9.2	16.8	1.3	36.7	145.7	81.4	82.9	6.6	138.6
16	26400.0	7333.3		114.2	75.8	153.8	66.7	143.6	35.4	18.2	19.1		21.4
17	32266.7	9466.7		35.3	14.4	19.1		14.3	50.0	28.5	44.0		37.0
18	8133.3	2160.0		16.7	7.1	4.1		8.5	36.0	17.5	11.9		16.8
19	28533.3	2733.3							19.9	11.6	25.4		14.6
20	2113.3	333.3		147.0	39.5	125.0	10.2	163.0	34.7	9.5	19.0		20.1
21	4466.7	2533.3		33.0	4.7	10.0	1.1	21.4	26.0	7.3	10.9	1.2	26.7
22	1980.0	613.3		14.1	5.4	1.5		1.9	566.0	216.0	159.2	90.0	238.0
23	6800.0	546.7		122.0	25.1	56.0	8.6	115.0	11.3	3.5	2.5	0.6	17.1
24	34000.0	15066.7		15.0	7.0	3.4		8.2	15.0	9.0	4.3		7.7
25	10666.7	3333.3		31.1	22.6	9.1	4.2	16.7	76.0	54.9	20.7	2.9	58.1
26	16200.0	7466.7		35.7	12.7	8.5		9.6	233.3	96.0	156.5	23.0	255.4
27	2133.3	810.0		148.5	54.1	60.3	7.3	82.0	267.8	89.3	110.0	30.4	130.7
28	1960.0	600.0		34.0	32.0	3.8			15.9	9.8			
29	12533.3	5866.7		46.7	44.0			30.0	80.7	36.7			60.0
30	39600.0	13333.3		198.0	137.0	178.0		159.0	265.0	172.0	285.0		229.0
31	260000.0	30666.7		739.2	177.8	257.0	39.6	369.6	766.7	142.0	360.0	65.3	440.0
32	2573.9			39.1	17.2	12.9	3.8	20.4	12.9	7.4	2.9		3.2
33	8800.0	3800.0	540.0	111.2	50.0	12.2	5.1	20.5	413.3	122.0	82.0	16.0	174.7
34	15466.7	1566.7		37.9	27.1	5.6		9.3	84.3	49.5	16.0		21.7



**Supplementary Table S3. Size of particles for 1 mL of plasma/BALF in scatter, membrane, and tetraspanin labeling**

Pt.	Plasma EVs			cBALF EVs					oBALF EVs				
	Scatter [nm]	CMDR [nm]	CD9 [nm]	Scatter [nm]	CMDR [nm]	CD63 [nm]	CD81 [nm]	CD9 [nm]	Scatter [nm]	CMDR [nm]	CD63 [nm]	CD81 [nm]	CD9 [nm]
1	94.6	105.9	88.6	195.8	193.9	80.9	79.6	93.2	197.3	201.2	78.9	84.5	89.7
2	102.7	113.2		167.0	181.1	83.5		105.1	153.7	171.0	95.7		95.7
3	99.6	98.4		217.9	243.0	274.2	227.5	185.6	151.4	177.5	78.0	84.8	81.5
4	109.2	154.5		147.4	154.0	105.2		125.5	161.4	170.4	85.5	176.0	97.1
5	83.4	102.0		140.0	128.2	84.3		102.1	167.7	178.9	107.6	160.0	125.3
6	98.9	123.8		159.6	161.6	104.4	79.2	103.0	151.1	152.1	88.8	78.4	92.9
7	104.4	117.5		179.0	162.8	161.5		138.0	179.5	206.6	97.7		108.3
8	91.4	117.3		152.7	164.8	92.9	96.0	100.6	150.4	160.2	87.0		84.0
9	112.4	129.0		196.3	192.0	103.0		100.1	158.8	165.4	94.1		113.3
10	102.9	106.0	77.8	196.3	192.0	103.0		100.1	170.5	164.2	78.6		85.4
11	98.4	108.0		154.1	161.3	79.0	89.4	90.6	161.0	164.7	83.2	176.2	86.9
12	89.5	128.5		166.2	175.3	81.9		96.8	164.3	169.8	92.9		111.8
13	95.3	114.4							173.6	169.7	131.2		120.0
14	119.1	132.1		191.6	208.4	80.2	196.1	84.0	189.0	195.1	85.5	79.0	91.5
15	104.3	110.6		158.3	169.8	102.6	109.4	90.2	166.2	175.6	112.0	92.7	98.3
16	109.2	131.3		163.6	174.9	80.0	92.3	81.5	156.7	162.4	76.1		85.8
17	107.5	118.9		185.1	188.0	86.7		102.1	173.4	172.1	80.7		92.7
18	106.1	126.5		211.2	256.5	84.3		88.1	189.0	182.6	86.6		106.2
19	112.8	154.8							169.3	179.9	76.3		82.0
20	95.0	122.1		169.0	209.1	79.3	87.8	87.4	161.8	198.7	78.6		82.0
21	83.7	88.9		177.2	214.7	84.9	117.8	89.0	171.8	192.9	93.6	152.4	90.6
22	93.9	110.7		163.5	188.8	97.1		140.9	160.1	159.9	89.4	157.2	98.3
23	102.2	140.6		150.2	218.9	78.4	93.7	81.5	179.4	217.6	83.7	91.3	88.4
24	89.4	98.1		185.9	218.9	121.5		109.5	173.4	196.0	97.1		92.1
25	84.3	95.6		153.6	156.6	82.7	159.1	97.9	150.8	157.7	80.8	205.9	80.6
26	83.8	88.9		157.5	169.7	87.0		109.3	147.3	155.8	78.8	222.9	87.0
27	89.6	101.8		159.3	167.9	82.6	83.7	97.3	162.5	178.4	89.5	170.6	91.3
28	95.5	119.1		235.1	242.8	166.5			186.3	184.9			
29	107.3	117.0		129.8	97.8			82.4	181.7	173.4			79.4
30	107.6	128.3		189.2	184.8	91.2		122.0	184.2	191.5	90.0		103.3
31	113.7	158.5		168.0	170.8	84.2		98.8	148.1	149.0	89.8	93.4	89.4
32	84.5			139.1	151.6	78.0	79.8	80.9	144.3	147.9	82.7		107.8
33	85.4	93.9	103.5	172.4	181.3	105.8	145.8	126.5	153.4	166.2	94.7	107.6	102.2
34	89.1	115.3		170.6	182.0	96.9		120.6	174.9	187.8	103.7		127.9

**Supplementary Table S4. The concentration of particles – the fraction of all particles [%] in six size fractions (< 50nm, 50–100 nm, 100–150 nm, 150–200 nm, 200–250 nm, >250 nm) for plasma, BALF, and cell line EVs**

[nm]	plasma EVs			oBALF EVs					NSCLC Cell line EVs				
	Scatter [%]	CD9 [%]	CMDR [%]	Scatter [%]	CD63 [%]	CD9 [%]	CD81 [%]	CMDR [%]	Scatter [%]	CD63 [%]	CD9 [%]	CD81 [%]	CMDR [%]
< 50	1.44	19.59	2.52	0.42	8.42	7.67	13.96	0.56	0.62	12.88	16.69	9.75	1.09
50–100	42.54	52.17	37.18	7.11	43.28	37.21	39.52	5.83	15.18	44.02	46.96	39.90	19.77
100–150	38.44	26.00	39.74	24.04	24.94	27.18	23.26	20.84	39.07	20.55	23.75	30.25	36.18
150–200	11.97	1.12	13.10	25.37	12.21	15.12	9.30	24.40	25.80	11.73	7.70	12.04	23.14
200–250	3.47	0.00	4.42	18.54	5.78	6.48	4.65	18.35	11.04	6.95	3.00	3.62	10.76
> 250	2.14	1.12	3.03	24.53	5.37	6.34	9.30	30.02	8.28	3.85	1.90	4.43	9.06

---

**Supplementary Table S5. Concentration of protein for 1 mL of plasma/BALF**

Patient no.	The concentration of protein in plasma EVs [ug/mL of plasma]	The concentration of protein in cBALF EVs [ug/mL of BALF]	The concentration of protein in oBALF EVs [ug/mL of BALF]
1	31.99	1.47	2.21
2	121.86	0.42	0.08
3	149.72	0.16	1.03
4	16.71	0.04	1.37
5	248.20	1.03	0.52
6	130.64	0.44	0.23
7	306.93	0.14	0.42
8	116.34	0.23	0.34
9	51.35	0.96	0.08
10	109.58	2.77	4.01
11	236.44	0.95	1.82
12	172.83	1.41	0.21
13	177.31		
14	211.36	0.13	0.23
15	67.22	0.07	0.50
16	112.19	1.79	
17	146.98	0.42	0.45
18	8.56	0.63	0.42
19	193.37	0.33	0.33
20	80.91	3.08	0.72
21	185.18	0.53	0.27
22	74.51	0.10	2.32
23	20.41	3.05	0.22
24	70.36	0.12	0.16
25	85.66	0.14	0.35
26	155.36	0.21	2.26
27	101.06	0.93	1.67
28	70.73		
29	84.90	0.84	2.41
30	139.12		
31	545.66	5.46	3.24
32	248.62	0.20	0.00
33	250.16	0.24	1.58
34	292.43	0.05	0.11

### Supplementary figure S1. EVs isolation from plasma - particle/protein ratio

Isolation of EVs from plasma was performed as described in Materials & Methods using 3 homemade columns (prepared 1 day before) and one new commercial Izon qEV/70 nm column. Fractions 1–8 (1 mL each) from the SEC columns were collected and measured for particle content by the NTA method and for protein content by the BCA method (Pierce). Most enriched in particles were fractions 4, 5 and 6 (mean concentration  $\pm$  SD was: F4:  $5.40 \times 10^{10} \pm 5.13 \times 10^9$ ; F5:  $1.70 \times 10^{11} \pm 6.17 \times 10^{10}$ ; F6:  $7.55 \times 10^{10} \pm 1.79 \times 10^{10}$  particles/mL) (**Fig. S 1a**). The protein concentration was below the detection limit of our BCA method in the first 4 fractions, was low in fractions 5-6, and increased rapidly in fractions 7-8 (**Fig. S 1b**). The particle/protein ratio was most beneficial (highest) in fractions 5 and 6 (ratio  $\pm$  SD was: F5:  $8.40 \times 10^9 \pm 1.53 \times 10^9$ ; F6:  $8.42 \times 10^8 \pm 1.01 \times 10^8$  particles/mL) (**Fig. S 1c**).

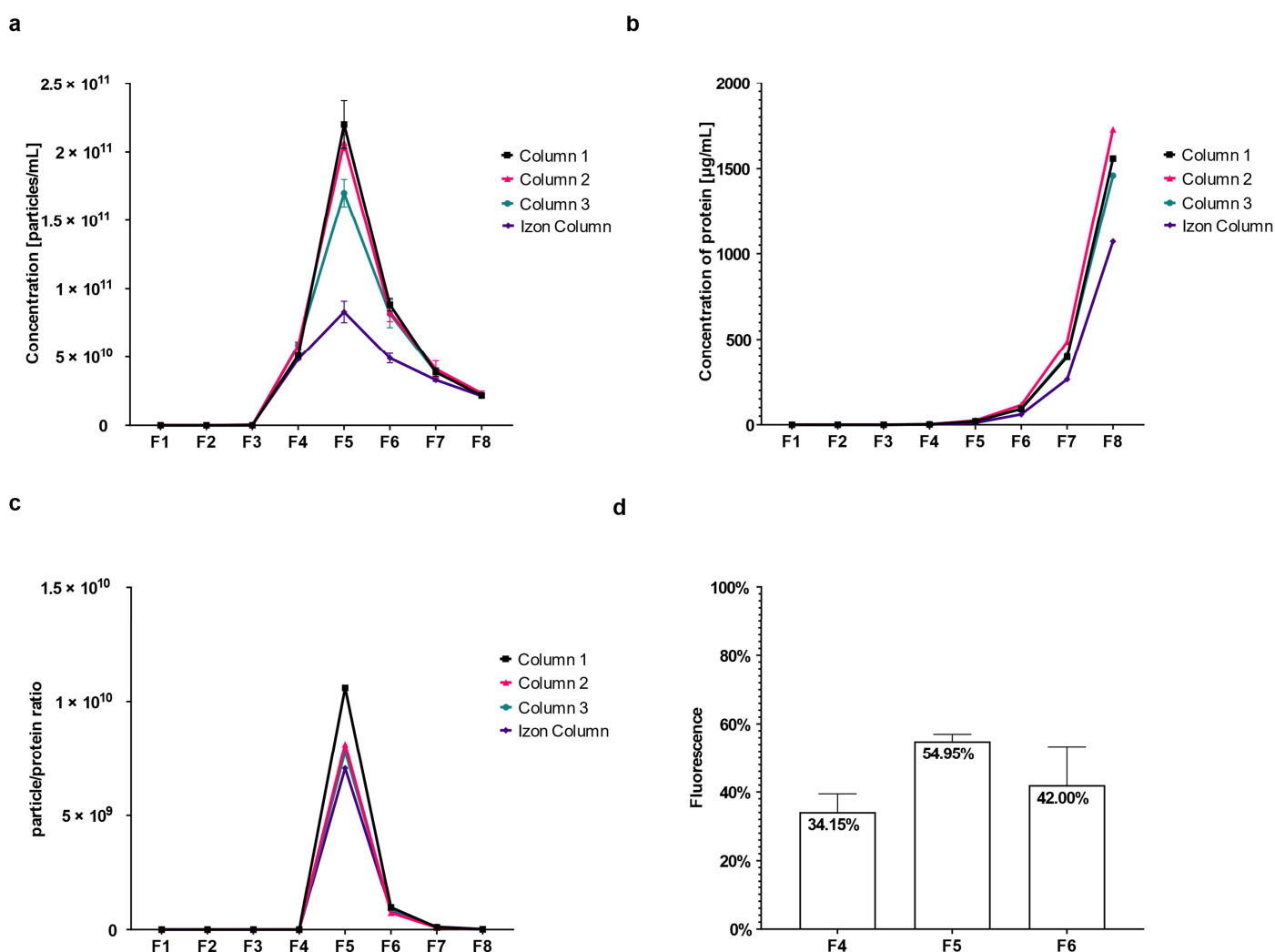
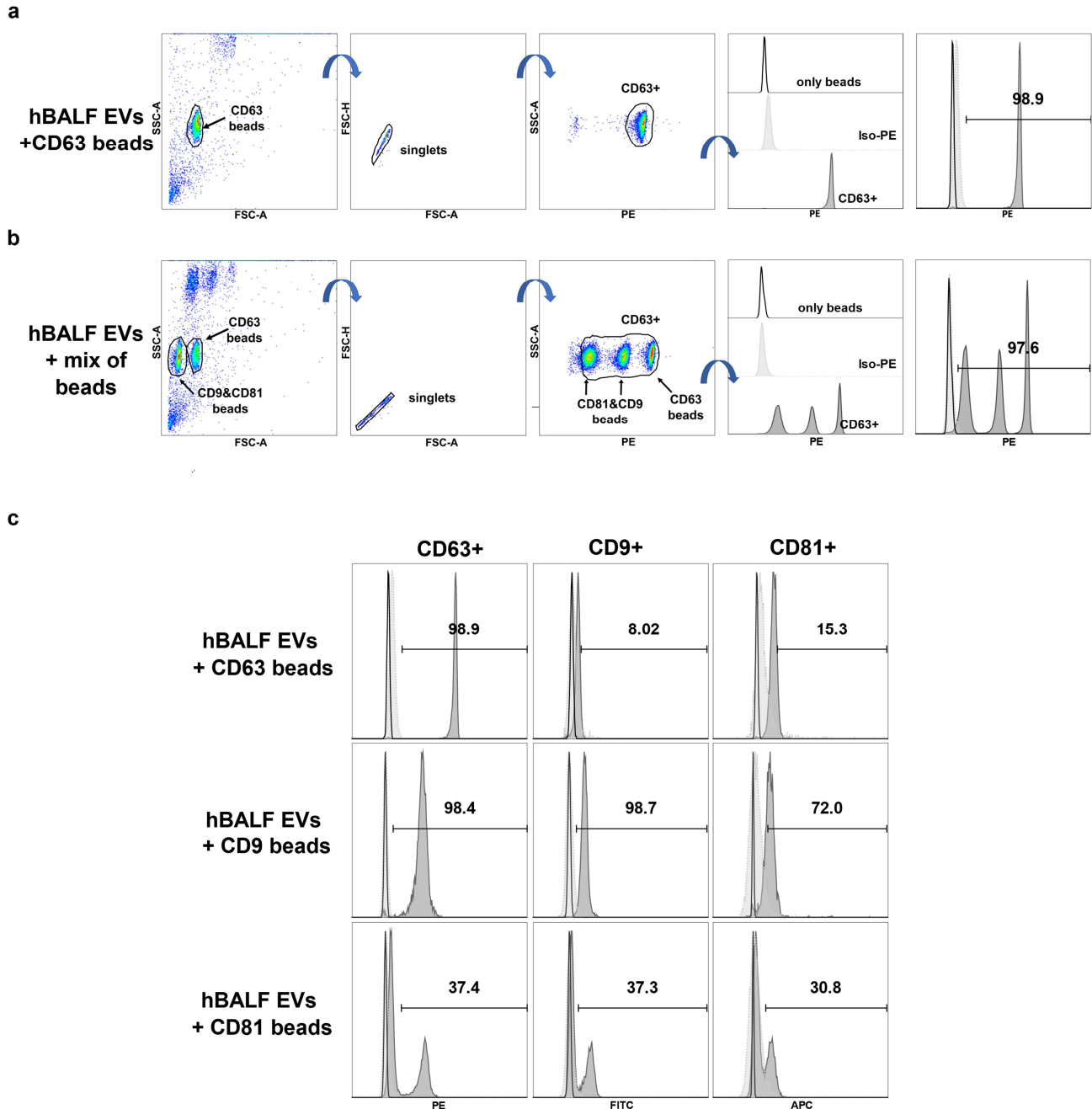


**Fig. S1. EVs separation from plasma on SEC - particle/protein ratio.** (a) The concentration of particles in fractions 1-8 from 3 home-made SEC columns and one commercial Izon column after separation of EVs from plasma. (b) The concentration of protein measured in 1-8 fraction for each column. (c) Particle/protein ratio in each fraction. (d) CMDR positive particles' fluorescence from all visible in the scatter of plasma EVs in fractions 4,5 and 6 from SEC. The experiment from figures (a-c) was conducted on two biological samples with three replicate measurements each. Graph d presents Mean and SD from two replicates. The experiment from graph (d) was created from measurements taken at Sensitivity 93.

Those results led us to further investigations on fractions 4, 5, and 6. We have performed membrane labeling of fractions 4, 5 and 6. The results showed that in F4 there was 34.15%, in F5 54.95%, and in F6 42.00% CMDR positive particles of all visible particles in scatter (**Fig. S1d**). All three fractions were enriched in EVs, but higher concentration of particles, the measurable concentration of protein, and higher percent of CMDR positive

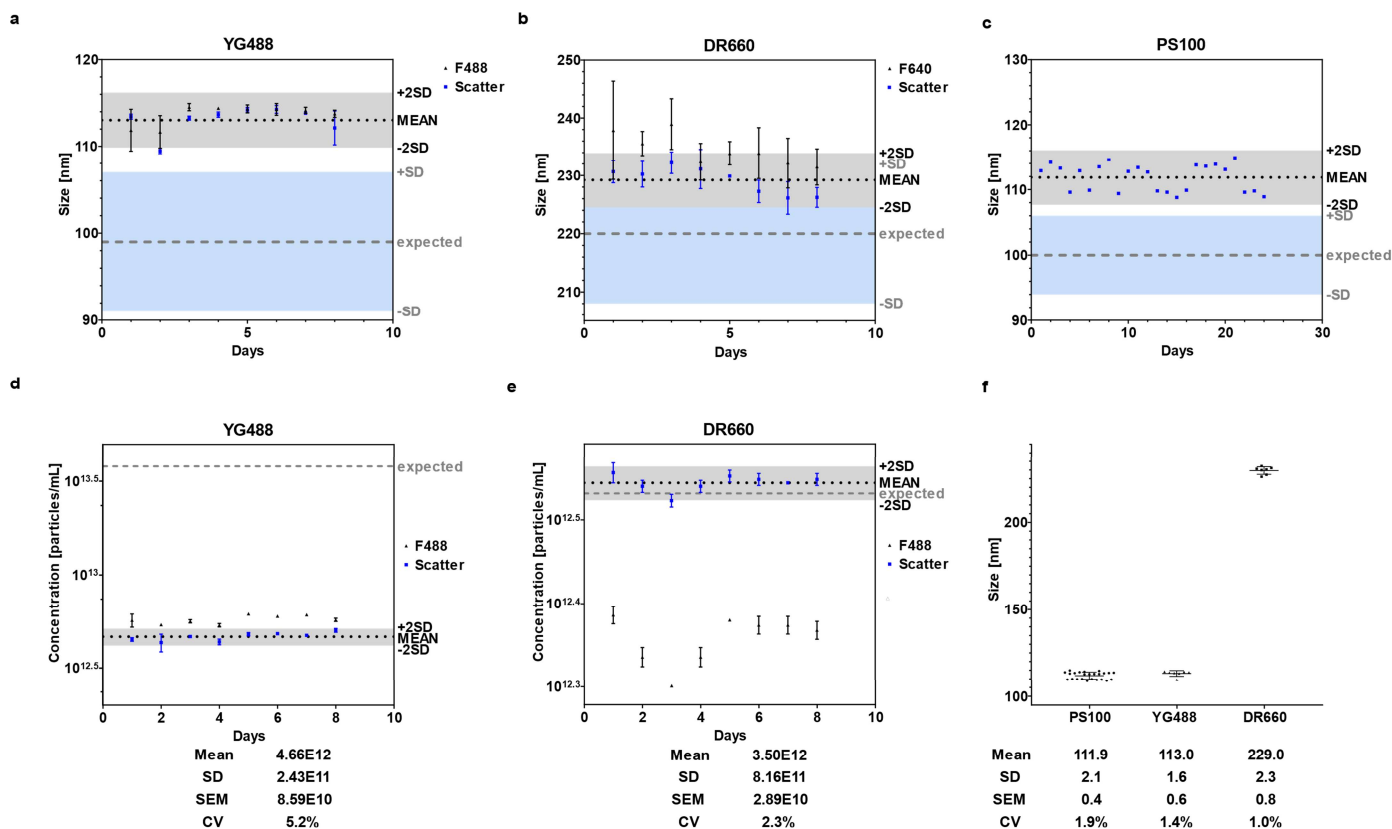
particles led us to choose fractions 5 and 6, which we pulled for further analysis of the NSCLC patient's plasma-EV samples.

**Supplementary figure S2. Flow cytometry of BALF-EVs after coupling to CD63-, CD9- and CD81-specific magnetic beads**



**Fig. S2. Flow cytometry analysis of oBALF-EVs bound to magnetic Dynabeads coated with antibodies against tetraspanins.** Figures (a & b) present examples of gating strategy and overlay creation. Gates were set first on single beads visible in the forward and side scatter, then on singlets. The gate for tetraspanin-positive events was set based on isotype control labeling so that a maximum of 5% of the isotype control was included in the gate. Samples with beads only, isotype labeled sample, and tetraspanin labeled sample were overlaid. (a) CD63 beads. (b) A mix of CD63, CD9, and CD81 beads. (c) One type of beads (CD63, CD9, or CD81) bound to oBALF-EVs and labeled with CD63-PE, CD9-FITC, and CD81-APC. The highest percentage and MFI for a given tetraspanin were usually achieved with beads specific for this given tetraspanin. An exemption were CD81-beads, where only up to 40% of beads captured any vesicles. EVs captured by CD9 beads showed the highest percent for all three markers (98.4% CD63, 98.7% CD9, and 72% CD81 positive particles). In the case of the CD63 beads, the highest percent had CD63 positive particles (98.9%), whereas there were only 8.02% CD9 and 15.3% CD81 positive particles. CD81 beads showed 37.4% of CD63, 37.3% CD9 and 30.8% CD81 positive particles.

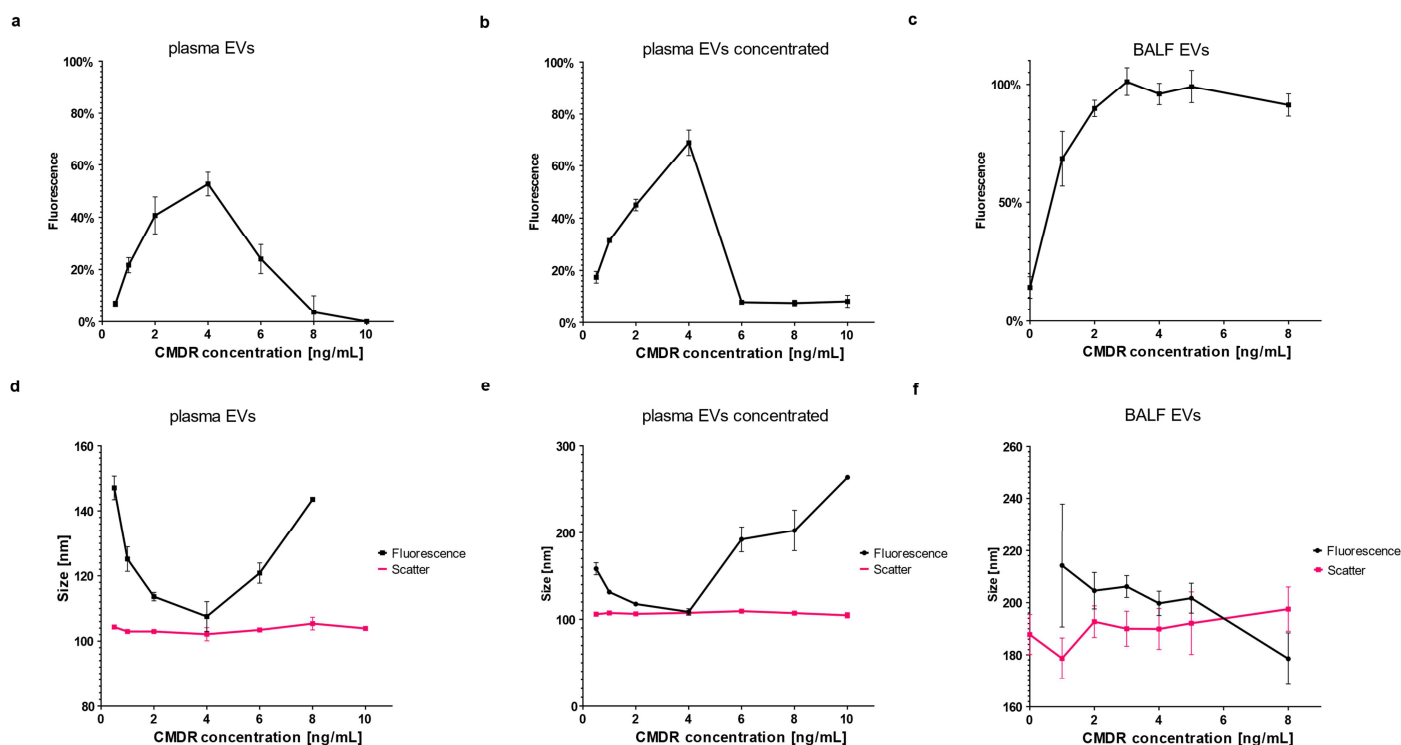
### Supplementary figure S3. Analytical variability of the NTA measurements



**Fig. S3. Variability of the measured size and concentration of standard beads on NTA.** (a) The size of YG488 particles in F488 (black) and scatter (blue) mode. (b) The size of DR660 particles in (black) and scatter (blue). (c) The size of PS100 particles in scatter mode - single data from calibration beads from 24 days. (d) The concentration of YG488 particles in (black) and scatter (blue). (e) The concentration of DR660 particles in F660 (black) and scatter (blue). (f) The mode size of PS100, YG488, and DR660 in the scatter mode with calculated Mean, SD, SEM, and CV. Graphs (a, b, d, e) were prepared from 3 replicate measurements performed for 8 days. Graphs (a, b, d, e) present the mean and SD of each replicate. MEAN  $\pm$  2 SD area is colored grey. MEAN value is marked with the black dotted line. The expected value from the beads certificate is marked with the grey dotted line (expected) with  $\pm$  SD area colored blue. All graphs were created from measurements in settings described in Materials & Methods dedicated to each type of beads.

### Supplementary figure S4. Optimization of dye concentration for measurements

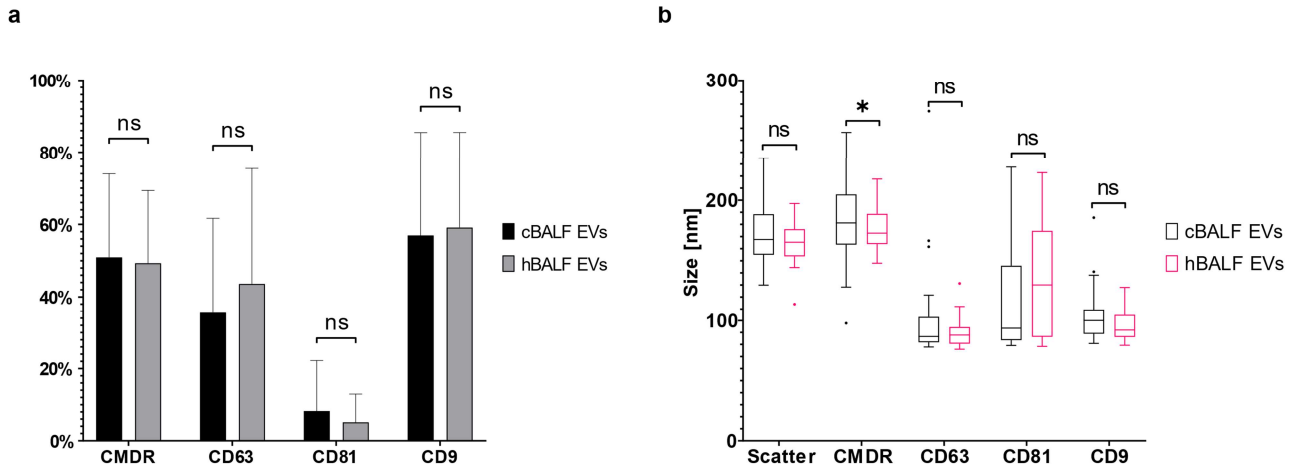
Staining mixtures were prepared by adding different amounts of CMDR (final concentration for NTA measurement 0.5/1/2/4/6/8/10 [ng/mL]) to a constant appropriate amount of EVs sample (optimal for NTA measurement after final dilution). Mixtures were filled with PBS to a total volume of 10  $\mu$ l. Samples were incubated for 2 h at RT in the dark. Then, the samples were diluted in PBS and measured on NTA. The optimization experiment was conducted on nonconcentrated (pulled fraction 5 and 6) and concentrated plasma-EVs (pulled fraction 4-6) from Healthy Normal Control and on BALF-EVs from NSCLC patient (**Fig. S4**).



**Fig. S4. Optimization of CMDR concentration.** (a-c) CMDR positive particles' fluorescence from all visible in scatter for fresh, pulled fraction 5 and 6 of plasma EVs (a), concentrated, thawed, pulled fractions 4-6 of plasma EVs (b), and BALF EVs (c). (d-f) The mode size of particles in scatter and fluorescence for fresh, pulled fraction 5 and 6 of plasma EVs (d), concentrated, thawed, pulled fractions 4-6 of plasma EVs (e), and BALF EVs (f). Experiments were conducted on 3-6 replicate measurements. Graphs (a-f) present Mean and SD. Graphs (a) and (d) were created from measurements in settings described in Materials & Methods. Graphs (b, c, e, f) were created from measurements taken at Sensitivity 93.

The results showed that in plasma-EVs (both concentrated and nonconcentrated), the fluorescence reaches the highest percent for 4 ng/mL of final CMDR concentration on NTA (nonconcentrated:  $52.67 \pm 4.51\%$ , concentrated:  $68.9 \pm 4.90\%$ ), and then drops when more CMDR is present (**Fig. S4a, b**). For plasma-EVs the difference between particles' size in fluorescent and scatter mode was the smallest at 4 ng/mL CMDR ( $\Delta$  mean size: nonconcentrated: 5.42 nm, concentrated: 1.1 nm) (**Fig. S4d, e**). In the case of BALF-EVs, the concentration of particles in fluorescent mode reached a plateau at concentration 3 ng/mL CMDR (**Fig. S4c**). The difference between particles' size in fluorescent and scatter mode was the smallest at 2-5 ng/mL CMDR (**Fig. S4f**). The concentration 4 ng/mL CMDR was chosen as optimal for further staining experiments.

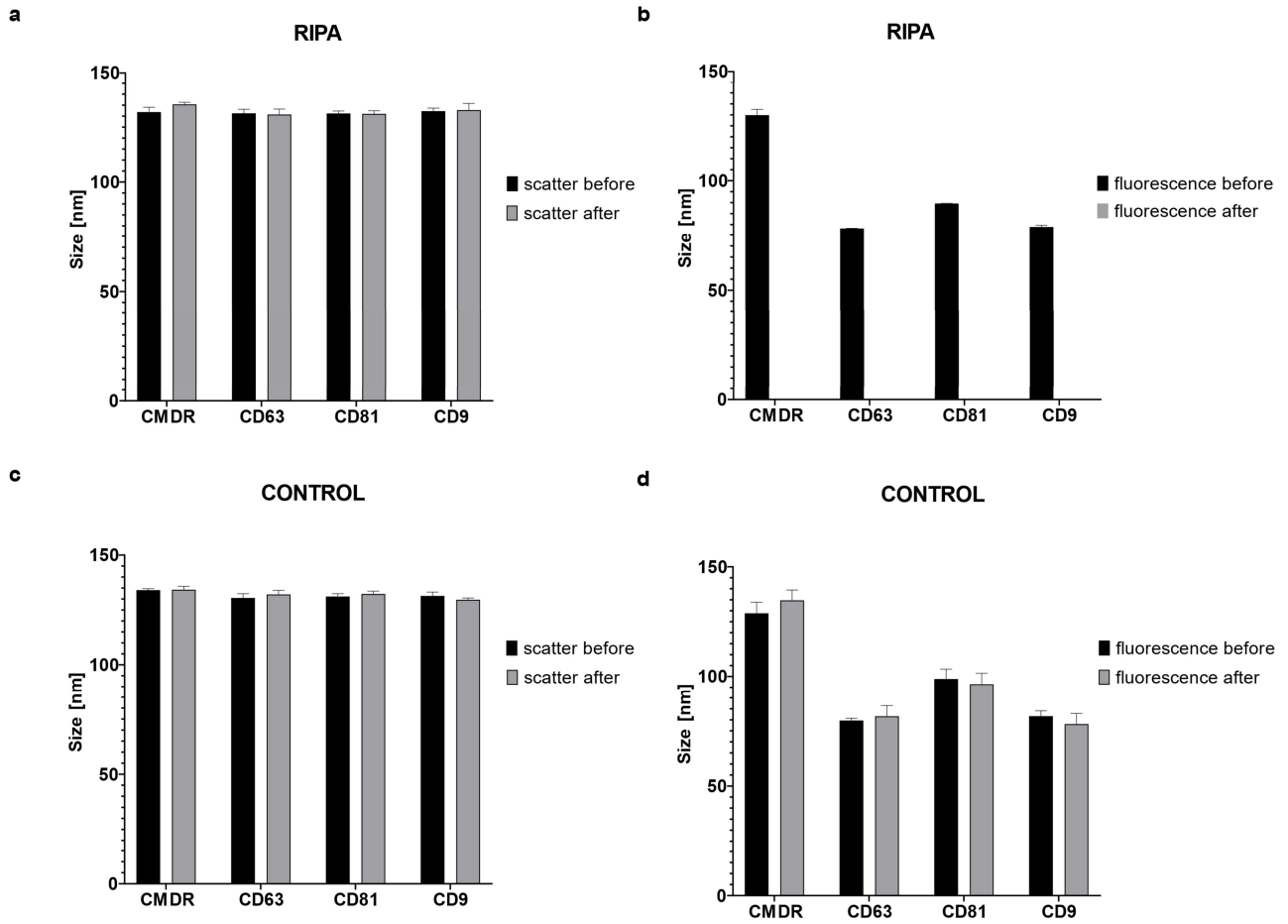
Supplementary figure S5. Antibody labeling of cBALF and oBALF EVs



**Fig. S5. Antibody labeling of cBALF and oBALF EVs.** (a) The percent of fluorescent particles in comparison to all particles visible in scatter mode for cBALF and oBALF EVs for all patients. (b) Measured mode sizes of particles in scatter and in fluorescent mode (488, 640 nm) for cBALF and oBALF EVs for all patients. Graph (a) present Mean and SD for all patients. Graph (b) presents the Tukey plot for all patients. \* refers to p value  $\leq 0.05$ , ns refers to p value  $> 0.05$  from Wilcoxon test-paired comparison.

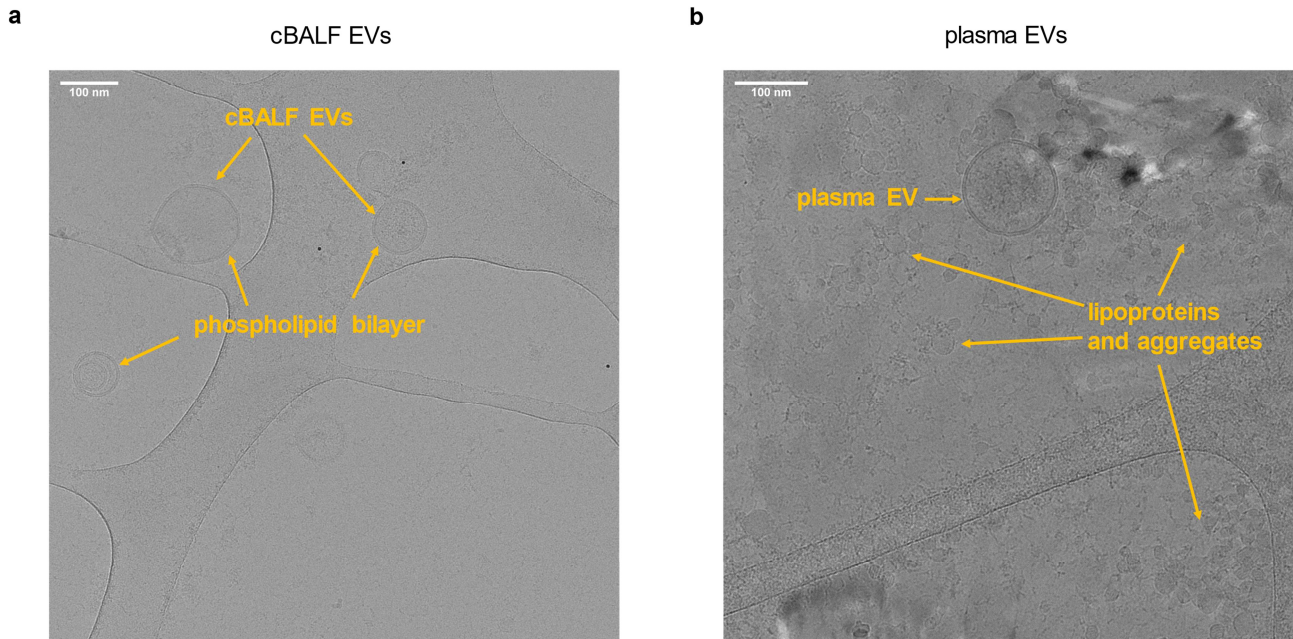


Supplementary figure S6. RIPA lysis of NSCLC Cell line EVs - size



**Fig. S6. RIPA lysis of EVs.** (a-b) Particles' mode size after labeling with CMDR and tetraspanin markers of NSCLC Cell line EVs before and after incubation with RIPA lysis buffer measured in the scatter mode (a) and fluorescent mode (b). (c-d) Particles' mode size after labeling with CMDR and tetraspanin markers of NSCLC Cell line EVs before and after incubation with PBS (Control) measured in the scatter mode (c) and fluorescent mode (d). Graphs a-d present Mean and SD from three replicates.

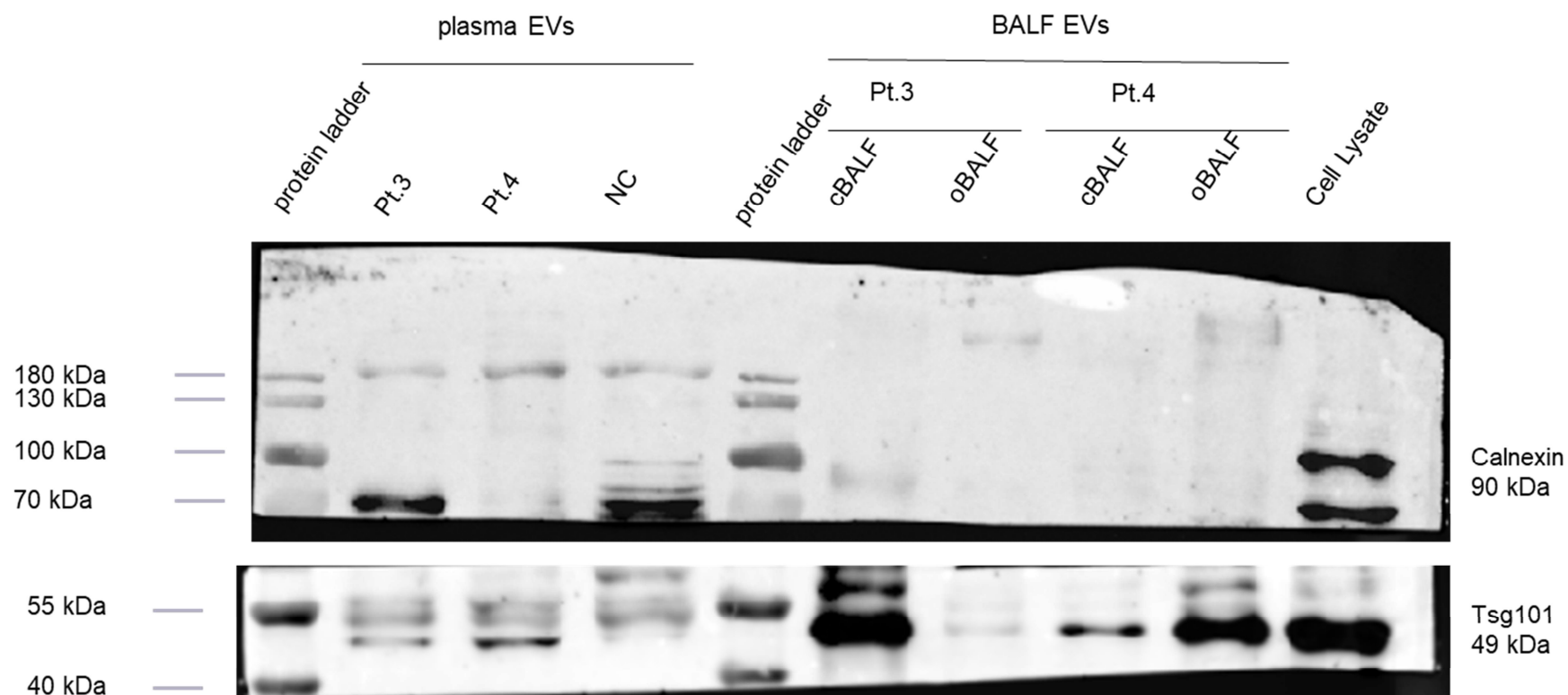
Supplementary figure S7. Cryo-TEM images of thawed cBALF EVs

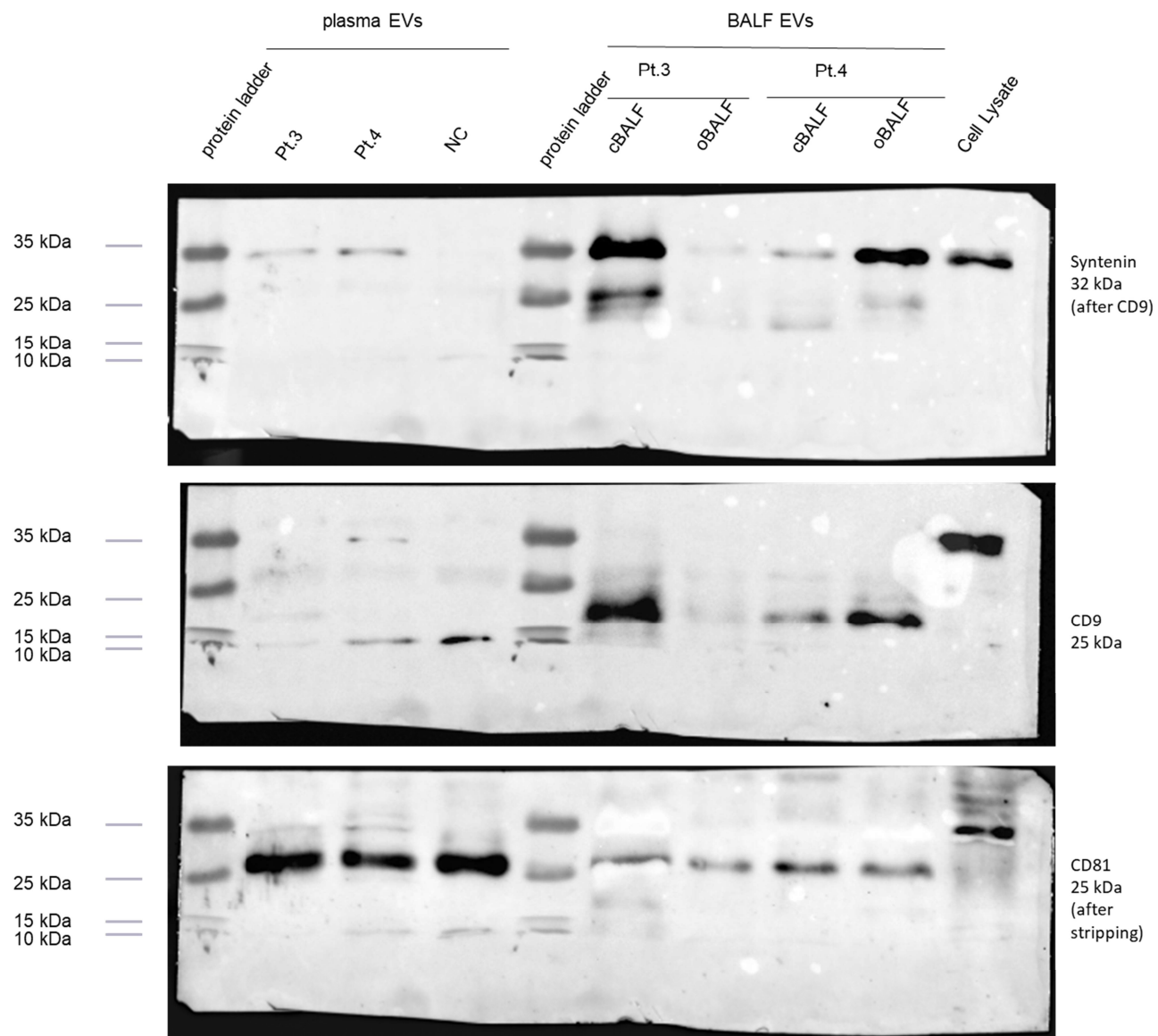


**Fig. S7. Cryo-TEM images of thawed cBALF EVs.** (a) Thawed cBALF EVs. There is a visible double phospholipid bilayer. (b) Plasma EVs. Besides EVs, particles with different morphology, like lipoproteins and aggregates, are visible.

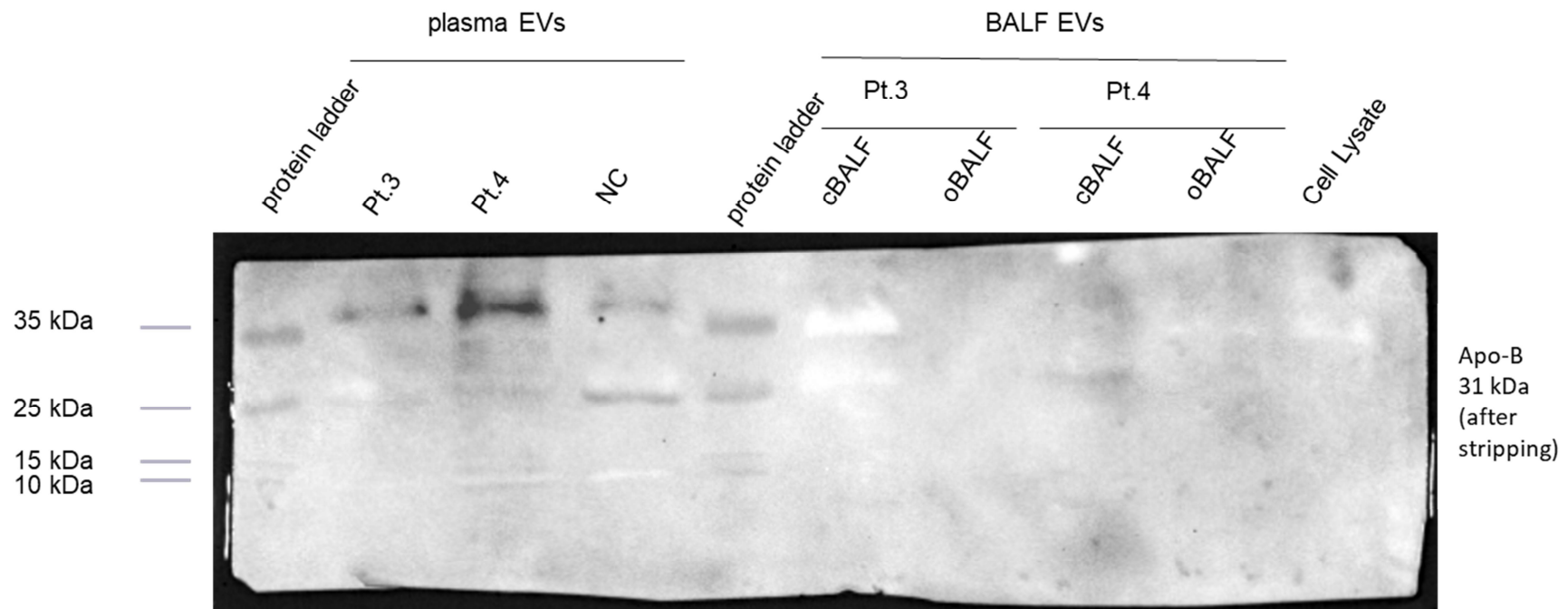
**Full blots from Fig.2 (a)**

Merged (chemiluminescence and colorimetric) blots with described protein ladder: Characterization of plasma/BAL EVs from NSCLC patients. Immunoblot analysis of EVs from Plasma and BALF of two NSCLC patients (Pt.3, Pt.4), a normal donor (NC) and a cell lysate (SEMK2). Each lane with plasma EVs represents the amount of protein present in 100  $\mu$ l of patients' plasma which was taken for the isolation. Each lane with BAL EVs represents the amount of protein present in 4 ml of Patients' BALF (from healthy or cancer lung) which was taken for the isolation. Cell lysate lane was loaded with 10  $\mu$ g of protein from cell lysate.





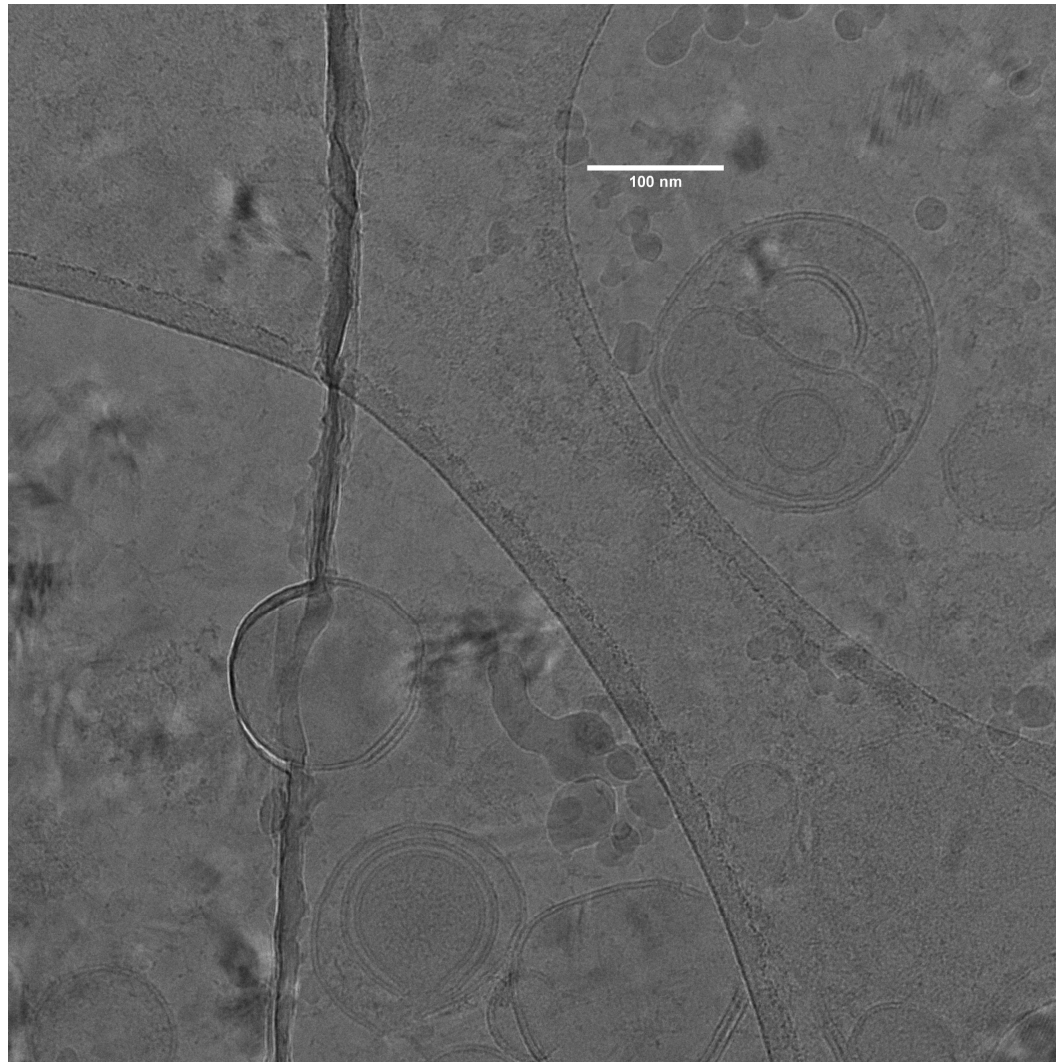
Supplementary figure S8. Lipoprotein marker Apo-B



---

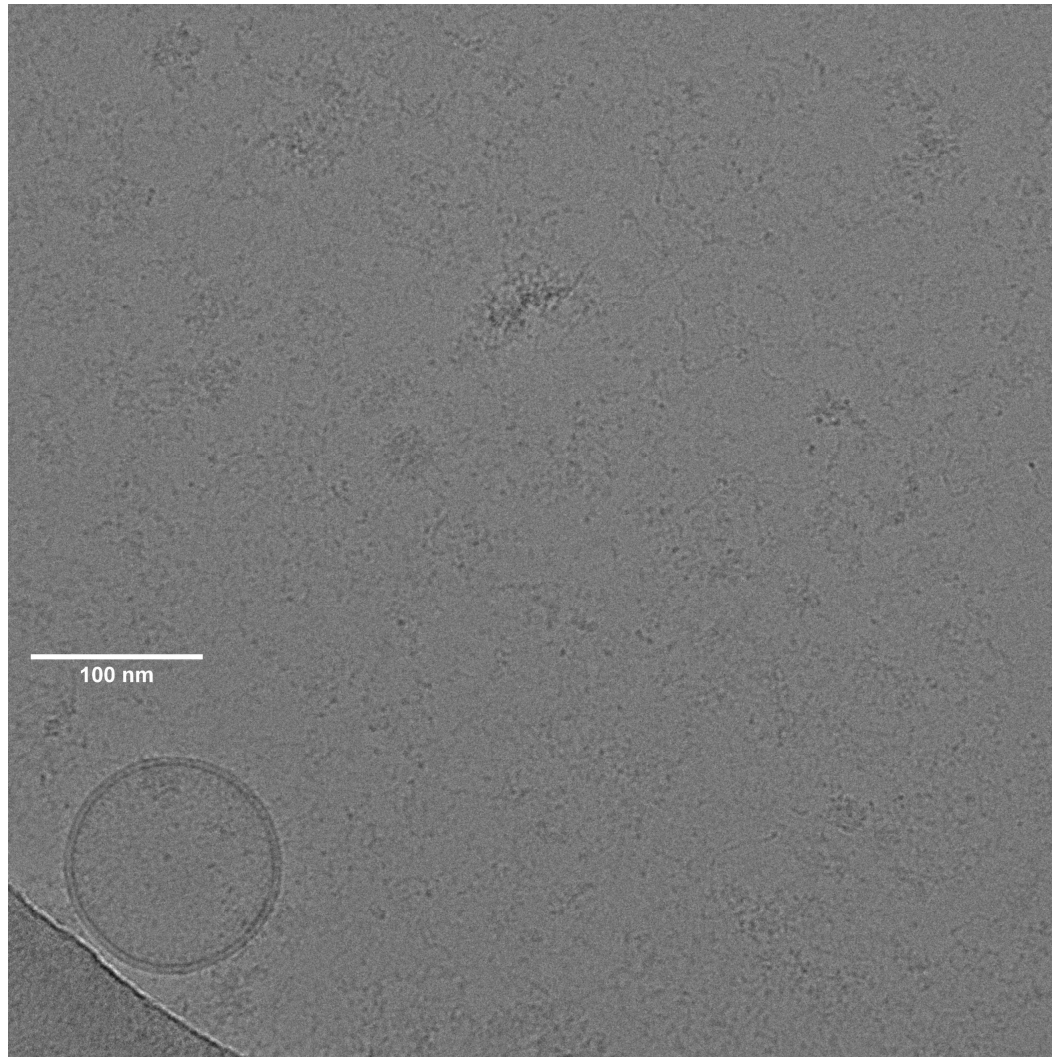
Raw pictures from Cryo-TEM from Fig. 2 (b)

cBALF  
EVs



---

oBALF  
EVs





---

plasma  
EVs





2. Długolecka M, Czystowska-Kuźmich M. Factors to consider before choosing EV labeling method for fluorescence-based techniques. *Front. Bioeng. Biotechnol. Sec. Nanobiotechnology*. Volume 12 – 2024.



## OPEN ACCESS

## EDITED BY

Wojciech Chrzanowski,  
The University of Sydney, Australia

## REVIEWED BY

Venkatesh Srinivasan,  
University of Maryland, Baltimore County,  
United States

Xiao Cheng,  
North Carolina State University, United States

## \*CORRESPONDENCE

Malgorzata Czystowska-Kuzmicz,  
✉ mczystowska@wum.edu.pl

RECEIVED 12 August 2024

ACCEPTED 05 September 2024

PUBLISHED 18 September 2024

## CITATION

Dlugolecka M and Czystowska-Kuzmicz M  
(2024) Factors to consider before choosing EV  
labeling method for fluorescence-  
based techniques.

*Front. Bioeng. Biotechnol.* 12:1479516.  
doi: 10.3389/fbioe.2024.1479516

## COPYRIGHT

© 2024 Dlugolecka and Czystowska-Kuzmicz.  
This is an open-access article distributed under  
the terms of the [Creative Commons Attribution  
License \(CC BY\)](https://creativecommons.org/licenses/by/4.0/). The use, distribution or  
reproduction in other forums is permitted,  
provided the original author(s) and the  
copyright owner(s) are credited and that the  
original publication in this journal is cited, in  
accordance with accepted academic practice.  
No use, distribution or reproduction is  
permitted which does not comply with these  
terms.

# Factors to consider before choosing EV labeling method for fluorescence-based techniques

Magdalena Dlugolecka and  
Malgorzata Czystowska-Kuzmicz \*

Chair and Department of Biochemistry, Medical University of Warsaw, Warsaw, Poland

A well-designed fluorescence-based analysis of extracellular vesicles (EV) can provide insights into the size, morphology, and biological function of EVs, which can be used in medical applications. Fluorescent nanoparticle tracking analysis with appropriate controls can provide reliable data for size and concentration measurements, while nanoscale flow cytometry is the most appropriate tool for characterizing molecular cargoes. Label selection is a crucial element in all fluorescence methods. The most comprehensive data can be obtained if several labeling approaches for a given marker are used, as they would provide complementary information about EV populations and interactions with the cells. In all EV-related experiments, the influence of lipoproteins and protein corona on the results should be considered. By reviewing and considering all the factors affecting EV labeling methods used in fluorescence-based techniques, we can assert that the data will provide as accurate as possible information about true EV biology and offer precise, clinically applicable information for future EV-based diagnostic or therapeutic applications.

## KEYWORDS

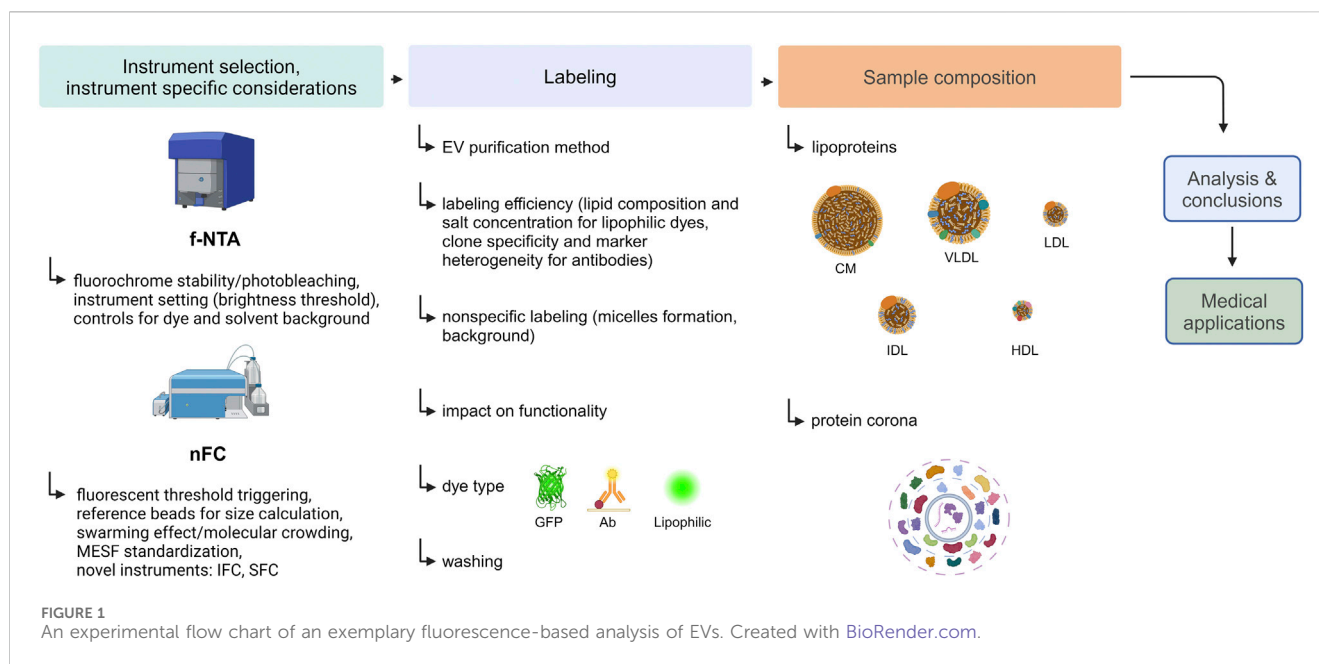
extracellular vesicles, f-NTA, nanoscale flow cytometry, fluorescent staining, corona, lipophilic dyes, lipoproteins

## 1 Introduction

Small extracellular vesicles (EVs) are sized 30–150 nm and play a significant role in cell-to-cell communication because they are secreted by all eukaryotic cells and carry a specific cargo of lipids, nucleic acids, and proteins derived from the origin cell (Colombo et al., 2014). They are present in all body fluids and can be easily obtained by minimally invasive methods. Because EVs contain molecular cargo similar to that of the parent cells, they seem to be a promising source of biomarkers as so called “liquid biopsy” (Imanbekova et al., 2022).

Direct measurement of sEVs using conventional flow cytometry is impossible because their size is below the limit of detection of the instruments (Arraud et al., 2016; Botha et al., 2021; van der Pol et al., 2022). Moreover, their small size also has some implications in the way we can label EVs and how labeling impacts the measurement. Often, there is no possibility of washing the unbound dye/antibody; we can only dilute it, but it is still present and may interfere with results.

To address these challenges, several highly sensitive instruments capable of directly measuring fluorescently labeled small EVs have been developed. Methods on which the performance of these instruments is based, with the focus on fluorescence-based Nanoparticle Tracking Analysis (f-NTA) and Nanoscale Flow Cytometry (nFC), are



presented in this review. Subsequently, important fluorescent labeling parameters influencing EV measurement, such as labeling efficiency, specificity, and impact on EV functionality, are discussed. Next, factors that may interfere with EV analysis, such as lipoproteins and the protein corona (PC) will be considered. Finally, mistakes commonly made during the planning and conducting of fluorescent labeling experiments of EVs, as well as typical pitfalls and misinterpretations of results, are discussed. A flowchart presenting the steps of an exemplary fluorescence-based analysis of EVs and listing the interfering factors that should be considered is shown in Figure 1.

## 2 Fluorescent methods

The most frequently used methods capable of directly measuring fluorescently labeled particles smaller than 300 nm are f-NTA and nFC, which are discussed in more detail in this chapter. Additionally, other methods that can be applied to a limited extent for EV characterization have recently been developed, such as those based on direct stochastic optical reconstruction (dSTORM), or a single-particle interferometric reflectance imaging sensor (SP-IRIS) coupled with fluorescence microscopy.

In brief, the dSTORM method allows for single-molecule localization super-resolution microscopy (with an optical resolution of ~20 nm) using regular, photostable, and bright organic fluorophores (Endesfelder and Heilemann, 2015; Chambers et al., 2021; Zhang et al., 2023). Notably, Bağcı et al. described a novel approach for characterizing EVs using the dSTORM method, in which particles are immobilized on a microscope slide prior to antibody staining of specific EV proteins. They used the reflectance mode of a confocal microscope to locate the EVs plane precisely. They then identified EVs labeled with specific proteins in the fluorescence mode of confocal microscopy. This approach allowed them to

distinguish labeled proteins on EVs from free proteins. The disadvantage of this method is that it requires fixation and immobilization of EVs, which affects their functionality. In addition, the true size of EVs cannot be measured and is not suitable for identifying single EVs because of the diffraction limit of confocal microscope (Bağcı et al., 2022). In turn, SP-IRIS coupled with fluorescence microscopy allows multiplexed characterization and digital counting of EVs caught on a solid chip in the form of a microarray (Avci et al., 2015; Daaboul et al., 2016; Mizenko et al., 2021; Breitwieser et al., 2022).

Examples of the most common instruments with a short description of their advantages and disadvantages, along with representative references, are presented in Table 1.

### 2.1 Fluorescent NTA

It is well established that NTA in the scatter mode is a very sensitive method for measuring the concentration and size of particles in the nanometric size range. This method uses Brownian motion (random movement) of particles in a solution for measurement. Brownian motion is strictly related to the hydrodynamic size of particles. Because smaller particles move faster than larger ones, NTA software can calculate the hydrodynamic diameter using the Stokes-Einstein equation (Malloy and Carr, 2006).

In addition, by counting the particles in a known volume of the sample within the flow cell, the software calculates the concentration of the particles. Moreover, during NTA measurements, light is scattered by the nanoparticles, which enables their visualization using a microscope. The scattering effect depends on the refractive index of the nanoparticles and the solution in which they are dissolved. The differences in the refractive indices of the different particles enabled the differentiation of these nanoparticles in NTA. However, the value of the refractive indices significantly affects the

TABLE 1 Instruments capable of direct measurement of nanosized particles with fluorescence detection.

Name of the instrument	type	company	size range of particles	cost <sup>a</sup>	throughput <sup>a</sup>	advantages	disadvantages	References
ZetaView	NTA	Particle Metrics	10 nm–2000 nm	low	high	high resolution, real-time analysis; short time is needed for sample preparation and measurements (<1 h); EVs can be analyzed in their native form in solution	limited sensitivity to smaller particles (<50 nm), biases the detection of larger particles, less precise in heterogenous samples containing differently sized vesicles, sample has to meet the detection concentration range, possibility of co-localization studies still under development	<a href="#">Desgeorges et al. (2020)</a> , <a href="#">George et al. (2021)</a> , <a href="#">Bagci et al. (2022)</a>
Nanosight (NS300, LM10, LM20, LM14)	NTA	Malvern Panalytical	10 nm–2000 nm	low	medium	EVs can be analyzed in their native form in solution, high sensitivity	requires trained personnel, careful sample preparation, limited concentration range for measurements, technical issues related to measurements of sample in flow, difficulties in determining the size of particles in heterogenous samples	<a href="#">Dragovic et al. (2011)</a> , <a href="#">Koksal et al. (2023)</a>
Nanoimager	dSTORM	ONI	10 nm–2000 nm	medium	low	high spatial resolution, single molecule sensitivity, co-localization studies possible, intra-vesicular staining possible	limited to relatively small sample volumes, EV concentration of sample has to be known, low through-put	<a href="#">Roseborough et al. (2023)</a> , <a href="#">Zhang et al. (2023)</a>
ExoView	SP-IRIS coupled with fluorescence microscopy	NanoView Biosciences	from 20 nm	low	medium	quick, automated platform, enables biomarker colocalization, low sample volume, no need for sample purification	limited to specific particle types – only detected by tetraspanin antibodies	<a href="#">Bachurski et al. (2019)</a> , <a href="#">Breitwieser et al. (2022)</a> , <a href="#">Bhagwan Valjee et al. (2024)</a>
Cytoflex	nFC	Beckman Coulter	not specified	medium	high	high sensitivity, multi-color analysis, flexibility	variable performance depending on sample quality, high background interference, limited sensitivity to dim particles, swarming effect	<a href="#">George et al. (2021)</a> , <a href="#">Mizenko et al. (2021)</a> , <a href="#">Salmond et al. (2021)</a>
Aurora/Northern Lights	nFC	Cytex Biosciences	not specified	medium	high	high resolution, high throughput, unmixing, removal of autofluorescence	high background interference, limited sensitivity to dim particles, swarming effect	<a href="#">Welsh et al. (2021)</a> , <a href="#">Voss et al. (2022)</a> , <a href="#">Aibaidula et al. (2023)</a>
ImageStream	nFC	Luminex Corporation	not specified	high	high	imaging flow cytometry, multiparametric analysis direct EV measurement in biological fluids	complex data analysis using dedicated idea software, need for high quality computer equipment for data storage and analysis, complex optimisation for every single dye or Ab	<a href="#">Corso et al. (2019)</a> , <a href="#">Tertel et al. (2020)</a> , <a href="#">Botha et al. (2021)</a> , <a href="#">Tertel et al. (2022)</a> , <a href="#">Wu et al. (2023)</a>

(Continued on following page)

TABLE 1 (Continued) Instruments capable of direct measurement of nanosized particles with fluorescence detection.

Name of the instrument	type	company	size range of particles	cost <sup>a</sup>	throughput <sup>a</sup>	advantages	disadvantages	References
CellStream	nFC	Merck Millipore	not specified	low	high	high sensitivity multiparametric analysis direct EV measurement in biological fluids	limited options for advanced applications, unintuitive software, need for high quality computer equipment for data storage and analysis, complex optimisation for every single dye or Ab	Zheng et al. (2023), von Lersner et al. (2024)
nanoFCM	nFC	NanoFCM Inc	not specified	low	medium	high sensitivity, rapid analysis, colocalization analysis	limited sample throughput, accuracy relies on calibrating using silica beads causes bias	Fortunato et al. (2022), Chen et al. (2023)
MoFlo Astrios-EQ	nFC	Beckman Coulter	not specified	high	high	high sensitivity, single cell sorting	limited to specific applications, complex operation	Morales-Kastresana et al. (2017), Morales-Kastresana et al. (2019)
Apogee A50-Micro	nFC	Apogee Flow Systems	100–1000 nm	medium	high	linear detection of particles, multiplex detection	high initial investment, need for negative and positive controls, need to modify the gains for each PMT	Gomes et al. (2018), Padda et al. (2019), Botha et al. (2021), Roseborough et al. (2023)
Gallios	nFC	Beckman Coulter	from 100 to 150 nm (fluorescence threshold triggering, calculated value)	medium	high	high sensitivity compared to conventional FC, reproducible, simplicity of use, can be applied do unprocessed biological fluids	unspecific signal from unbound dye and dye aggregates, risk of swarming effect, only stained EVs visible, detection of 300 nm fluorescent beads with efficiency of 50% ± 2%, limited sensitivity of sEVs	Arraud et al. (2016), George et al. (2021)
Influx (modified for small-particle detection)	nFC	BD Biosciences	from 100 nm (fluorescence threshold triggering)	customized	high	high sensitivity, multicolor antibody labeling	unspecific signal from unbound dye and dye aggregates, risk of swarming effect, only stained EVs visible, lack of reproducibility because of custom made equipment	Nolte-'t Hoen et al. (2012), van der Vlist et al. (2012)
FACS Canto (custom constructed)	nFC	BD Biosciences	from 70 to 80 nm (fluorescence threshold triggering)	customized	high	high sensitivity	high cost for custom made equipment, unspecific signal from unbound dye and dye aggregates, risk of swarming effect, only stained EVs visible, lack of reproducibility because of custom made equipment	Stoner et al. (2016)

<sup>a</sup>More details on cost and throughput are available on the website: <https://exrna.org/resources/ercc2-tech-detail/?particles=&methods=>.

instrument's precision and resolution. Larger nanoparticles, which have a higher refractive index, scatter light more intensely, making them easier to detect and track. Smaller particles with a relatively small refractive index present in the same sample may not be detected or underestimated in their number, as their signal will be covered by larger particles. Populations with a close size range may not be distinguished and will be considered as one population. Therefore, the analysis of heterogeneous particle solutions, such as biofluids, with conventional scatter-based NTA may be difficult. Furthermore, if the refractive index of the nanoparticles is close to that of the solvent, they may be more difficult to detect because they scatter light less efficiently (Malloy and Carr, 2006; Filipe et al., 2010; Gardiner et al., 2014; van der Pol et al., 2014; Midtvedt et al., 2020; Kashkanova et al., 2022).

Consequently, the sensitivity and use of light scattering are limitations of conventional NTA because particulates with a similar refraction index and/or size cannot be differentiated from actual EVs. These can be dust or powder, plastic particles, lipoproteins, or other impurities. They can influence both concentration and size measurements. NTA has a strictly defined concentration range in which samples can be measured, and in most cases, the sample must be diluted to meet this concentration range. Notably, the solvent used may contain particles that are visible in the NTA, which may affect the results. Therefore, it is crucial to prepare appropriate controls, such as size and concentration calibration using commercial PS beads (with a certificate of size and concentration) and buffer-only controls (for instance, phosphate-buffered saline, PBS). In addition, one should check the quality of plastics and always use fresh deionized water or other buffers as instrument rinse solutions and sample diluents (Snyder et al., 2021). Another important requirement of NTA that ensures the accuracy and reproducibility of the readout is to maintain the same conditions for each measurement, which have been previously optimized for a given sample type (temperature, sensitivity, frame rate, threshold, etc.). These conditions should be reported when results have been published. Even if one meets all these requirements to improve reproducibility, it is important to remember that EVs are very heterogeneous and polydisperse, and their size distribution on NTA usually does not follow a Gaussian or log-normal distribution. The population of smaller EVs may be covered by a population of larger EVs with a higher refractive index, and populations in a close size range may not be distinguished and will be considered as one population.

This imperfection of the traditional light scatter-based NTA was noticed, among others, by a team investigating urinary EVs, comparing the impact of different isolation methods (different combinations of ultracentrifugation (UCF), size-exclusion chromatography, PEG precipitation and ultrafiltration) on chosen EV analysis methods (NTA, flow cytometry, transmission electron microscopy) (Droste et al., 2021). The authors showed that EV enumeration by NTA was highly affected by typical urine non-vesicular impurities like uromodulin. Another group confirmed that protein aggregates, such as albumin, which are created in urine, were visible on NTA as small particles undistinguishable from urinary EVs (McNicholas et al., 2017). Therefore, scatter-based NTA is highly dependent on the chosen EV isolation method that determines the levels of co-isolated non-vesicular impurities. This is particularly true for biological fluids, where impurities are usually highly abundant. Indeed, the impact of myosin aggregates, IgG

immunoglobulins, and alpha-synuclein on NTA scatter measurements has been reported previously (Filipe et al., 2010; Hoover and Murphy, 2020).

To increase the specificity and sensitivity of NTA measurements and prevent the detection of non-EV particles, additional fluorescent labeling of particles was introduced for NTA. Fluorescent NTA (f-NTA), which measures particles in fluorescent mode, enables the visualization of only particles that are specifically fluorescently labeled. Using lipophilic or nucleic acid-specific dyes, we can detect particles that have biological membranes or DNA/RNA cargo, whereas fluorescent antibodies allow the detection of specific EV-surface antigens and phenotypic characterization. Whereas traditional light-scatter-based NTA measurements offer only an estimation of the total particle number in a solution, f-NTA enables the measurement of individual particle fractions determined through specific fluorescent labeling. Furthermore, small EVs that reflect insufficient light to be detected in scatter mode may become visible after labeling in the fluorescent mode owing to their fluorescence. Therefore, f-NTA may be a solution for the main drawbacks of conventional NTA, such as underestimation of the content of small EVs in a heterogeneous particle solution and poor distinction between "real" EVs and impurities of similar size. However, many factors that can influence readout and introduce bias remain, as outlined below.

### 2.1.1 Fluorophore properties and instrument settings

The most well-known aspects that may affect the fluorescent staining of EVs, but also affect traditional cell analysis, are the stability and intensity of the fluorophore. In the case of f-NTA, this impact is even more pronounced, since the measurement lasts longer than on a flow cytometer; therefore, the fluorophore needs to emit fluorescence longer for signal collection and is more prone to photobleaching. Modern NTA devices are equipped with a special function (for instance, the "low bleach" option in the ZetaView device, or laser pulsing on and off in synchronization with the camera shutter in the case of the Nanosight NS300) to prevent photobleaching. To lessen the impact of photobleaching, it is important to use bright and stable fluorochromes like Alexa Fluor (488, 647), Cyanine Dyes (Cy3, Cy5) or quantum dots (Thane et al., 2019; Desgeorges et al., 2020; Fortunato et al., 2021). Although the relative high sensitivity of the NTA instruments enables to detect the much lower fluorescent signal of EVs, in comparison to cells (usually 2-3 magnitudes lower), but on the other hand it also means a higher susceptibility to background noise and contaminations (Midekessa et al., 2021). The sensitivity of the instrument for the fluorescence signal can usually be set by the brightness threshold setting. In the fluorescent mode, it affects the distribution, number, and size of the detected particles and the zeta potential (Midekessa et al., 2021). It is important to balance the dye concentration and fluorescence threshold based on appropriate controls (dye-only control and solvent-only control) before the measurement of actual samples.

## 2.2 Nanoscale flow cytometry

A noteworthy advancement in Flow Cytometry (FC) instrumentation utilized for EV analysis involves the



implementation of nanoscale FC (nFC, nanoFACS). This upgrade of conventional flow cytometry includes special enhancements in optical and fluidic systems, which allows for more accurate and targeted analysis of EVs (Lian et al., 2019). In this technology a fluorescence threshold triggering instead of side scattered light (SSC) triggering is used (Gomes et al., 2018; Padma et al., 2019; Salmond et al., 2021). The wavelength of visible light is longer, which causes lower resolution, however the usage of fluorescence and a shorter wavelength – 405 nm, enables a better resolution. Simultaneously, the use of fluorescence triggering determines that, from the beginning, only distinct labeled populations of EVs are visible. The lack of a “scatter mode” in nFC differs from NTA, where the sample can be measured simultaneously in both the scatter and fluorescent modes. On the other hand, the nFC method enables often measurements directly in the original biological samples without EV isolation, which cannot be done in case of NTA because of high background (Gorgens et al., 2019). Moreover, combining nFC with size exclusion chromatography (SEC) purification after labeling enables to keep a low false positive event rate, because SEC washes unbound dye or antibody from the sample (Aibaidula et al., 2023). Thanks to nFC, characterization of the molecular EV cargo, and colocalization of different markers on single EVs is possible. However, similar to NTA, several factors must be considered for a successful nFC analysis. The importance of the specificity and effectiveness of EV labeling and the removal of unbound dye and dye aggregates are discussed in detail in the labeling section. Other factors are discussed below.

### 2.2.1 EV size characterization using nFC

EV size characterization in scattered light using nFC remains biased because the reference beads from polystyrene and silica, which are available on the market so far, have higher refractive indices (RI) than EVs. This results in inaccurate measurements both in term of size and concentration (Gul et al., 2022). Recently a new kind of reference - hollow organosilica beads (HOBs) have been evaluated (Deumer et al., 2024). In the study authors used HOBs with different shell thickness and determined the size distribution and their concentration using several techniques including Small-Angle X-ray Scattering (SAXS), Atomic Force Microscopy (AFM) and Single Particle Inductively Coupled Plasma Mass Spectrometry (spICP-MS). They then used two different flow cytometers, A60-Micro, Apogee, and Nothern Lights, Cytex, for flow cytometry measurements and NS300, Malvern Panalytical, for NTA. The determined side scattering cross-sections in the case of HOBs were two orders of magnitude smaller than those for the PS beads but similar to that of EVs. Moreover, the measured RI value could be tuned by adjusting the shell thickness of the HOBs and for 11-HOB it was about 1.363–1.373 – which is similar to the RI of EVs in human urine. These results are promising for the future use of nFC for size measurements of EVs.

An indirect way to perform EV quantitative measurements on nFC was described by von Lersner et al., 2024. The authors used Di8-ANNEPS-stained EVs in serial dilution with addition of dextran to evaluate the advantages of the so-called molecular crowding (MC). Detecting single extracellular vesicles (EVs) in a flow cytometer often requires a significant dilution of the source material to prevent the detector from being overwhelmed by multiple particles. However, this dilution reduces the molecular density, which can

increase the nonspecific interactions between microparticles and macromolecules. Therefore, the authors used dextran to compensate for the reduction in protein and other buffering components caused by the sample dilution. They found that it improved single-particle detection of labeled beads and EVs by 100%–400%. They established a 3.25% final concentration of dextran as the optimal condition for particle detection, which was also verified using synthetic beads. Moreover, in their study they developed a method named “EV Fingerprinting”, that determines separate EV populations using dimensional reduction of multiparametric data collected by nFC (von Lersner et al., 2024). This method allows to identify and characterize distinct EV populations in complex biological samples. EV fingerprinting uses multiparametric analysis of the fluorescence data of EVs stained with a lipophilic dye that is sensitive to the membrane environment. Di-8-ANEPPS changes its fluorescence properties depending on the order of the lipid membranes, allowing EVs to be distinguished based on their size and structure of their lipid membrane. Thus, it is possible to obtain more detailed information on EV heterogeneity than with traditional cytometric methods.

### 2.2.2 Impact of the swarming effect in nFC

An important factor in nFC is the swarming effect, which means that many single particles are detected as one event by a flow cytometer (Libregts et al., 2018). When many small molecules pass through the detector simultaneously, their signals can overlap. This results in one large signal being recorded instead of several smaller ones, which can lead to incorrect conclusions regarding the size and number of measured particles and the mean fluorescent intensity (MFI) of the detected molecules. The swarming effect was detected by comparing the fluorescence intensities of different sample concentrations. If the ratio of the particle number to MFI remains constant, there is no swarming effect; however, if the intensity increases rapidly, many particles are measured together. To prevent swarming low flow rates and serial dilutions of the samples are recommended (Kuiper et al., 2021).

### 2.2.3 MESF standardization

The fluorescent signal from the nFC is reported in arbitrary units, which cannot be compared between the instruments. To enable validation of measurements and comparison between different flow cytometers and laboratories, a so called MESF (Molecules of Equivalent Soluble Fluorophore) calibration with standard MESF beads must be performed (Schwartz et al., 2002; Padma et al., 2019; Kuiper et al., 2021; Hajji et al., 2022). Fluorescence intensity given in MESF units can be then compared to other flow cytometers.

### 2.2.4 Novel instruments

Notably, there are some custom-made nFC instruments that enable the detection of nanoscale particles; however, the repeatability between instruments constructed in this manner is unknown. There are also newly developed instruments dedicated to small-particle analysis using nFC that may provide valuable information about EV molecular cargo after proper validation. All these instruments are listed in Table 1. However, their performance requires time to be comprehensively evaluated and compared to other instruments, along with the establishment and evaluation of consistent labeling protocols (Lopez-Pacheco et al., 2021; Salmond et al., 2021).

#### 2.2.4.1 Imaging flow cytometry

Another type of FC that provides higher fluorescence sensitivity and resolution than traditional FC and can be used for EV analysis is imaging flow cytometry (IFC). The main change in conventional FC is the way in which the optical signal is detected and processed. These cytometers use charge-coupled device (CCD) cameras, which have lower noise and broader dynamic range than PMTs from conventional cytometers. Additionally, IFC instruments have a so-called time delay integration (TDI) of pixel intensities on CCD cameras and slower flow rates; therefore, the signal has longer integration for each particle, which increases the sensitivity. Moreover, the images of all events in all channels are stored so that they can be processed for further data analysis (Botha et al., 2021). Still, most EVs are below the diffraction limit and are visualized as diffraction-limited spots.

IFC encounters several technical issues related to signal processing, that cause the necessity for appropriate calibration, gating strategy, controls and serial dilutions (Woud et al., 2022; Welsh et al., 2023; Wu et al., 2023). Interestingly, in case of IFC, staining intensity and sample recovery vary depending on the temperature of the incubation with fluorescent antibodies (Tertel et al., 2020). To prevent coincident detection in imaging FC, Woud et al. proposed a specific gating strategy, where they collected events displaying 0 or 1 fluorescent spot on acquired images. This ensured that they analyzed only single particles and not multiple particles. The authors also suggested standardizing SSC signal intensities for the estimation of particle sizes and colocalization of at least two fluorophores to assess the presence of two markers on the same particle. They underlined the importance of a detergent-treated sample as a control; the disappearance of the signal after detergent treatment ensures that the detected fluorescent events are associated with lipid membranes of biological origin (Woud et al., 2022).

#### 2.2.4.2 Spectral flow cytometry

An additional type of FC for EV characterization is spectral flow cytometry (SFC) (Aibaidula et al., 2023). In which optical signals are collected from the full emission spectrum, not only from the section where each fluorochrome has an emission peak. Collecting the entire spectrum reveals differences in the pattern between fluorophores with similar emission peaks and allows more fluorochromes to be used to stain a single sample. These spectrometers apply a spectral unmixing procedure to unravel the signal from each fluorophore. However, the use of SFC for EV analysis is limited by the small surface area and dim signals of EVs similar to nFC (Welsh et al., 2023).

## 3 Labeling

### 3.1 Sample handling: impact of EV isolation method, sample concentration and background

EV labeling protocols are often based on protocols and dyes that were initially dedicated to cells. However, owing to the several orders of magnitude smaller size of EVs, these protocols must be adapted to

meet the special requirements and challenges connected to EVs, which are discussed in more detail later in this chapter.

In general, it is important to optimize dye concentration, staining temperature, and EV purification methods before conducting actual sample measurements. Midekessa et al. showed, for example, that the size of fluorescent particles decreases and their number increases with higher concentrations of the lipophilic dye Cell Mask Green (CMG) (Midekessa et al., 2021). Those differences may be related to the differences in apparatus sensitivity in the scatter and fluorescent modes. Because of the low refractive indices of sEVs, they may not reflect enough light to be detected in the scatter mode; however, after labeling, the fluorescent signal is much more intense, and these particles can be detected in the fluorescent mode. Because, as mentioned above, particular impurities affect fluorescent staining and subsequent f-NTA measurements, the chosen EV isolation method will influence the subsequent staining and f-NTA results. Midekessa et al. observed that the number of CMG-stained EVs increased slightly with the incubation temperature. This can be explained by the higher fluidity of the double phospholipid bilayer of EVs at higher temperatures, which favors intercalation of dye molecules into the membrane. The EV purification method impacted their NTA results - in the case of combination of tangential flow filtration (TFF) and SEC the authors detected fewer particles but with a bigger size than using only the SEC method (Midekessa et al., 2021). The authors explained that these results showed the impact of the purification method used for EV preparation on f-NTA measurements - by combining TFF and SEC they obtained a different particle composition in the analyzed sample, which was reflected by the EV profile detected by NTA.

Interestingly, Koksall et al. mentioned that every precipitation and centrifugation step during EV preparation for analysis due to mechanical stress influences the EV conformation and activity of surface markers. Consequently, fewer EVs can be detected using fluorescent antibody labeling methods (Koksall et al., 2023). The authors admitted that f-NTA is a time-consuming and operator-specific method. The duration of the entire analysis must be within the range of fluorochrome optimal glowing properties to prevent the impact of photobleaching. The samples were protected from light during the entire protocol for all the washing and measurement steps. Altogether, the difficulties described above limit the applicability of f-NTA as an EV analytical method, particularly in the clinical context.

Another important factor affecting NTA results is the sample concentration. Although the sample dilution factor is considered by the analysis software for concentration calculations, one must be within the optimal concentration range of the sample for the measurement. Salaga-Zalewska et al. noticed that too high or too low sample dilution during measurement distorts the determination of the total number of particles per milliliter (Salaga-Zaleska et al., 2023). Too many particles in the field of view during NTA measurement can lead to particle interaction, collision, and overlapping, which may interfere with particle movement and give unreliable results (Yahata et al., 2021). It is also a known effect in flow cytometry measurements of EVs and is recognized as the swarming effect. Therefore, the sample concentration for the measurement must be carefully optimized. Furthermore, in the case of f-NTA, the optimal concentrations for the scatter and fluorescent



modes may be different. In most cases, we aim to determine the absolute number or percentage of our fluorescent-positive particle (EV) population relative to the total particles, and a measurement in both modes (scatter and fluorescent) of exactly the same sample loaded into the flow cell is needed. The concentration of the sample optimal for scatter light analysis may be too low for measurement in fluorescent mode, especially if the percentage of the fluorescent-positive EV population is low, for example, the number of tetraspanin CD9 positive EVs—Thus, we have too few fluorescent particles in the field of view for accurate concentration calculations by the software. In contrast, when we adjust the sample concentration to be optimal for fluorescence measurement, it might be too high for the scatter mode, where many more particles will be detected by the instrument, and there is a risk of the swarming effect. Furthermore, the optimal sample dilution for an f-NTA measurement also depends on the background of the dye or fluorescent antibody and sample impurities.

Often, as previously mentioned, other compounds are co-isolated with EVs, such as large protein complexes, soluble proteins, and cell culture media components. These compounds can significantly influence the effectiveness of the labeling and results. Their influence is discussed in the third section of this review. There should always be a negative (the sample containing the solvent without EVs, but treated and labeled the same way as EV sample) and a background control (the sample containing only the solvent or the sample matrix) to provide reliable results (Fortunato et al., 2021). In addition, depending on the dye or type of fluorescent antibody, staining may also give a more or less high background signal in the fluorescent mode due to the formation of micelles or aggregates detectable by the instrument, unspecific binding to sample contaminants, or other undefined reasons. This background influence can be reduced by a high dilution of the sample after staining for measurement on the NTA instrument. However, the requirement for this is an initially highly concentrated EV sample for the staining step, which ensures that after the high dilution for measurement (at least 100 times), the EV number in the field of view remains sufficiently high to be in the range required for the measurement. Therefore, it is necessary to balance the initial EV sample concentration for staining, dye or antibody concentration, and dilution for measurement to obtain an optimal result, which has been shown in our study (Dlugolecka et al., 2021). Alternatively, a washing step can be performed after staining to remove unbound dye or antibody (discussed in detail below); however, this step is not always applicable and can contribute to the loss of EV samples.

### 3.2 EV labeling efficiency, nonspecific labeling

EV labeling techniques used for fluorescence analysis by f-NTA, nFC, or other methods present many challenges. One of the important issues is labeling efficiency. During analysis, the concentration of total particles in scatter (on NTA) and labeled particles (f-NTA) can be compared, but the actual efficiency of labeling “real” EVs is unknown (Dlugolecka et al., 2021). The total particle concentration, in fact, counts particles that are EVs and are

labeled, particles that are EVs but because of labeling efficiency will not be labeled and particles that are not EVs. Researchers must be aware of this during the data analysis.

Interestingly, Chen et al., using nFC, noticed a large variation in the labeling performance of lipophilic dyes or lipophilic membrane probes, probably because of the heterogeneous nature of EVs and the differences in their lipid composition. Their results showed that the labeling efficiency of EVs differed according to different biological sources, such as different cell lines, and varied within individuals for EVs from plasma (Chen et al., 2023).

Similar observations were made by Tertel et al., who compared the efficiency and specificity of common EV dyes. They stained MSC-derived EVs with a few conventionally used dyes (BODIPY TR ceramide, calcein AM, CFDA-SE, PKH67, and Exoria) and analyzed them by Imaging FC. Additionally, to determine specificity, labeled objects were treated with detergent NP-40. Only events that disappeared after detergent treatment were considered true EVs. The objects labeled with CCFDA-SE and BODIPY TR ceramide were not affected by detergent treatment; therefore, the authors concluded that those were not small EVs. Calcein AM failed to stain any object. Only PKH67 and Exoria dyes successfully stained EVs based on light-scattering properties and detergent control. Co-staining using fluorescently labeled antibodies against tetraspanins showed that, in the case of MSC-derived EVs Exoria was more specific to tetraspanin-positive particles than PKH67. The authors also mentioned that the labeling results differed depending on the source of EVs and their molecular content. For instance, different cell types secrete EVs with varying esterase contents, which limits the utility of CFSE as a dye for cell types with low intracellular and intra-vesicular esterase concentrations (Tertel et al., 2022).

Notably, Melling et al. performed an interesting study in which they labeled EVs previously tagged with mEmerald-CD81 with two types of dyes, PKH26 and C5-maleimide-Alexa633. They performed colocalization tests for both the dyes and CD81 using confocal microscopy. The results showed that most of the tagged EVs were not labeled with either PKH26 (only  $4.6\% \pm 1.6$  was labeled), or C5-maleimide-Alexa633 ( $35.4\% \pm 1.8$  was labeled) (Melling et al., 2022). The authors noticed that a significant fraction of the dye was not associated with EVs. They observed additional particles by NTA and confocal microscopy in the dye controls, which corresponded to macromolecular dye self-aggregates and micelles. Notably, after an additional cleaning step using SEC, the authors noticed the elimination of this maleimide signal and the reduction of the PKH26 signal in the dye controls. A substantial amount of signal from both dyes was detected after an analogous cleaning step with an Exospin column. The authors suggested that EV-staining dyes can form large molecular aggregates, but certain techniques can be employed to minimize their occurrence (Melling et al., 2022).

The formation of micelles and aggregates in the PKH26 dye was also reported by Morales-Kastresana et al., 2017. The researchers observed a higher event rate in the EV sample labeled with PKH26 on nFC and NTA than in the unstained EV sample. A non-EV control (PBS + PKH dye) also showed a differentiated particle distribution, corresponding to the presence of micelles or PKH26 aggregates (Morales-Kastresana et al., 2017). Furthermore, the authors also assessed CFSE as an EV dye and observed that there was no evidence of micelle or aggregate formation, since the concentration and size distribution of the labeled sample

remained similar to that of the unstained EVs. However, there was a shift in the fluorescence of the background reference noise events on the nFC, which corresponded to the unbound dye. To reduce background fluorescence, the authors used several techniques (SEC, UCF, sucrose cushions, or CFSE sequestration with BSA-coated beads) and reported that SEC was the most effective in removing unbound labels (Morales-Kastresana et al., 2017).

Additionally, Fortunato et al. emphasizes that, for example, CFSE can give an unspecific signal from the contamination with soluble esterases (Fortunato et al., 2021). Loconte et al. analyzed EVs labeled with several dyes: MG-488, CFDA-SE, or labeled through the expression of a mp-sfGFP and evaluated uptake experiments by spectral flow cytometry and imaging flow cytometry. They found that EVs labeled with MG-488 were present in all cell types, EVs stained with CFSE were only visible in a minor subset of cells, and EVs labeled with mp-sfGFP were mostly detected in CD14<sup>+</sup> monocytes. The authors stated that all combined methods provided complementary information about EVs (Loconte et al., 2023).

Some studies have described possible solutions to increase the efficiency of lipophilic dyes. Cha et al. proposed reducing the NaCl concentration of the buffer during labeling to 20 mM NaCl to help lipophilic dyes enter the membrane (Cha et al., 2023). They explain that lipophilic dyes are not getting efficiently incorporated into vesicle membranes in an aqueous buffer because of their low water solubility. At lower salt concentrations, the dye was more dispersed and better available for vesicle membrane incorporation. After labeling, they suggested increasing the ionic strength to 150 mM NaCl because the dye forms macromolecular aggregates that can be easily separated from vesicles by regular syringe filtration using 0.2  $\mu$ m filters. A comparison between conventional staining and salt-change staining showed a much higher efficiency of the salt-change method. It has been shown to work with several types of vesicles and lipophilic dyes, such as DiI, DiD and PKH67 (Cha et al., 2023). Moreover, their experiments showed that, using the salt change method, less dye is needed for satisfactory results, and because there is a small amount of dye molecules per vesicle, the impact of the dye on vesicle characteristics such as size and functionality is minimal.

In antibody labeling, the selection of a specific type and clone is critical, as their performance can vary depending on the assay type and conditions. To assist in the selection of the appropriate antibody and to minimize the need for extensive optimization studies, the EV Antibody Database has been established (Morey et al., 2024). Although currently limited, the database is open access and is intended to provide detailed information on assay variables and protocols in the future, to support the sharing of relevant antibody data in EV research. It includes information on antibodies tested in Western blots, flow cytometry, and other assays, helping researchers eliminate inefficient antibodies from their protocols and select more effective ones. Also, the proper antibody to sample ratio during the staining process is critical to results, and this information can also be included in the database.

According to staining with fluorescent antibodies directed against certain EV surface markers, the observed variability in staining efficiency is an effect not only on the staining performance of a given antibody, but also on the heterogeneous marker expression of EV populations. Interestingly, Spitzberg et al. performed a multiplexed analysis of EVs using high-resolution

microscopy (MASEV), the method of direct stochastic optical reconstruction (dSTORM), and self-made microfluidic devices (Spitzberg et al., 2023). In which the authors investigated whether common EV markers used in bulk methods, such as Western blotting and ELISA, are present in variable concentrations in all EVs or if some EVs are enriched in specific proteins. Their analysis revealed that there is in fact a heterogeneous distribution of specific markers across all EV groups. The most abundant protein was CD9 (47.9%) in the PANC-1 cell line. They also evaluated the concomitance of the different biomarkers in each vesicle. The results revealed that many of the tested EVs had a low percentage or no tetraspanins depending on the cell line. This implies that in the case of affinity purification of EVs using one of the tetraspanin markers from biological fluids, an unknown, but in some cases, a substantial number of EVs could be missed. The authors suggested that it is worth to use pan-tetraspanin affinity purification to raise the ratio of isolated vesicles and increase the detection yield (Spitzberg et al., 2023). Other studies also show that tetraspanins are not expressed evenly across different EV sources and that the tetraspanin profile changes depending on EV size, subclass and source (Mizenko et al., 2021).

These studies indicate that none of the methods currently used for labeling EVs offers accurate quantitative measurements. Rather, samples can only be compared among themselves, as the number of stained EVs is often overestimated owing to dye and background aggregates. In addition, it is difficult to assess staining efficiency, which affects the precision and reliability of the obtained results.

### 3.3 Does the EV staining method impact the functionality of EVs?

Loconte et al., in their work mentioned in the previous chapter, reported that the labeling of EVs considerably influences their interactions with recipient cells, including their uptake and cargo delivery. EVs labeled with MG-488 were found in all cell types, and the same EVs labeled with other dyes were detected in only some cell subsets. This indicated that the labeling type considerably affected EV functionality in the uptake experiments. Therefore, the authors concluded that combined labeling methods could provide more complete information about the interaction of EVs with cells (Loconte et al., 2023).

Furthermore, Chen et al. performed a functionality test of EVs labeled with the lipophilic membrane probe DSPE-PEG<sub>2000</sub>-biotin to check if there was a steric hindrance effect impacting surface protein analysis during labeling with PE-conjugated antibodies against CD9, CD63, and CD81. No impact of this lipophilic membrane probe on the antibody staining or functionality of EVs was observed (Chen et al., 2023).

In their review of labeling techniques, Bao et al. highlighted the advantages of using aptamer particles instead of classical antibodies. Conventional antibodies can induce immunological reactions and EV aggregation, which can affect EV properties and functionality *in vivo*. Aptamers are short stretches of nucleic acids (DNA or RNA) or peptides that can bind specifically to specific molecules, such as proteins, small organic molecules, metal ions, and even whole cells. Aptamers act similarly to antibodies, showing high specificity and affinity for their targets but differ in structure and production

TABLE 2 Common label types.

Name of the label	company	type	advantages	disadvantages	impact of staining on EV function	application	References
CellMask	Thermo Fisher Scientific	lipophilic membrane dye	membrane-specific labeling, compatible with live-cell imaging, slow internalization, can be used after fixation	label every biological compound with a lipid membrane, not only EVs, cannot be used after permeabilization, detergent sensitive, impacts the size of EVs	may affect EV uptake and cargo distribution	EV membrane labeling	Długolecka et al. (2021), Midekessa et al. (2021), Bao et al. (2023)
Specific antibody conjugate with fluorescent probe like CD9-PE, CD9-AF488, etc.	Various	immunospecific, protein-specific	highly specific labeling of target proteins	potential for nonspecific binding, binding many proteins causes increase of EVs size, for most applications only labeling of surface markers, fluorophore size may cause steric hindrance	may influence EV protein function and sorting, obscure functional receptors on EV surface, affects EV physiochemical properties and biological functions	EV protein labeling	Długolecka et al. (2021), Bao et al. (2023)
CFDA-SE (CFSE)	Thermo Fisher Scientific	amine-reactive become fluorescent after enzymatic reactions	stable and covalent labeling of cellular components, allows to study EV internalization and content transfer <i>in vitro</i> , allows the detection of intact EVs and their content delivery	limited to intact EV labeling, EVs from different sources can differ in esterase content and therefore its staining efficiency depends strongly on source of EVs	may alter EV uptake and cargo distribution; do not perturb the size of EVs nor their biodistribution	EV labeling, tracking	Morales-Kastresana et al. (2017), Dehghani et al. (2020), Barrachina et al. (2022), Tertel et al. (2022), Loconte et al. (2023)
PKH67	Sigma-Aldrich	lipophilic dye	bright fluorescence, compatible with various imaging modalities	limited to lipid membrane labeling, creates aggregates and micelles, so washing step is necessary	may affect EV membrane properties, impacts EV size	EV labeling, imaging <i>in vivo</i> and <i>in vitro</i>	Liebel et al. (2020), Droste et al. (2021), Bao et al. (2023), Cha et al. (2023), Chen et al. (2023)
PKH26	Sigma-Aldrich	lipophilic dye	high stability, long-lasting fluorescence	requires optimization for different EV types, creates aggregates and micelles, so washing step is necessary	impacts EV size	EV tracking, imaging <i>in vivo</i> and <i>in vitro</i> , functional studies	Morales-Kastresana et al. (2017), Puzar Dominkus et al. (2018), Dehghani et al. (2020), Melling et al. (2022), Bao et al. (2023), Chen et al. (2023)
DiI, DiO, DiL, DiD, DiR	Thermo Fisher Scientific	lipophilic dye	bright fluorescence, long-term labeling, minimal background fluorescence, stable staining, almost no staining transfer between EVs	photobleaching over time, creates aggregates and micelles	may alter EV uptake and cellular response	EV labeling, imaging <i>in vitro</i> ; DiD, DiR <i>in vivo</i> imaging	Rautaniemi et al. (2021), Bao et al. (2023), Cha et al. (2023), Chen et al. (2023)
Azido-dPEG-TFP ester, linked inhouse with AF350, AF488, or AF647	Quanta Bio-design	fluorescently label free amines of EV-surface proteins	labels any accessible EV surface protein equally well, bright, stable, PEG linker increases water solubility, labeling efficiency and reduce nonspecific EV binding/aggregation	increases size of EV, impairs function of EV surface proteins	may influence EV biodistribution and interactions with target cells	total EV labeling	Ferguson et al. (2022), Spitzberg et al. (2023)
C5-maleimide-Alexa633	Thermo Fisher Scientific	thiol-reactive	strong fluorescence, selective labeling	potential for nonspecific binding	may influence EV stability and uptake	EV labeling, imaging	Roberts-Dalton et al. (2017), Melling et al. (2022)

(Continued on following page)

TABLE 2 (Continued) Common label types.

Name of the label	company	type	advantages	disadvantages	impact of staining on EV function	application	References
MemBright	BioActs	membrane-specific	high specificity, compatible with live-cell imaging, simple handling, great specificity, low working concentration, no cytotoxicity, compatible with many fluorescence imaging techniques, no aggregates	limited to membrane labeling	may alter EV membrane properties	EV membrane labeling	Collot et al. (2019), Melling et al. (2022), Bao et al. (2023), Boudna et al. (2024)
MemGlow (MG)	BioActs	membrane-specific	bright fluorescence, minimal background; creates non-fluorescent aggregates, allows the detection of short/transient interactions	potential photobleaching, possible dye transfer through brief interaction with the recipient cell	may affect EV uptake and cargo distribution	EV membrane labeling	Loconte et al. (2023), Rodriguez et al. (2023)
ExoGlow	System Biosciences	membrane-specific	bright, intact membrane specific	can also label liposomes and lipoproteins	may alter EV membrane properties	EV membrane labeling	Kamei et al. (2021), Roseborough et al. (2023)
ExoTracker	SBI	fluorescent	compatible with EV tracking in live cells	limited to fluorescence microscopy	may alter EV distribution and cargo sorting	EV tracking	Zhou et al. (2020), Loconte et al. (2023)
DHPE	Sigma-Aldrich	lipophilic dye	stable incorporation into lipid bilayers	limited compatibility with certain imaging modalities	may influence EV membrane properties	EV labeling, membrane studies	Nazarenko et al. (2013), Rautaniemi et al. (2021)
Ptx-OG (paclitaxel Oregon Green)	Creative Bioarray	fluorescent dye conjugate of the chemotherapy drug paclitaxel	selective labeling, minimal interference, high fluorescence quantum yield, photostability	potential for nonspecific binding, paclitaxel cytotoxicity	may impact EV protein function and sorting	EV uptake and intracellular trafficking	Saari et al. (2018), Rautaniemi et al. (2021)
SYTO RNASelect	Thermo Fisher Scientific	nucleic acid-specific	highly specific for RNA, compatible with flow cytometry	limited signal intensity in EVs with low RNA content	minimal impact on EV function	analysis of EV RNA cargo	Popena et al. (2018), Adamo et al. (2019), Melling et al. (2022)
Exoria	AAT Bioquest	lipophilic dye	high photostability, compatible with flow cytometry	limited spectral range, potential cytotoxicity	may affect EV uptake and cargo distribution	EV labeling, tracking	Chong et al. (2022), Tertel et al. (2022), Johnson et al. (2023)
Calcein AM	Abcam	fluorescent dye	non-toxic, suitable for live-cell imaging	limited membrane permeability	minimal impact on EV function	monitoring EV release dynamics	Gray et al. (2015), Tertel et al. (2022)
BODIPY and derivatives (Dp ceramide, BPC12, BP and others)	AAT Bioquest, Creative Bioarray	lipophilic dye	bright fluorescence, high quantum yield, long-term labeling, sharp absorption, and emission peaks, and good photostability, easy to modify to adjust photophysical properties, biocompatible	possible unspecific binding, time consuming modification procedure, limited effectiveness in deep tissue imaging	may alter EV membrane properties	uptake and trafficking inside the cell	Rautaniemi et al. (2021), Tertel et al. (2022)
CellTracker Red CMTPX	Invitrogen	fluorescent dye	highly stable, compatible with live-cell imaging	moderate photostability, pH-dependent fluorescence	minimal impact on EV function	studying EV uptake and trafficking	Tong et al. (2017), Reginald-Opara et al. (2022), Song et al. (2023)

(Continued on following page)

TABLE 2 (Continued) Common label types.

Name of the label	company	type	advantages	disadvantages	impact of staining on EV function	application	References
Di-8-ANEPPS	Invitrogen	lipophilic dye	high sensitivity to membrane potential changes, Suitable for membrane potential imaging in live cells, high effectiveness of EV labeling	toxic at high concentrations, Limited selectivity for specific membranes, creates aggregates and micelles	potential disruption of EV membrane integrity	membrane potential imaging, live-cell studies	Chen et al. (2023), von Lersner et al. (2024)
DSPE-PEG <sub>2000</sub> -biotin	Avanti Polar Lipids, Inc	lipophilic membrane probe	biotinylated for specific interaction with streptavidin or avidin, PEG linker enhances solubility and stability	potential alteration of lipid bilayer properties, requires streptavidin or avidin for detection	minimal impact on EV function in case of interaction with antibodies for tetraspanins	biotinylation of EVs for isolation or detection	Wan et al. (2017), Chen et al. (2023)
GFP	-	fluorescent protein	adequate to follow the first steps of uptake, bright green fluorescence	requires genetic engineering for expression, may interfere with protein function if fused improperly	may interfere with protein function if fused improperly	visualization and tracking of proteins, organelles, cellular structures (including EVs) in living cells	Corso et al. (2019), Loconte et al. (2023)

methods. Compared to classical fluorescent antibodies, aptamers are much smaller, have higher biocompatibility, and do not affect the physicochemical and biological functions of EVs. In addition, aptamers can be chemically synthesized, allowing precise control of their sequences and properties. The aptamer selection process can be performed completely *in vitro*, whereas antibodies are typically produced in living organisms (Bao et al., 2023).

Moreover, Arifin et al. described current state-of-the-art imaging techniques for studying EV uptake and distribution *in vivo*, focusing on the biodistribution and pharmacokinetic profiles of EVs after administration *in vivo*. The authors reported cytotoxicity at higher label concentrations, which may severely impact EV and cell functionality; therefore, optimizing the label concentration is important to lessen the cytotoxic effect *in vivo*. Additionally, the authors observed an altered surface charge or size distribution of EVs at high label concentrations, which may also influence EV functionality (Arifin et al., 2022).

The most common labels used in EV studies are listed in Table 2, which also addresses their advantages, disadvantages, and impact on EV function.

### 3.4 Washing after labeling

As presented above, a substantial amount of background and unspecific staining can be expected under certain circumstances during fluorescent labeling of EVs, and a washing step is highly recommended. There are a few ways to perform washing after labeling, like SEC, UCF, ultracentrifugation with a discontinuous density gradient (UCG), ultrafiltration (UF), anion exchange chromatography (AEC) or with affinity beads (Morales-Kastresana et al., 2017; Fortunato et al., 2021; Rautaniemi et al., 2021). Unfortunately, washing always causes some losses of the

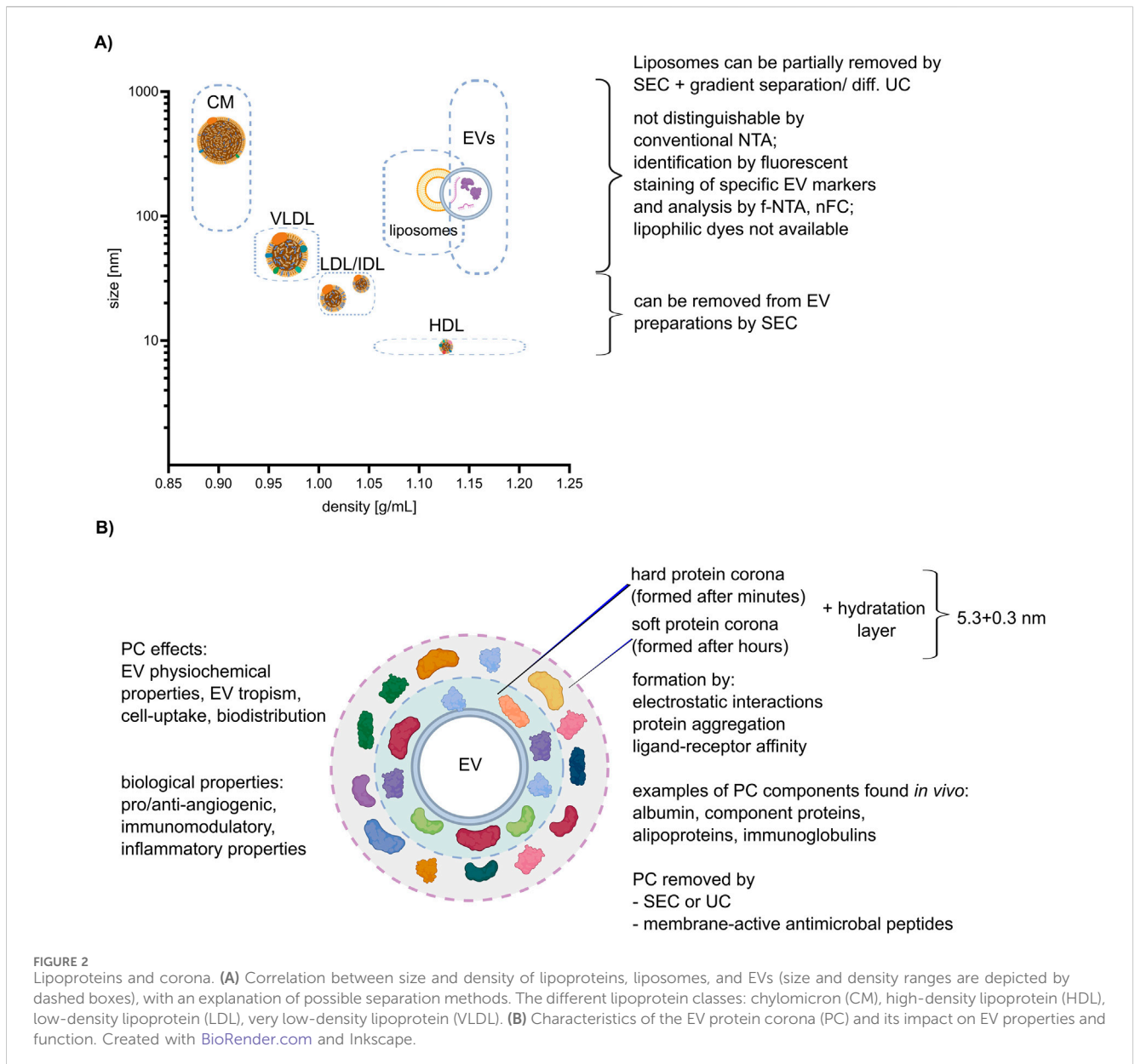
stained material, which is especially problematic in the case of small amount of original sample material (for instance, from biological fluids), and also due to this losses the following quantitative measurement is biased. Moreover, the efficiency of the removal of unbound dyes is strongly dependent on dye properties. Rautniemi et al. concludes that for a good purification the relative purification efficiency ( $E_{rp}$ ; recovery of the EVs divided by the recovery of the dye) should be higher than one (Rautaniemi et al., 2021). The best method of EV purification after labeling found in their work was SEC. However, after purification, stained EVs need to have a sufficiently high fluorescence intensity to be visible in the target application, and in their case, the fluorescence of labeled and purified EVs was too weak to be detected after administration to cells.

In some cases, when the amount of biological sample is very limited, dilution can be performed instead of washing to reduce the background from the unbound dye as much as possible. This is often done in the case of NTA, where the sample has to be strongly diluted to be within the detection range. Detergent lysis controls, buffer controls without EVs, and unstained samples for antibody labeling must be provided even after washing to control for background signal and unspecific staining (Gorgens et al., 2019; Dlugolecka et al., 2021; von Lersner et al., 2024).

## 4 Lipoproteins and corona

Lipoproteins are biochemical complexes of lipids such as triglycerides and phospholipids, with special proteins called apolipoproteins. Their primary function is to transport hydrophobic lipids (also known as fat) in the blood plasma or other extracellular fluids. Plasma lipoproteins are typically divided into five main groups based on their size, lipid composition, and





apolipoprotein content, which are very low-density lipoproteins (VLDLs), intermediate- and low-density lipoproteins (IDLs and LDLs), high-density lipoproteins (HDLs), and chylomicrons (Simonsen, 2017). They outnumber plasma EVs by orders of magnitude and can be co-isolated with EVs during the separation process, leading to potential contamination or interference with the EV staining process as shown on Figure 2A (Chen et al., 2023; Lozano-Andres et al., 2023; Boudna et al., 2024). In conventional light scattering, NTA EVs cannot be distinguished from lipoproteins of similar size. Labeling with lipophilic dyes, as shown recently, will unfortunately not help to distinguish EVs from lipoproteins, since both EVs and lipoproteins are labeled due to their phospholipid membrane. Therefore, lipoproteins affect the accuracy and specificity of labeling (Chen et al., 2023). The most frequently used method for plasma EV separation is SEC (Pang et al.,

2020). It enables the purification of EVs from LDLs and HDLs because of their difference in size, but not from VLDLs and chylomicrons. A combination of SEC and additional gradient separation or differential UC can additionally remove more lipoproteins, although it also lowers the total particle count (Karimi et al., 2018). Notably, in case of plasma sample collection it was proven that, regardless of the chosen EV purification method, it is advisory to collect blood samples in pre-prandial state to reduce lipoproteins contamination (Tushuizen et al., 2012).

The protein corona (PC) is the areola of biomolecules, including proteins and lipids, which form around EVs when they come into contact with biological fluids as shown on Figure 2B (Toth et al., 2021). Those molecules are attached to EVs not covalently but by other interactions, such as hydrogen bonds, van der Waals

interactions, and electrostatic interactions. Varga et al. shows that the thickness of the hydration layer (including PC) can be calculated by combining optical methods like dynamic light scattering (DLS) and NTA, and non-optical methods like microfluidic resistive pulse sensing (MRPS) and very small-angle neutron scattering (VSANS) and is around  $(5.3 \pm 0.3)$  nm (Varga et al., 2020).

The PC can alter the surface properties and size of EVs and impact their interactions with recipient cells (Varga et al., 2020). During the labeling process, the PC may affect the accessibility of the labeling agent to the surface of EV, potentially reducing labeling efficiency or specificity. In addition, some proteins or lipids present in the PC can be labeled, but they are not a physical part of the EV themselves. With standard staining, we cannot distinguish between what is a real EVs surface marker and what is only a component of the corona, and it can be distinguished only after removing it. Yahata et al. claimed that the observed differences between liposome and EVs properties potentially originated from the PC (Yahata et al., 2021).

To remove the PC Singh et al. proposed the use of membrane-active antimicrobial peptides (AMPs). Those AMPs typically have a short sequence (10–50 residues), mostly a net positive charge, and contain ~ 50% hydrophobic residues that make them membrane active (Mangoni et al., 2015; Nayab et al., 2022). They can approach the surface of a lipid bilayer in such a way that associated proteins can be removed from EV surfaces. Comparison of control EVs with AMP-treated samples revealed detachment of proteins adsorbed on the lipid bilayer of EVs (Singh et al., 2020; Singh et al., 2023).

Interestingly, Wolf et al. demonstrated the significant influence of PC removal (by a subsequent process of EV separation using TFF followed by SEC or UCF) on angiogenesis and immunomodulation. Their results showed that these functions are closely linked to the presence of the PC, and once it is removed, these functions are lost (Wolf et al., 2022). Additionally, Toth et al. showed that the labeling results differed greatly depending on the composition of the PC. They incubated medium-sized EVs (100–800 nm in diameter, typically sedimented at  $10,000\text{--}20,000 \times g$ ) isolated from THP-1 cells with EV-depleted blood plasma from patients and then characterized the coated EVs using several methods. Nascent EVs, plasma protein aggregates, nascent EVs incubated with fibrinogen, and annexin V-positive plasma EVs were used as the controls. In addition, the authors demonstrated that EVs with an external plasma protein cargo, in contrast to nascent EVs, induced increased expression of TNF- $\alpha$ , IL-6, CD83, CD86, and HLA-DR in human monocyte-derived dendritic cells (Toth et al., 2021).

Notably, an increasing number of studies suggest that PC and lipoproteins should not always be perceived as contamination but may play an important role in the biological function of EVs, and functional studies should carefully investigate whether isolating EVs from PC is the best solution (Dietz et al., 2023; Liam-Or et al., 2024; Welsh et al., 2024). When researchers plan labeling approaches for their isolated EV samples for functional testing, they need to consider the impact of PC and lipoproteins on their results.

## 5 Development of EV labeling towards medical applications - challenges

The number of studies using fluorescent labeling of EV for the development of future clinical diagnostic or prognostic applications is

increasing exponentially every year. However, many published studies present controversial results or outcomes that are difficult to assess, interpret, and compare with other results. The reason for this is often an incomplete description of the methods and results in manuscripts, an inappropriate experimental design, lack of appropriate calibration and standardization and mistakes in interpreting results—like, for example, considering actual measurement artifacts as “true” EVs. A few years ago, EV researchers proposed a flow-cytometry-specific reporting framework of EV studies that included detailed guidelines regarding methods and data reporting, which will allow a full interpretation and validation of flow cytometry data of EVs (Welsh et al., 2020). These guidelines, although initially referring only to flow cytometry, it can be easily applied to all other EV analysis methods that are based on fluorescent staining. A broad implementation of this reporting framework in experimental practice is necessary for the development of standardized, reliable, and validated fluorescence-based EV analysis methods that can be implemented as clinical diagnostic or prognostic tools in the future.

Although an increasing number of researchers have attempted to follow in their manuscripts the guidelines mentioned above, there are still studies that lack important controls or information about critical variables. In many of these studies, the authors failed to provide all the necessary information for evaluation if all relevant disruptive factors for staining have been appropriately reviewed and assessed. Based on selected examples of reported studies, we briefly discuss the common mistakes and misinterpretations within fluorescent-staining-based EV experiments and propose possible improvements.

In his study, Koksai et al. presented a quantitation of cancer-derived EVs in clinical samples of hepatocellular carcinoma (HCC), based on fluorescent staining of typical HCC markers and subsequent f-NTA analysis (Koksai et al., 2023). The authors showed that by this method they can discriminate between HCC patients and cirrhosis patients, and that the presented EV quantification correlated with the size of the liver tumor assessed by liver imaging. The authors have correctly reported the NTA instrument settings and staining procedures in detail. However, they did not avoid mistakes in experimental design or reporting. The optimization of antibody and dye concentrations was performed only on EVs isolated from the liver cancer cell line Huh7, even though the assay was performed directly in the serum. Admittedly, the authors mentioned in the Methods section that they had also tested several antibody dilutions in serum samples, but they did not show or report any results. It is expected that in the tested serum samples, there will be many proteins and impurities that will impact fluorescent staining and may lead to a much higher number of staining artifacts in comparison to the isolated EV samples from cell culture used for staining optimization. The much higher percentage of membrane-stained particles observed in the serum samples compared to the cell-culture EV-samples implies not necessarily, as interpreted by the authors, a higher EV content, but may be also a sign of unspecific staining due to the serum background. Staining and analysis of appropriate controls, consisting of Huh7-derived EVs spiked into serum samples or EV-free serum samples, would help to evaluate the impact of background staining. The signal linearity and concentration dependence of NTA measurements with serially diluted serum samples are not presented. Additionally, antibody and dye concentrations were reported only as relative

TABLE 3 List of factors that should be considered in the fluorescent analysis of EVs.

Article	Koksal et al. (2023)	Piibor et al. (2023)	Bhagwan Valjee et al. (2024)
Method type	F-NTA	F-NTA	Plasmon resonance
Device name for fluorescence detection	Nanosight, Malvern Panalytical	ZetaView, Particle Metrix	ExoView, NanoView Biosciences
Labeling type	immunospecific, lipophilic	lipophilic	immunospecific
Washing step	+	-	+
Measurement of dye efficiency	-	-	-
Measuring the efficiency of the rinsing step	-	-	-
Stability and intensity of the fluorophore	PE - bright, rapidly photobleached; CellMask -bright, stable for 4 h	CellMask -bright, stable for 4 h	AF488, AF647, AF555 – relatively bright and stable fluorophores
Brightness threshold setting	set on 5 on Nanosight	sensitivity 90, shutter 100, min Brightness 25, frame rate 30 fps (two frames)	no information
Dye concentration	only relative dilution stated, no absolute units; optimized on HCC-derived EVs but not in target serum sample	only relative dilution stated, no absolute units, no information about optimization	adjusted according to the manufacturer's instructions
Temperature	overnight at 4°C with agitation for antibodies; 2 h, RT for CellMask	at RT for 1 h in dark	adjusted according to the manufacturer's instructions
EV purification method	direct labeling of serum, SEC after labeling	TFF, SEC	precipitation
Compounds co-isolated with EVs	lipoproteins, protein aggregates	protein aggregates	lipoproteins, protein aggregates
Assessment of background influence	no information about dye-only, buffer-only controls; staining optimization only on isolated EVs and not directly in serum	no information about dye-only, buffer-only controls	no information about antibody-only, buffer-only controls; immunoaffinity control of an EV-free plasma sample is lacking
Sample concentration	adjusted to $10^4$ – $10^8$ particles/mL	adjusted to $1 \times 10^{10}$ particles/mL	adjusted according to the manufacturer's instructions
Precipitation and centrifugation step during EV preparation	-	+	+
Anticipated Labeling specificity	high for immunolabeling, low for CellMask	low	high
Reported pre-analytical variables	no information about serum collection variables (centrifugation steps, time between blood draw and serum preparation, etc.)	+	no information about plasma collection variables (type of anti-coagulant, centrifugation steps, time between blood draw and plasma preparation, etc.)
Impact on functionality of EVs	not tested	not tested	not tested

dilutions and not in appropriate absolute units, such as mole/L or mg/mL. Furthermore, it was not stated if any antibody/dye-only controls were used to assess background dye staining. It is not clear how the SEC washing step was optimized, especially how EV recovery was evaluated against EV quality performance. The actual fractions that were collected and analyzed after sample application on the given column were not stated. It is not clear why the recovery and quality assessment of the samples after the column wash were analyzed only in scatter mode, which does not provide any information regarding the number of stained EVs. A high particle number in this case may indicate a high impurity content and pure column performance, rather than a high EV recovery. The pre-analytical variables according to serum collection were reported very superficially and did not provide details about the blood collection and centrifugation steps to obtain the serum.

In another study, the authors perform labeling only with the CMG dye and did not check for specificity, staining saturation, or background staining (Piibor et al., 2023). The significantly higher particle concentration of the “Total-NP” fraction after CMG-staining compared to the “EV only” fraction of unlabeled particles measured in the scatter mode may imply the formation of some kind of aggregates (e.g., of CMG) during staining. The possible impact of their presence on NTA measurements in fluorescent mode was not evaluated (e.g., by the measurement of a dye-only sample at the same concentration).

Table 3 presents a summarized list of factors that should be considered in the fluorescence analysis of EVs in selected studies, including those discussed above. Researchers must be cautious when attempting to draw clinical conclusions based on limited information. None of these studies have examined the impact of labeling on EV functionality, which can have a substantial meaning



for clinical outcomes. This table shows that there is still a long road to make solid, evidence-based conclusions from EV-based studies. Substantial dose improvements and additional experiments are required to provide reliable data.

## 6 Study limitations

EV characterization studies are a rapidly growing field, with our understanding of EV biology expanding every year. This study addresses key aspects of fluorescent EV staining for analysis on currently available instruments and discussed in recent publications, although these factors may evolve with the development of new, more sensitive tools capable of easily distinguishing EVs from background and EV detection in biological samples. In addition, our study does not cover non-fluorescent labeling methods, which are also used in EV characterization and are discussed in detail in the Imanbekova study (Imanbekova et al., 2022).

## 7 Summary

Since the recognition that EVs may be promising non-invasive disease indicators, the scientific community has made enormous efforts to develop EV-specific biomarkers for routine clinical use. Diverse high-resolution techniques for single-vesicle analysis have been developed. Soon it has become clear that fluorescent labeling of specific EV markers may be the only way to discriminate EVs in complex, heterogeneous samples and to quantitatively evaluate specific EV populations, often present only in extremely low abundance, for diagnostic and prognostic purposes. Advanced instruments using fluorescence to analyze EVs, such as f-NTA and nFC, allow researchers to gain insights into EVs properties, with each method providing slightly different information.

A wide spectrum of compounds with fluorescent properties have been developed and used to label vesicles. The choice of an appropriate compound should be made consciously because each type has its advantages and disadvantages, allowing for the discovery of different EV properties. Dyes are often not specific only to EVs; the staining efficiency varies greatly depending on the source and composition of EVs, and some compounds may affect the biological functionality of the vesicles. Regardless of the staining methodology and analysis instrument used, appropriate controls are indispensable. Whenever possible, dye removal or dilution steps should be incorporated. A suitable dye removal method is often dye- and EV-specific and must be chosen based on the sample, anticipated EV recovery, quality ratio, and subsequent downstream EV analysis (Rautaniemi et al., 2021).

## References

- Adamo, A., Brandi, J., Caligola, S., Delfino, P., Bazzoni, R., Carusone, R., et al. (2019). Extracellular vesicles mediate mesenchymal stromal cell-dependent regulation of B cell PI3K-akt signaling pathway and actin cytoskeleton. *Front. Immunol.* 10, 446. doi:10.3389/fimmu.2019.00446
- Aibaidula, A. Z., Fain, C. E., Garcia, L. C., Wier, A., Bouchal, S. M., Bauman, M. M., et al. (2023). Spectral flow cytometry identifies distinct nonneoplastic plasma extracellular vesicle phenotype in glioblastoma patients. *Neurooncol Adv.* 5 (1), vdad082. doi:10.1093/oa/njnl/vdad082
- Arifin, D. R., Witwer, K. W., and Bulte, J. W. M. (2022). Non-Invasive imaging of extracellular vesicles: quo vadit in vivo? *J. Extracell. Vesicles* 11 (7), e12241. doi:10.1002/jev2.12241
- Arraud, N., Gounou, C., Turpin, D., and Brisson, A. R. (2016). Fluorescence triggering: a general strategy for enumerating and phenotyping extracellular vesicles by flow cytometry. *Cytom. A* 89 (2), 184–195. doi:10.1002/cyto.a.22669

Furthermore, analysis should be performed with the awareness of the presence of lipoproteins in biological fluids, which are sometimes challenging to distinguish from EVs. One should also consider the impact of the PC of EVs, which affects their properties and may provide additional EV cargo and completely different, additional biological functions.

Currently, there is an increasing number of publications utilizing EV staining for clinical purposes, including their use as biomarkers. Therefore, it is important for the authors of such studies to be aware of the limitations of the used instruments staining protocols and dyes. This will ensure that their results can be properly interpreted and will have true clinical value in expanding our understanding of EV biology.

## Author contributions

MD: Conceptualization, Funding acquisition, Investigation, Software, Visualization, Writing—original draft, Writing—review and editing. MC-K: Conceptualization, Funding acquisition, Project administration, Supervision, Writing—original draft, Writing—review and editing.

## Funding

The author(s) declare that financial support was received for the research, authorship, and/or publication of this article. National Science Centre - OPUS14 2017/27/B/NZ6/01990; NAWA BPI/PST/2021/1/00071/U/00001; Medical University of Warsaw 1WK/2/M/MB/N/22/22.

## Conflict of interest

The authors declare that the research was conducted in the absence of any commercial or financial relationships that could be construed as a potential conflict of interest.

## Publisher's note

All claims expressed in this article are solely those of the authors and do not necessarily represent those of their affiliated organizations, or those of the publisher, the editors and the reviewers. Any product that may be evaluated in this article, or claim that may be made by its manufacturer, is not guaranteed or endorsed by the publisher.

- Avci, O., Unlu, N. L., Ozkumur, A. Y., and Unlu, M. S. (2015). Interferometric reflectance imaging sensor (IRIS)--A platform technology for multiplexed diagnostics and digital detection. *Sensors (Basel)* 15 (7), 17649–17665. doi:10.3390/s150717649
- Bachurski, D., Schuldner, M., Nguyen, P. H., Malz, A., Reiners, K. S., Grenzi, P. C., et al. (2019). Extracellular vesicle measurements with nanoparticle tracking analysis - an accuracy and repeatability comparison between NanoSight NS300 and ZetaView. *J. Extracell. Vesicles* 8 (1), 1596016. doi:10.1080/20013078.2019.1596016
- Bagci, C., Sever-Bahcekapili, M., Belder, N., Bennett, A. P. S., Erdener, S. E., and Dalkara, T. (2022). Overview of extracellular vesicle characterization techniques and introduction to combined reflectance and fluorescence confocal microscopy to distinguish extracellular vesicle subpopulations. *Neurophotonics* 9 (2), 021903. doi:10.1117/1.NPh.9.2.021903
- Bao, C., Xiang, H., Chen, Q., Zhao, Y., Gao, Q., Huang, F., et al. (2023). A review of labeling approaches used in small extracellular vesicles tracing and imaging. *Int. J. Nanomedicine* 18, 4567–4588. doi:10.2147/IJN.S416131
- Barrachina, F., Battistone, M. A., Castillo, J., Mallofre, C., Jodar, M., Breton, S., et al. (2022). Sperm acquire epididymis-derived proteins through epididymosomes. *Hum. Reprod.* 37 (4), 651–668. doi:10.1093/humrep/deac015
- Bhagwan Valjee, R., Mackraj, I., Moodley, R., and Ibrahim, U. H. (2024). Investigation of exosomal tetraspanin profile in sepsis patients as a promising diagnostic biomarker. *Biomarkers* 29 (2), 78–89. doi:10.1080/1354750X.2024.2319296
- Botha, J., Pugsley, H. R., and Handberg, A. (2021). Conventional, high-resolution and imaging flow cytometry: benchmarking performance in characterisation of extracellular vesicles. *Biomedicine* 9 (2), 124. doi:10.3390/biomedicine9020124
- Boudna, M., Campos, A. D., Vychytilova-Faltejskova, P., Machackova, T., Slaby, O., and Souckova, K. (2024). Strategies for labelling of exogenous and endogenous extracellular vesicles and their application for *in vitro* and *in vivo* functional studies. *Cell Commun. Signal* 22 (1), 171. doi:10.1186/s12964-024-01548-3
- Breitwieser, K., Koch, L. F., Tertel, T., Proestler, E., Burgers, L. D., Lipps, C., et al. (2022). Detailed characterization of small extracellular vesicles from different cell types based on tetraspanin composition by ExoView R100 platform. *Int. J. Mol. Sci.* 23 (15), 8544. doi:10.3390/ijms23158544
- Cha, M., Jeong, S. H., Bae, S., Park, J. H., Baeg, Y., Han, D. W., et al. (2023). Efficient labeling of vesicles with lipophilic fluorescent dyes via the salt-change method. *Anal. Chem.* 95 (14), 5843–5849. doi:10.1021/acs.analchem.2c05166
- Chambers, M. G., McNamara, R. P., and Dittmer, D. P. (2021). Direct stochastic optical reconstruction microscopy of extracellular vesicles in three dimensions. *JoVE* 174, e62845. doi:10.3791/62845
- Chen, C., Cai, N., Niu, Q., Tian, Y., Hu, Y., and Yan, X. (2023). Quantitative assessment of lipophilic membrane dye-based labelling of extracellular vesicles by nano-flow cytometry. *J. Extracell. Vesicles* 12 (8), e12351. doi:10.1002/jev2.12351
- Chong, M. C., Silva, A., James, P. F., Wu, S. S. X., and Howitt, J. (2022). Exercise increases the release of NAMPT in extracellular vesicles and alters NAD(+) activity in recipient cells. *Aging Cell* 21 (7), e13647. doi:10.1111/accel.13647
- Collet, M., Ashokkumar, P., Anton, H., Boutant, E., Faklaris, O., Galli, T., et al. (2019). MemBright: a family of fluorescent membrane probes for advanced cellular imaging and neuroscience. *Cell Chem. Biol.* 26 (4), 600–614.e7. doi:10.1016/j.chembiol.2019.01.009
- Colombo, M., Raposo, G., and Thery, C. (2014). Biogenesis, secretion, and intercellular interactions of exosomes and other extracellular vesicles. *Annu. Rev. Cell Dev. Biol.* 30, 255–289. doi:10.1146/annurev-cellbio-101512-122326
- Corso, G., Heusermann, W., Trojer, D., Gorgens, A., Steib, E., Voshol, J., et al. (2019). Systematic characterization of extracellular vesicle sorting domains and quantification at the single molecule - single vesicle level by fluorescence correlation spectroscopy and single particle imaging. *J. Extracell. Vesicles* 8 (1), 1663043. doi:10.1080/20013078.2019.1663043
- Daaboul, G. G., Gagni, P., Benussi, L., Bettotti, P., Ciani, M., Cretich, M., et al. (2016). Digital detection of exosomes by interferometric imaging. *Sci. Rep.* 6, 37246. doi:10.1038/srep37246
- Dehghani, M., Gulvin, S. M., Flax, J., and Gaborski, T. R. (2020). Systematic evaluation of PKH labelling on extracellular vesicle size by nanoparticle tracking analysis. *Sci. Rep.* 10 (1), 9533. doi:10.1038/s41598-020-66434-7
- Desgeorges, A., Hollerweger, J., Lassacher, T., Rohde, E., Helmbrecht, C., and Gimona, M. (2020). Differential fluorescence nanoparticle tracking analysis for enumeration of the extracellular vesicle content in mixed particulate solutions. *Methods* 177, 67–73. doi:10.1016/j.jmeth.2020.02.006
- Deumer, J., Schurmann, R., Gaal, A., Varga, Z., Bettin, B., van der Pol, E., et al. (2024). Traceable characterization of hollow organosilica beads as potential reference materials for extracellular vesicle measurements with optical techniques. *Discov. Nano* 19 (1), 14. doi:10.1186/s11671-024-03956-3
- Dietz, L., Oberlander, J., Mateos-Maroto, A., Schunke, J., Fichter, M., Kramer-Albers, E. M., et al. (2023). Uptake of extracellular vesicles into immune cells is enhanced by the protein corona. *J. Extracell. Vesicles* 12 (12), e12399. doi:10.1002/jev2.12399
- Długolecka, M., Szymanski, J., Zareba, L., Homonick, Z., Domagala-Kulawik, J., Polubiec-Kownacka, M., et al. (2021). Characterization of extracellular vesicles from bronchoalveolar lavage fluid and plasma of patients with lung lesions using fluorescence nanoparticle tracking analysis. *Cells* 10 (12), 3473. doi:10.3390/cells10123473
- Dragovic, R. A., Gardiner C Fau - Brooks, A. S., Brooks As Fau - Tannetta, D. S., Tannetta Ds Fau - Ferguson, D. J. P., Ferguson Dj Fau - Hole, P., Hole P Fau - Carr, B., et al. (2011). *Sizing and phenotyping of cellular vesicles using Nanoparticle Tracking Analysis*, 1549–9642. (Electronic).
- Droste, M., Tertel, T., Jeruschke, S., Dittrich, R., Kontopoulou, E., Walkenfort, B., et al. (2021). Single extracellular vesicle analysis performed by imaging flow cytometry and nanoparticle tracking analysis evaluate the accuracy of urinary extracellular vesicle preparation techniques differently. *Int. J. Mol. Sci.* 22 (22), 12436. doi:10.3390/ijms222212436
- Endesfelder, U., and Heilemann, M. (2015). “Direct stochastic optical reconstruction microscopy (dSTORM),” in *Advanced fluorescence microscopy: methods and protocols*. Editor P. J. Verwee, (New York, NY: Springer), 263–276.
- Ferguson, S., Yang, K. S., Zelga, P., Liss, A. S., Carlson, J. C. T., Del Castillo, C. F., et al. (2022). Single-EV analysis (sEVA) of mutated proteins allows detection of stage 1 pancreatic cancer. *Sci. Adv.* 8 (16), eabm3453. doi:10.1126/sciadv.abm3453
- Filipe, V., Hawe, A., and Jiskoot, W. (2010). Critical evaluation of Nanoparticle Tracking Analysis (NTA) by NanoSight for the measurement of nanoparticles and protein aggregates. *Pharm. Res.* 27 (5), 796–810. doi:10.1007/s11095-010-0073-2
- Fortunato, D., Giannoukakis, S., Gimenez-Capitan, A., Hackenberg, M., Molina-Vila, M. A., and Zarovni, N. (2022). Selective isolation of extracellular vesicles from minimally processed human plasma as a translational strategy for liquid biopsies. *Biomark. Res.* 10 (1), 57. doi:10.1186/s40364-022-00404-1
- Fortunato, D., Mladenovic, D., Criscuoli, M., Loria, F., Veiman, K. L., Zocco, D., et al. (2021). Opportunities and pitfalls of fluorescent labeling methodologies for extracellular vesicle profiling on high-resolution single-particle platforms. *Int. J. Mol. Sci.* 22 (19), 10510. doi:10.3390/ijms221910510
- Gardiner, C., Shaw, M., Hole, P., Smith, J., Tannetta, D., Redman, C. W., et al. (2014). Measurement of refractive index by nanoparticle tracking analysis reveals heterogeneity in extracellular vesicles. *J. Extracell. Vesicles* 3, 25361. doi:10.3402/jev.v3.25361
- George, S. K., Laukova, L., Weiss, R., Semak, V., Fendl, B., Weiss, V. U., et al. (2021). Comparative analysis of platelet-derived extracellular vesicles using flow cytometry and nanoparticle tracking analysis. *Int. J. Mol. Sci.* 22 (8), 3839. doi:10.3390/ijms22083839
- Gomes, J., Lucien, F., Cooper, T. T., Kim, Y., Williams, K. C., Liao, X., et al. (2018). Analytical considerations of nanoscale flow cytometry of extracellular vesicles to achieve data linearity. *Thromb. Haemost.* 118 (9), 1612–1624. doi:10.1055/s-0038-1668544
- Gorgens, A., Bremer, M., Ferrer-Tur, R., Murke, F., Tertel, T., Horn, P. A., et al. (2019). Optimisation of imaging flow cytometry for the analysis of single extracellular vesicles by using fluorescence-tagged vesicles as biological reference material. *J. Extracell. Vesicles* 8 (1), 1587567. doi:10.1080/20013078.2019.1587567
- Gray, W. D., Mitchell, A. J., and Searles, C. D. (2015). An accurate, precise method for general labeling of extracellular vesicles. *MethodsX* 2, 360–367. doi:10.1016/j.mex.2015.08.002
- Gul, B., Syed, F., Khan, S., Iqbal, A., and Ahmad, I. (2022). Characterization of extracellular vesicles by flow cytometry: challenges and promises. *Micron* 161, 103341. doi:10.1016/j.micron.2022.103341
- Hajji, N., Hau, C. M., Nieuwland, R., and van der Pol, E. (2022). “Protocol for measuring concentrations of extracellular vesicles in human blood plasma with flow cytometry,” in *Extracellular vesicles in diagnosis and therapy*. Editors M. Federico, and B. Ridolfi, (New York, NY: Springer US), 55–75.
- Hoover, B. M., and Murphy, R. M. (2020). Evaluation of nanoparticle tracking analysis for the detection of rod-shaped particles and protein aggregates. *J. Pharm. Sci.* 109 (1), 452–463. doi:10.1016/j.xphs.2019.10.006
- Imanbekova, M., Suarasan, S., Lu, Y., Jurchuk, S., and Wachsmann-Hogiu, S. (2022). Recent advances in optical label-free characterization of extracellular vesicles. *Nanophotonics* 11 (12), 2827–2863. doi:10.1515/nanoph-2022-0057
- Johnson, J., Law, S. Q. K., Shojaae, M., Hall, A. S., Bhuiyan, S., Lim, M. B. L., et al. (2023). First-in-human clinical trial of allogeneic, platelet-derived extracellular vesicles as a potential therapeutic for delayed wound healing. *J. Extracell. Vesicles* 12 (7), e12332. doi:10.1002/jev2.12332
- Kamei, N., Nishimura, H., Matsumoto, A., Asano, R., Muranaka, K., Fujita, M., et al. (2021). Comparative study of commercial protocols for high recovery of high-purity mesenchymal stem cell-derived extracellular vesicle isolation and their efficient labeling with fluorescent dyes. *Nanomedicine* 35, 102396. doi:10.1016/j.nano.2021.102396
- Karimi, N., Cvjetkovic, A., Jang, S. C., Crescitelli, R., Hosseinpour Feizi, M. A., Nieuwland, R., et al. (2018). Detailed analysis of the plasma extracellular vesicle proteome after separation from lipoproteins. *Cell Mol. Life Sci.* 75 (15), 2873–2886. doi:10.1007/s00018-018-2773-4
- Kashkanova, A. D., Blessing, M., Gemeinhardt, A., Soulat, D., and Sandoghdar, V. (2022). Precision size and refractive index analysis of weakly scattering nanoparticles in polydispersions. *Nat. Methods* 19 (5), 586–593. doi:10.1038/s41592-022-01460-z
- Koksai, A. R., Ekmen, N., Aydin, Y., Nunez, K., Sandow, T., Delk, M., et al. (2023). A single-step immunocapture assay to quantify HCC exosomes using the highly sensitive fluorescence nanoparticle-tracking analysis. *J. Hepatocell. Carcinoma* 10, 1935–1954. doi:10.2147/JHC.S423043

- Kuiper, M., van de Nes, A., Nieuwland, R., Varga, Z., and van der Pol, E. (2021). Reliable measurements of extracellular vesicles by clinical flow cytometry. *Am. J. Reprod. Immunol.* 85 (2), e13350. doi:10.1111/aji.13350
- Liam-Or, R., Faruq, F. N., Walters, A., Han, S., Xu, L., Wang, J. T., et al. (2024). Cellular uptake and *in vivo* distribution of mesenchymal-stem-cell-derived extracellular vesicles are protein corona dependent. *Nanotechnol.* 19 (6), 846–855. doi:10.1038/s41565-023-01585-y
- Lian, H., He, S., Chen, C., and Yan, X. (2019). Flow cytometric analysis of nanoscale biological particles and organelles. *Rev. Anal. Chem. (Palo Alto Calif.)* 12 (1), 389–409. doi:10.1146/annurev-anchem-061318-115042
- Libregts, S., Arksteijn, G. J. A., Nemeth, A., Nolte- $\dot{t}$  Hoen, E. N. M., and Wauben, M. H. M. (2018). Flow cytometric analysis of extracellular vesicle subsets in plasma: impact of swarm by particles of non-interest. *J. Thromb. Haemost.* 16 (7), 1423–1436. doi:10.1111/jth.14154
- Liebel, M., Ortega Arroyo, J., Beltran, V. S., Osmond, J., Jo, A., Lee, H., et al. (2020). 3D tracking of extracellular vesicles by holographic fluorescence imaging. *Sci. Adv.* 6 (45), eabc2508. doi:10.1126/sciadv.abc2508
- Loconte, L., Arguedas, D., El, R., Zhou, A., Chipont, A., Guyonnet, L., et al. (2023). Detection of the interactions of tumour derived extracellular vesicles with immune cells is dependent on EV-labelling methods. *J. Extracell. Vesicles* 12 (12), e12384. doi:10.1002/jev.12384
- Lopez-Pacheco, C., Bedoya-Lopez, A., Olguin-Alor, R., and Soldevila, G. (2021). Analysis of tumor-derived exosomes by nanoscale flow cytometry. *Methods Mol. Biol.* 2174, 171–191. doi:10.1007/978-1-0716-0759-6\_11
- Lozano-Andres, E., Enciso-Martinez, A., Gijbsbers, A., Ridolfi, A., Van Niel, G., Libregts, S., et al. (2023). Physical association of low density lipoprotein particles and extracellular vesicles unveiled by single particle analysis. *J. Extracell. Vesicles* 12 (11), e12376. doi:10.1002/jev.12376
- Malloy, A., and Carr, B. (2006). NanoParticle tracking analysis – the Halo™ system. *Part. and Part. Syst. Charact.* 23 (2), 197–204. doi:10.1002/ppsc.200601031
- Mangoni, M. L., Luca, V., and McDermott, A. M. (2015). Fighting microbial infections: a lesson from amphibian skin-derived esculentin-1 peptides. *Peptides* 71, 286–295. doi:10.1016/j.peptides.2015.04.018
- McNicholas, K., Li, J. Y., Michael, M. Z., and Gleadle, J. M. (2017). Albuminuria is not associated with elevated urinary vesicle concentration but can confound nanoparticle tracking analysis. *Nephrol. Carl.* 22 (11), 854–863. doi:10.1111/nep.12867
- Melling, G. E., Conlon, R., Pantazi, P., Dellar, E. R., Samuel, P., Baena-Lopez, L. A., et al. (2022). Confocal microscopy analysis reveals that only a small proportion of extracellular vesicles are successfully labelled with commonly utilised staining methods. *Sci. Rep.* 12 (1), 262. doi:10.1038/s41598-021-04225-4
- Midekessa, G., Godakumara, K., Dissanayake, K., Hasan, M. M., Reshi, Q. U. A., Rinken, T., et al. (2021). Characterization of extracellular vesicles labelled with a lipophilic dye using fluorescence nanoparticle tracking analysis. *Membr. (Basel)* 11 (10), 779. doi:10.3390/membranes11100779
- Midtvedt, D., Eklund, F., Olsen, E., Midtvedt, B., Swenson, J., and Hook, F. (2020). Size and refractive index determination of subwavelength particles and air bubbles by holographic nanoparticle tracking analysis. *Anal. Chem.* 92 (2), 1908–1915. doi:10.1021/acs.analchem.9b04101
- Mizenko, R. R., Brostoff, T., Rojalin, T., Koster, H. J., Swindell, H. S., Leiserowitz, G. S., et al. (2021). Tetraspanins are unevenly distributed across single extracellular vesicles and bias sensitivity to multiplexed cancer biomarkers. *J. Nanobiotechnology* 19 (1), 250. doi:10.1186/s12951-021-00987-1
- Morales-Kastresana, A., Musich, T. A., Welsh, J. A., Telford, W., Demberg, T., Wood, J. C. S., et al. (2019). High-fidelity detection and sorting of nanoscale vesicles in viral disease and cancer. *J. Extracell. Vesicles* 8 (1), 1597603. doi:10.1080/20013078.2019.1597603
- Morales-Kastresana, A., Telford, B., Musich, T. A., McKinnon, K., Clayborne, C., Braig, Z., et al. (2017). Labeling extracellular vesicles for nanoscale flow cytometry. *Sci. Rep.* 7 (1), 1878. doi:10.1038/s41598-017-01731-2
- Morey, A., Ng, M., Spanos, M., Zhang, P., Xu, T., Cheung, W., et al. (2024). The EV antibody database: an interactive database of curated antibodies for extracellular vesicle and nanoparticle research. *Extracell. Vesicle* 3, 100040. doi:10.1016/j.vesic.2024.100040
- Nayab, S., Aslam, M. A., Rahman, S. u., Sindhu, Z. u.D., Sajid, S., Zafar, N., et al. (2022). A review of antimicrobial peptides: its function, mode of action and therapeutic potential. *Int. J. Peptide Res. Ther.* 28 (1), 46. doi:10.1007/s10989-021-10325-6
- Nazarenko, I., Rupp, A.-K., and Altevogt, P. (2013). “Exosomes as a potential tool for a specific delivery of functional molecules,” in *Ovarian cancer: methods and protocols*. Editors A. Malek, and O. Tchernitsa, (Totowa, NJ: Humana Press), 495–511.
- Nolte- $\dot{t}$  Hoen, E. N., van der Vlist, E. J., Aalberts, M., Mertens, H. C., Bosch, B. J., Bartelink, W., et al. (2012). Quantitative and qualitative flow cytometric analysis of nanosized cell-derived membrane vesicles. *Nanomedicine* 8 (5), 712–720. doi:10.1016/j.nano.2011.09.006
- Padda, R. S., Deng, F. K., Brett, S. I., Biggs, C. N., Durfee, P. N., Brinker, C. J., et al. (2019). Nanoscale flow cytometry to distinguish subpopulations of prostate extracellular vesicles in patient plasma. *Prostate* 79 (6), 592–603. doi:10.1002/pros.23764
- Pang, B., Zhu, Y., Ni, J., Ruan, J., Thompson, J., Malouf, D., et al. (2020). Quality assessment and comparison of plasma-derived extracellular vesicles separated by three commercial kits for prostate cancer diagnosis. *Int. J. Nanomedicine* 15, 10241–10256. doi:10.2147/IJN.S283106
- Piibor, J., Dissanayake, K., Midekessa, G., Andronowska, A., Kavak, A., Waldmann, A., et al. (2023). Characterization of bovine uterine fluid extracellular vesicles proteomic profiles at follicular and luteal phases of the oestrous cycle. *Vet. Res. Commun.* 47 (2), 885–900. doi:10.1007/s11259-022-10052-3
- Popena, I., Abols, A., Saulite, L., Pleiko, K., Zandberga, E., Jekabsons, K., et al. (2018). Effect of colorectal cancer-derived extracellular vesicles on the immunophenotype and cytokine secretion profile of monocytes and macrophages. *Cell Commun. Signal* 16 (1), 17. doi:10.1186/s12964-018-0229-y
- Puzar Dominkus, P., Stenovec, M., Sitar, S., Lasic, E., Zorec, R., Plemenitas, A., et al. (2018). PKH26 labeling of extracellular vesicles: characterization and cellular internalization of contaminating PKH26 nanoparticles. *Biochim. Biophys. Acta Biomembr.* 1860 (6), 1350–1361. doi:10.1016/j.bbmem.2018.03.013
- Rautaniemi, K., Zini, J., Lofman, E., Saari, H., Haapalehto, I., Laukka, J., et al. (2021). Addressing challenges in the removal of unbound dye from passively labelled extracellular vesicles. *Nanoscale Adv.* 4 (1), 226–240. doi:10.1039/d1na00755f
- Reginald-Opara, J. N., Svirskis, D., Paek, S. Y., Tang, M., O’Carroll, S. J., Dean, J. M., et al. (2022). The involvement of extracellular vesicles in the transcytosis of nanoliposomes through brain endothelial cells, and the impact of liposomal pH-sensitivity. *Mater Today Bio* 13, 100212. doi:10.1016/j.mtbio.2022.100212
- Roberts-Dalton, H. D., Cocks A Fau - Falcon-Perez, J. M., Falcon-Perez Jm Fau - Sayers, E. J., Sayers Ej Fau - Webber, J. P., Webber Jp Fau - Watson, P., Watson P Fau - Clayton, A., et al. (2017). Fluorescence labelling of extracellular vesicles using a novel thiol-based strategy for quantitative analysis of cellular delivery and intracellular traffic. *Nanoscale* 9 (36), 13693–13706. doi:10.1039/c7nr04128d
- Rodriguez, B. V., Wen, Y., Shirk, E. N., Vazquez, S., Gololobova, O., Maxwell, A., et al. (2023). An *ex vivo* model of interactions between extracellular vesicles and peripheral mononuclear blood cells in whole blood. *J. Extracell. Vesicles* 12 (12), e12368. doi:10.1002/jev.12368
- Roseborough, A. D., Myers, S. J., Khazae, R., Zhu, Y., Zhao, L., Iorio, E., et al. (2023). Plasma derived extracellular vesicle biomarkers of microglia activation in an experimental stroke model. *J. Neuroinflammation* 20 (1), 20. doi:10.1186/s12974-023-02708-x
- Saari, H., Lisitsyna, E., Rautaniemi, K., Rojalin, T., Niemi, L., Nivaro, O., et al. (2018). FLIM reveals alternative EV-mediated cellular up-take pathways of paclitaxel. *J. Control Release* 284, 133–143. doi:10.1016/j.jconrel.2018.06.015
- Salaga-Zaleska, K., Kuchta, A., Bzoma, B., Chyla-Danil, G., Safianowska, A., Ploska, A., et al. (2023). Nanoparticle tracking analysis of urinary extracellular vesicle proteins as a new challenge in laboratory medicine. *Int. J. Mol. Sci.* 24 (15), 12228. doi:10.3390/ijms241512228
- Salmond, N., Khanna, K., Owen, G. R., and Williams, K. C. (2021). Nanoscale flow cytometry for immunophenotyping and quantitating extracellular vesicles in blood plasma. *Nanoscale* 13 (3), 2012–2025. doi:10.1039/d0nr05525e
- Schwartz, A., Wang, L., Early, E., Gaigalas, A., Zhang, Y. Z., Marti, G. E., et al. (2002). Quantitating fluorescence intensity from fluorophore: the definition of MESF assignment. *J. Res. Natl. Inst. Stand Technol.* 107 (1), 83–91. doi:10.6028/jres.107.009
- Simonsen, J. B. (2017). What are we looking at? Extracellular vesicles, lipoproteins, or both? *Circ. Res.* 121 (8), 920–922. doi:10.1161/CIRCRESAHA.117.311767
- Singh, P., Szzygarto, I. C., Ricci, M., Gaal, A., Queme-Pena, M. M., Kitka, D., et al. (2023). Removal and identification of external protein corona members from RBC-derived extracellular vesicles by surface manipulating antimicrobial peptides. *J. Extracell. Biol.* 2 (3), e78. doi:10.1002/jex.278
- Singh, P., Szzygarto, I. C., Ricci, M., Zsila, F., Juhász, T., Mihály, J., et al. (2020). Membrane active peptides remove surface adsorbed protein corona from extracellular vesicles of red blood cells. *Front. Chem.* 8, 703. doi:10.3389/fchem.2020.00703
- Snyder, O. L., Campbell, A. W., Christenson, L. K., and Weiss, M. L. (2021). Improving reproducibility to meet minimal information for studies of extracellular vesicles 2018 guidelines in nanoparticle tracking analysis. *J. Vis. Exp.* 177. doi:10.3791/63059
- Song, P., Anna, B., G. E. S., and Chamley, L. W. (2023). The interaction of placental micro-EVs with immune cells *in vivo* and *in vitro*. *Am. J. Reprod. Immunol.* 90 (3), e13766. doi:10.1111/aji.13766
- Spitzberg, J. D., Ferguson, S., Yang, K. S., Peterson, H. M., Carlson, J. C. T., and Weissleder, R. (2023). Multiplexed analysis of EV reveals specific biomarker composition with diagnostic impact. *Nat. Commun.* 14 (1), 1239. doi:10.1038/s41467-023-36932-z
- Stoner, S. A., Duggan, E., Condello, D., Guerrero, A., Turk, J. R., Narayanan, P. K., et al. (2016). High sensitivity flow cytometry of membrane vesicles. *Cytom. A* 89 (2), 196–206. doi:10.1002/cyto.a.22787
- Tertel, T., Bremer, M., Maire, C., Lamszus, K., Peine, S., Jawad, R., et al. (2020). High-resolution imaging flow cytometry reveals impact of incubation temperature on labeling of extracellular vesicles with antibodies. *Cytom. A* 97 (6), 602–609. doi:10.1002/cyto.a.24034

- Tertel, T., Schoppet, M., Stambouli, O., Al-Jipouri, A., James, P. F., and Giebel, B. (2022). Imaging flow cytometry challenges the usefulness of classically used extracellular vesicle labeling dyes and qualifies the novel dye Exoria for the labeling of mesenchymal stromal cell-extracellular vesicle preparations. *Cytotherapy* 24 (6), 619–628. doi:10.1016/j.jcyt.2022.02.003
- Thane, K. E., Davis, A. M., and Hoffman, A. M. (2019). Improved methods for fluorescent labeling and detection of single extracellular vesicles using nanoparticle tracking analysis. *Sci. Rep.* 9 (1), 12295. doi:10.1038/s41598-019-48181-6
- Tong, M., Chen, Q., James, J. L., Wise, M. R., Stone, P. R., and Chamley, L. W. (2017). *In vivo* targets of human placental micro-vesicles vary with exposure time and pregnancy. *Reproduction* 153 (6), 835–845. doi:10.1530/REP-16-0615
- Toth, E. A., Turiak, L., Visnovitz, T., Cserep, C., Mazlo, A., Sodar, B. W., et al. (2021). Formation of a protein corona on the surface of extracellular vesicles in blood plasma. *J. Extracell. Vesicles* 10 (11), e12140. doi:10.1002/jev2.12140
- Tushuizen, M. E., Diamant, M., Peypers, E. G., Hoek, F. J., Heine, R. J., Sturk, A., et al. (2012). Postprandial changes in the phospholipid composition of circulating nanoparticles are not associated with coagulation activation. *Thromb. Res.* 130 (1), 115–121. doi:10.1016/j.thromres.2011.09.003
- van der Pol, E., Coumans, F. A., Sturk, A., Nieuwland, R., and van Leeuwen, T. G. (2014). Refractive index determination of nanoparticles in suspension using nanoparticle tracking analysis. *Nano Lett.* 14 (11), 6195–6201. doi:10.1021/nl503371p
- van der Pol, E., Welsh, J. A., and Nieuwland, R. (2022). Minimum information to report about a flow cytometry experiment on extracellular vesicles: communication from the ISTH SSC subcommittee on vascular biology. *J. Thromb. Haemost.* 20 (1), 245–251. doi:10.1111/jth.15540
- van der Vlist, E. J., Nolte-'t Hoen, E. N., Stoorvogel, W., Arkesteijn, G. J., and Wauben, M. H. (2012). Fluorescent labeling of nano-sized vesicles released by cells and subsequent quantitative and qualitative analysis by high-resolution flow cytometry. *Nat. Protoc.* 7 (7), 1311–1326. doi:10.1038/nprot.2012.065
- Varga, Z., Feher, B., Kitka, D., Wacha, A., Bota, A., Berenyi, S., et al. (2020). Size measurement of extracellular vesicles and synthetic liposomes: the impact of the hydration shell and the protein corona. *Colloids Surf. B Biointerfaces* 192, 111053. doi:10.1016/j.colsurfb.2020.111053
- von Lersner, A. K., Fernandes, F., Ozawa, P. M. M., Jackson, M., Masureel, M., Ho, H., et al. (2024). Multiparametric single-vesicle flow cytometry resolves extracellular vesicle heterogeneity and reveals selective regulation of biogenesis and cargo distribution. *ACS Nano* 18 (15), 10464–10484. doi:10.1021/acsnano.3c11561
- Voss, S. C., Yassin, M., Grivel, J. C., Al Hmissi, S., Allahverdi, N., Nashwan, A., et al. (2022). Red blood cell derived extracellular vesicles during the process of autologous blood doping. *Drug Test. Anal.* 14 (11–12), 1984–1994. doi:10.1002/dta.3157
- Wan, Y., Cheng, G., Liu, X., Hao, S. J., Nisic, M., Zhu, C. D., et al. (2017). Rapid magnetic isolation of extracellular vesicles via lipid-based nanoprobes. *Nat. Biomed. Eng.* 1, 0058. doi:10.1038/s41551-017-0058
- Welsh, J. A., Arkesteijn, G. J. A., Bremer, M., Cimorelli, M., Dignat-George, F., Giebel, B., et al. (2023). A compendium of single extracellular vesicle flow cytometry. *J. Extracell. Vesicles* 12 (2), e12299. doi:10.1002/jev2.12299
- Welsh, J. A., Goberdhan, D. C. I., O'Driscoll, L., Buzas, E. I., Blenkiron, C., Bussolati, B., et al. (2024). Minimal information for studies of extracellular vesicles (MISEV2023): from basic to advanced approaches. *J. Extracell. Vesicles* 13 (2), e12404. doi:10.1002/jev2.12404
- Welsh, J. A., Killingsworth, B., Kepley, J., Traynor, T., McKinnon, K., Savage, J., et al. (2021). A simple, high-throughput method of protein and label removal from extracellular vesicle samples. *Nanoscale* 13 (6), 3737–3745. doi:10.1039/d0nr07830a
- Welsh, J. A., Van Der Pol, E., Arkesteijn, G. J. A., Bremer, M., Brisson, A., Coumans, F., et al. (2020). MIFlowCyt-EV: a framework for standardized reporting of extracellular vesicle flow cytometry experiments. *J. Extracell. Vesicles* 9 (1), 1713526. doi:10.1080/20013078.2020.1713526
- Wolf, M., Poupardin, R. W., Ebner-Peking, P., Andrade, A. C., Blochl, C., Obermayer, A., et al. (2022). A functional corona around extracellular vesicles enhances angiogenesis, skin regeneration and immunomodulation. *J. Extracell. Vesicles* 11 (4), e12207. doi:10.1002/jev2.12207
- Woud, W. W., van der Pol, E., Mul, E., Hoogduijn, M. J., Baan, C. C., Boer, K., et al. (2022). An imaging flow cytometry-based methodology for the analysis of single extracellular vesicles in unprocessed human plasma. *Commun. Biol.* 5 (1), 633. doi:10.1038/s42003-022-03569-5
- Wu, L., Woud, W. W., Baan, C. C., Hesselink, D. A., van der Pol, E., Jenster, G., et al. (2023). Isolation-free measurement of single urinary extracellular vesicles by imaging flow cytometry. *Nanomedicine* 48, 102638. doi:10.1016/j.nano.2022.102638
- Yahata, S., Hirose, M., Ueno, T., Nagumo, H., and Sakai-Kato, K. (2021). Effect of sample concentration on nanoparticle tracking analysis of small extracellular vesicles and liposomes mimicking the physicochemical properties of exosomes. *Chem. Pharm. Bull. (Tokyo)* 69 (11), 1045–1053. doi:10.1248/cpb.c21-00452
- Zhang, Z., Yu, K., You, Y., Jiang, P., Wu, Z., DeTure, M. A., et al. (2023). Comprehensive characterization of human brain-derived extracellular vesicles using multiple isolation methods: implications for diagnostic and therapeutic applications. *J. Extracell. Vesicles* 12 (8), e12358. doi:10.1002/jev2.12358
- Zheng, W., Schurz, M., Wiklander, R. J., Gustafsson, O., Gupta, D., Slovak, R., et al. (2023). Surface display of functional moieties on extracellular vesicles using lipid anchors. *J. Control Release* 357, 630–640. doi:10.1016/j.jconrel.2023.04.033
- Zhou, X., Zhang, J., Song, Z., Lu, S., Yu, Y., Tian, J., et al. (2020). ExoTracker: a low-pH-activatable fluorescent probe for labeling exosomes and monitoring endocytosis and trafficking. *Chem. Commun. (Camb)* 56 (94), 14869–14872. doi:10.1039/d0cc06208a



## Podsumowanie i wnioski

W pracy tej przedstawiono pierwszą kompleksową charakteryzację EVs pochodzących z BALF, oddzielnie dla płuca objętego zmianami chorobowymi (cBALF) oraz drugiego płuca (oBALF) i osocza od pacjentów z NDRP, na dużej grupie pacjentów (34 osoby), stosując klasyczne metody charakterystyki EVs oraz stosunkowo nową metodę f-NTA. Opracowano i zoptymalizowano metodę izolacji EVs z BALF z użyciem ultrawirowania oraz izolacji EVs z osocza metodą SEC. Przeprowadzono optymalizację stężenia barwników i przeciwciał stosowanych w f-NTA. Przeprowadzono charakteryzację uzyskanych izolatów metodami Western Blot, cytometrii przepływowej z użyciem kulek magnetycznych oraz wykonano obrazowanie metodą kriogenicznej transmisyjnej mikroskopii elektronowej (Cryo-TEM), pokazując czystość uzyskanych preparatów. Porównano ilościowo i jakościowo profil EVs z krwi i BALF z wykorzystaniem klasycznego pomiaru NTA, a także z użyciem f-NTA z wykorzystaniem barwienia błonowego i barwienia z wykorzystaniem przeciwciał specyficznych na tetraspaniny CD9, CD63 i CD81.

Porównanie preparatów z wykorzystaniem samego klasycznego pomiaru NTA w świetle rozproszonym ukazało, że EVs w badanych izolatach z osocza miały wyższe stężenie pęcherzyków oraz białka oraz mniejszy rozmiar niż EVs z BALF. Porównanie cBALF z oBALF w świetle rozproszonym wykazało brak statystycznie istotnych różnic między EVs ze zmienionego chorobowo płuca i płuca zdrowego pod względem w liczby oraz wielkości pęcherzyków, a także stężenia białka w preparatach.

Barwienie błonowe i użycie f-NTA pozwoliło pokazać, że tylko część cząstek widocznych w klasycznym NTA to istotnie są pęcherzyki. Wykazano, że odpowiednio 30.9 % cząstek w izolatach EVs z osocza oraz średnio 50.9% cząstek w izolatach z cBALF i 49.3% w izolatach z oBALF ulega barwieniu błonowemu, czyli zawiera błony biologiczne. Można podejrzewać, że pozostała część próbki to zanieczyszczenia, które są również mierzone przez NTA. Barwienie błonowe potwierdziło większe stężenie EVs z osocza oraz ich mniejszy rozmiar w porównaniu do EVs z BALF, jednak pęcherzyki po barwieniu były istotnie większe niż przed barwieniem. Porównanie cBALF z oBALF w barwieniu błonowym wykazało, że EVs z cBALF były większe niż te z oBALF.

Barwienie za pomocą specyficznych przeciwciał na typowe egzosomalne markery-tetraspaniny i analiza f-NTA dostarczyły kolejnych informacji. W przypadku EVs z osocza,

w przeciwieństwie do BALF, nie wykryto tetraspanin CD63 oraz CD81, a CD9 wykryto tylko u 3 pacjentów. Fluorescencyjna charakteryzacja BALF EVs wykazała brak różnic w profilu cBALF i oBALF EVs w zakresie stężenia oraz procencie fluorescencyjnych cząstek. W przypadku cBALF EVs odsetek cząstek fluorescencyjnych w porównaniu do wszystkich cząstek widocznych w trybie rozproszenia (scatter) był wysoki w CMDR (50.9%) i CD9 (56.0%), niższy w CD63 (35.5%), a najniższy w CD81 (8.2%). Wielkość pęcherzyków wykazujących obecność tetraspanin była znacząco mniejsza niż wszystkich cząstek mierzonych w trybie rozproszenia (średnia  $\pm$  SD: 171.95  $\pm$  23.72 nm) a także cząstek posiadających błonę lipidową (średnia  $\pm$  SD: 183.23  $\pm$  32.70 nm). Jednocześnie wielkość wszystkich pęcherzyków pozytywnych dla poszczególnych tetraspanin była zbliżona (średnia  $\pm$  SD: CD63: 100.76  $\pm$  38.62 nm; CD9: 104.21  $\pm$  22.11 nm; CD81: 115.81  $\pm$  46.01 nm). Uzyskane stosunki ilości zmierzonych cząstek do stężenia białek były 100 razy wyższe dla osocza i 10 razy wyższe dla BALF-EVs niż stosunki uzyskane dla hodowli komórkowej lub EV z moczu podane we wcześniejszych badaniach (35).

Zestawienie wyników f-NTA oraz danych klinicznych 34 pacjentów (z czego sześć okazało się nie mieć NDRP tylko inne schorzenia, a u trzech nowotwór nie został jednoznacznie potwierdzony) wykazało brak istotnych różnic oraz korelacji dla wszystkich badanych parametrów między grupą pacjentów z potwierdzonym NDRP a pacjentami z innymi zmianami chorobowymi płuc. Mogło to być spowodowane zbyt małymi liczbami pacjentów w poszczególnych grupach, bądź faktem, że nasze izolaty BALF EV zawierały zarówno EV pochodzenia rakowego, jak EV pochodzące od komórek normalnie występujących w tym środowisku i na podstawie ogólnej charakterystyki nie da się ich rozróżnić.

Podsumowując, potwierdzono wcześniejsze doniesienia, że EVs zawierające tetraspaniny należą do mniejszych mikropecherzyków poniżej 120 nm (nazywanych też egzosomami) i stanowią tylko część wszystkich mikropecherzyków o nieco większej średniej wielkości. Pokazano, że znakowanie EVs z użyciem trybu fluorescencyjnego analizy NTA może dostarczyć informacji o koncentracji, rozmiarze, dystrybucji i fenotypie powierzchniowym w postaci tetraspanin izolatów EVs z heterogenicznych roztworów, pod warunkiem, że nie zawierają one zbyt dużo zanieczyszczeń. Wykonując analizę f-NTA EVs pochodzących z BALF w porównaniu do EVs z osocza, ujawniono, że metoda ta, szczególnie w przypadku oznaczania poziomu tetraspanin, nadaje się tylko do stosunkowo czystych preparatów EV, takich jak BALF lub nadsącz z hodowli komórkowych. Preparaty EV z osocza lub surowicy, zawierające bardzo niskie poziomy EV w porównaniu do zanieczyszczających

lipoprotein, są mniej odpowiednie do charakteryzowania metodą f-NTA, gdyż obecne zanieczyszczenia mogą zaburzać proces barwienia a także dodatkowo maskować już i tak stosunkowo słaby sygnał fluorescencji takich markerów jak tetraspaniny. Udowodniono, że specyficzne znakowanie błony barwnikami lipidowymi nie pozwala w pełni odróżnić „prawdziwych” EVs od lipoprotein podobnej wielkości, jednakże zastosowanie metody usuwania lipoprotein może poprawić specyficzność i wydajność barwienia.

Przeprowadzona po raz pierwszy na tak dużej grupie pacjentów z podejrzeniem NDRP porównawcza analiza profilu EVs uzyskanych z osocza oraz BALF wykazała spodziewane różnice ilościowe i jakościowe profilu EVs z tych dwóch źródeł. Jednakże wbrew oczekiwaniom nie znaleziono różnic w profilu EVs między płucem chorym (cBALF) a zdrowym (oBALF), co może wskazywać na to, że płuca stanowią w tym wypadku jedno mikrośrodowisko niezależnie od umiejscowienia guza. Ponieważ niestety nie zaobserwowano statystycznie znaczących korelacji między zbadanym profilem EVs a danymi klinicznymi w badanej grupie 34 pacjentów, nie udało się rozstrzygnąć na tym etapie badań, czy badane EVs z osocza i BALF mogą mieć znaczenie diagnostyczne.

Wiedza uzyskana w trakcie optymalizacji metod izolacji i charakteryzacji EVs metodami fluorescencyjnymi pozwoliła na przygotowanie pracy przeglądowej podsumowującej informacje, jakie należy wziąć pod uwagę przy projektowaniu badań fluorescencyjnych EVs dotyczące doboru sprzętu do analizy, metod izolacji i barwienia oraz wpływu czynników zakłócających. Pokazano, że wybór odpowiedniej metody analizy fluorescencyjnej EVs wymaga dokładnego rozważenia wielu czynników, takich jak: rodzaj płynu biologicznego z którego izolowane są EVs, metody izolacji, które cechy EVs chcemy zbadać, możliwe czynniki zakłócające, wrażliwość sprzętu do analizy na zanieczyszczenia, wpływ wybranej metody barwienia na funkcjonalność EVs, itd. Na podstawie najnowszych danych literaturowych przedyskutowano wpływ każdego z omawianych czynników na analizę fluorescencyjną EVs i wykazano, że odpowiednio zaprojektowane badanie z wykorzystaniem fluorescencji pozwala na dokładniejsze i bardziej specyficzne pomiary rozmiaru i stężenia EVs. Przedstawiono zaawansowane metody wykorzystujące fluorescencję do analizy EVs, takie jak NTA i nFC, ujmując w formie tabelarycznej informacje na temat zalet i wad, kosztów i przepustowości wybranych sprzętów do analizy fluorescencyjnej EVs oraz dostępnego szerokiego spektrum związków i przeciwciał o właściwościach fluorescencyjnych do znakowania pęcherzyków.

Bazując na doświadczeniach w trakcie opisanych wyżej prac eksperymentalnych podkreślono w pracy przeglądowej fakt, że konwencjonalne NTA dostarcza tylko ogólnych informacji o liczbie i wielkości cząstek zawartych w badanej próbce, z których, jak udowodniono, tylko część jest pochodzenia biologicznego, a jeszcze mniej jest samych EVs. Dopiero analiza f-NTA, z wykorzystaniem odpowiednich barwień błonowych czy przeciwciał dla specyficznych markerów, pozwala na dokładniejsze określenie rzeczywistych stężeń oraz wielkości pęcherzyków. Z kolei do poznania dokładniejszego składu molekularnego pęcherzyków najczęściej używa się dedykowanych lub specjalnie zmodyfikowanych urządzeń do cytometrii przepływowej dla cząstek mniejszych niż 300 nm.

Na podstawie wybranych prac zwrócono uwagę na fakt, że analiza EVs z płynów biologicznych różni się znacząco od analizy EVs uzyskanych z hodowli komórkowych, głównie z uwagi na dużo bardziej zróżnicowany skład matrycy próbki oraz jej znacznie ograniczoną objętość. Analiza taka powinna być przeprowadzana z uwzględnieniem obecności lipoprotein (w przypadku próbek z osocza) oraz innych substancji zakłócających w płynach biologicznych, które czasami trudno odróżnić od EVs. Należy również uwzględnić białkową koronę EVs, która wpływa na ich właściwości i może zapewniać zupełnie inne, dodatkowe funkcje biologiczne, które mogą zostać utracone, jeśli wybrana metoda izolacji EVs usunie białkową koronę. Na podstawie wybranych prac przedyskutowano, jak zastosowane metody izolacji EVs, zanieczyszczenia występujące w danym typie płynu biologicznego oraz wybrane metody barwienia i analizy pęcherzyków mogą prowadzić do znacząco innych wyników i wniosków z nich płynących. Podkreślono, że w badaniach warto wykorzystywać równoległe kilka sposobów znakowania, ponieważ pozwoli to uzyskać więcej informacji na temat analizowanych pęcherzyków.

W ramach kontynuacji przedstawionych w ramach Publikacji nr. 1 badań, powiększono badaną grupę o kolejnych pacjentów i prowadzone są dalsze badania, tj. analiza f-NTA dla w sumie 82 pacjentów oraz analiza z wykorzystaniem obrazowej cytometrii przepływowej poziomu dodatkowych specyficznych markerów obecnych na powierzchni EVs, związanych z ich funkcjami prozapalnymi i promującymi wzrost nowotworu. Ponadto wykonano kompleksową analizę fenotypu komórek immunologicznych wyizolowanych równoległe z EVs z osocza i BALF pacjentów, takich jak limfocyty CD8<sup>+</sup> i CD4<sup>+</sup>, limfocyty T regulatorowe oraz zbadano ich poziom apoptozy w klasycznej cytometrii przepływowej (dane nieopublikowane). Korelacja między danymi uzyskanymi z f-NTA oraz obrazowej cytometrii przepływowej z profilem komórek immunologicznych oraz danymi klinicznymi w tej znacznie poszerzonej



grupie pacjentów pozwoli znaleźć odpowiedź na pytanie, czy EVs z osocza i/lub BALF danego pacjenta mogą odzwierciedlać jego status immunologiczny i stopień immunosupresji charakterystyczny dla nowotworów i czy mogą spełniać potencjalną rolę diagnostyczną czy prognostyczną dla rozwoju choroby i postępu w terapii. Dodatkowo, prowadzona jest dalsza analiza wpływu lipoprotein na wyniki analizy f-NTA w ramach przyznanego mi Grantu Młodego Badacza na WUM, gdzie próbki osocza zostaną podzielone na dwie części. Z pierwszej części będą usuwane lipoproteiny a następnie przeprowadzona zostanie izolacja EVs metodą SEC i analiza f-NTA i za pomocą cytometrii przepływowej w nanoskali. Z drugiej części przeprowadzone zostaną analogiczne analizy, tylko bez usuwania lipoprotein. Następnie przeprowadzone zostanie porównanie wyników.

Dążenie wielu badaczy do wykorzystania EVs jako biomarkerów do celów klinicznych wymaga w pierwszej kolejności wypracowania powtarzalnych, dokładnych i wiarygodnych metod charakteryzacji ilościowej i jakościowej tych mikropęcherzyków. Przedstawiona praca jako jedna z pierwszych tego typu podejmuje próbę optymalizacji i weryfikacji takiej metody bazującej na barwieniu fluorescencyjnym i nowatorskiej technologii f-NTA EVs uzyskanych z rzeczywistych próbek klinicznych.

## Bibliografia

1. Zhang C, Ji Q, Yang Y, Li Q, Wang Z. Exosome: Function and Role in Cancer Metastasis and Drug Resistance. *Technol Cancer Res Treat*. 2018;17:1533033818763450.
2. Mathivanan S, Simpson RJ. ExoCarta: A compendium of exosomal proteins and RNA. *Proteomics*. 2009;9(21):4997-5000.
3. Lugini L, Cecchetti S, Huber V, Luciani F, Macchia G, Spadaro F, et al. Immune surveillance properties of human NK cell-derived exosomes. *J Immunol*. 2012;189(6):2833-42.
4. Soung YH, Ford S, Zhang V, Chung J. Exosomes in Cancer Diagnostics. *Cancers (Basel)*. 2017;9(1).
5. Guo L, He B. Extracellular vesicles and their diagnostic and prognostic potential in cancer. *Translational Cancer Research*. 2017;6(3):599-612.
6. Kumar MA, Baba SK, Sadida HQ, Marzooqi SA, Jerobin J, Altemani FH, et al. Extracellular vesicles as tools and targets in therapy for diseases. *Signal Transduct Target Ther*. 2024;9(1):27.
7. Hirsch FR, Scagliotti GV, Mulshine JL, Kwon R, Curran WJ, Jr., Wu YL, et al. Lung cancer: current therapies and new targeted treatments. *Lancet*. 2017;389(10066):299-311.
8. Zheng M. Classification and Pathology of Lung Cancer. *Surg Oncol Clin N Am*. 2016;25(3):447-68.
9. Pink RC, Beaman EM, Samuel P, Brooks SA, Carter DRF. Utilising extracellular vesicles for early cancer diagnostics: benefits, challenges and recommendations for the future. *Br J Cancer*. 2022;126(3):323-30.
10. Carreca AP, Tinnirello R, Miceli V, Galvano A, Gristina V, Incorvaia L, et al. Extracellular Vesicles in Lung Cancer: Implementation in Diagnosis and Therapeutic Perspectives. *Cancers (Basel)*. 2024;16(11).
11. Nicoś M, Krawczyk P, Szczyrek M, Mandziuk S, Jarosz B, Wojas-Krawczyk K, et al. Do we apply a personalised lung cancer therapy? Use of molecular tests in scheduling a multilineage treatment in a patient with lung adenocarcinoma. *Oncology in Clinical Practice*. 2017;13(1):24-9.
12. Kris MG, Johnson BE, Berry LD, Kwiatkowski DJ, Iafrate AJ, Wistuba II, et al. Using Multiplexed Assays of Oncogenic Drivers in Lung Cancers to Select Targeted Drugs. *Jama*. 2014;311(19).
13. Cooper AJ, Sequist LV, Lin JJ. Third-generation EGFR and ALK inhibitors: mechanisms of resistance and management. *Nat Rev Clin Oncol*. 2022;19(8):499-514.
14. Brahmer JR. PD-1-targeted immunotherapy: recent clinical findings. (1543-0790 (Print)).
15. Antonia SJ, Villegas A, Daniel D, Vicente D, Murakami S, Hui R, et al. Durvalumab after Chemoradiotherapy in Stage III Non-Small-Cell Lung Cancer. *N Engl J Med*. 2017;377(20):1919-29.
16. Gandhi L, Rodriguez-Abreu D, Gadgeel S, Esteban E, Felip E, De Angelis F, et al. Pembrolizumab plus Chemotherapy in Metastatic Non-Small-Cell Lung Cancer. *N Engl J Med*. 2018;378(22):2078-92.
17. Schoenfeld AJ, Arbour KC, Rizvi H, Iqbal AN, Gadgeel SM, Girshman J, et al. Severe immune-related adverse events are common with sequential PD-(L)1 blockade and osimertinib. *Ann Oncol*. 2019;30(5):839-44.
18. Whiteside TL. The potential of tumor-derived exosomes for noninvasive cancer monitoring: an update. *Expert Rev Mol Diagn*. 2018;18(12):1029-40.
19. Stevic I, Buescher G, Ricklefs FL. Monitoring Therapy Efficiency in Cancer through Extracellular Vesicles. *Cells*. 2020;9(1).
20. Czystowska-Kuzmicz M, Whiteside TL. The potential role of tumor-derived exosomes in diagnosis, prognosis, and response to therapy in cancer. *Expert Opin Biol Ther*. 2021;21(2):241-58.
21. Whiteside TL, Diergaarde B, Hong CS. Tumor-Derived Exosomes (TEX) and Their Role in Immuno-Oncology. *Int J Mol Sci*. 2021;22(12).
22. Zhou E, Li Y, Wu F, Guo M, Xu J, Wang S, et al. Circulating extracellular vesicles are effective biomarkers for predicting response to cancer therapy. *EBioMedicine*. 2021;67:103365.

23. Asleh K, Dery V, Taylor C, Davey M, Djeungoue-Petga MA, Ouellette RJ. Extracellular vesicle-based liquid biopsy biomarkers and their application in precision immuno-oncology. *Biomark Res.* 2023;11(1):99.
24. Pang B, Zhu Y, Ni J, Ruan J, Thompson J, Malouf D, et al. Quality Assessment and Comparison of Plasma-Derived Extracellular Vesicles Separated by Three Commercial Kits for Prostate Cancer Diagnosis. *Int J Nanomedicine.* 2020;15:10241-56.
25. Simonsen JB. What Are We Looking At? Extracellular Vesicles, Lipoproteins, or Both? *Circ Res.* 2017;121(8):920-2.
26. Chen C, Cai N, Niu Q, Tian Y, Hu Y, Yan X. Quantitative assessment of lipophilic membrane dye-based labelling of extracellular vesicles by nano-flow cytometry. *J Extracell Vesicles.* 2023;12(8):e12351.
27. Lozano-Andres E, Enciso-Martinez A, Gijsbers A, Ridolfi A, Van Niel G, Libregts S, et al. Physical association of low density lipoprotein particles and extracellular vesicles unveiled by single particle analysis. *J Extracell Vesicles.* 2023;12(11):e12376.
28. Boudna M, Campos AD, Vychytilova-Faltejskova P, Machackova T, Slaby O, Souckova K. Strategies for labelling of exogenous and endogenous extracellular vesicles and their application for in vitro and in vivo functional studies. *Cell Commun Signal.* 2024;22(1):171.
29. Tushuizen ME, Diamant M, Peypers EG, Hoek FJ, Heine RJ, Sturk A, et al. Postprandial changes in the phospholipid composition of circulating microparticles are not associated with coagulation activation. *Thromb Res.* 2012;130(1):115-21.
30. Muller L, Hong CS, Stolz DB, Watkins SC, Whiteside TL. Isolation of biologically-active exosomes from human plasma. *J Immunol Methods.* 2014;411:55-65.
31. van der Pol E, Welsh JA, Nieuwland R. Minimum information to report about a flow cytometry experiment on extracellular vesicles: Communication from the ISTH SSC subcommittee on vascular biology. *J Thromb Haemost.* 2022;20(1):245-51.
32. Botha J, Pugsley HR, Handberg A. Conventional, High-Resolution and Imaging Flow Cytometry: Benchmarking Performance in Characterisation of Extracellular Vesicles. *Biomedicines.* 2021;9(2).
33. Arraud N, Gounou C, Turpin D, Brisson AR. Fluorescence triggering: A general strategy for enumerating and phenotyping extracellular vesicles by flow cytometry. *Cytometry A.* 2016;89(2):184-95.
34. They C, Witwer KW, Aikawa E, Alcaraz MJ, Anderson JD, Andriantsitohaina R, et al. Minimal information for studies of extracellular vesicles 2018 (MISEV2018): a position statement of the International Society for Extracellular Vesicles and update of the MISEV2014 guidelines. *J Extracell Vesicles.* 2018;7(1):1535750.
35. Dong L, Zieren RC, Horie K, Kim CJ, Mallick E, Jing Y, et al. Comprehensive evaluation of methods for small extracellular vesicles separation from human plasma, urine and cell culture medium. *J Extracell Vesicles.* 2020;10(2):e12044.

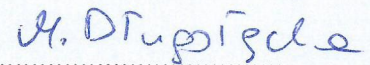
## **Oświadczenia współautorów publikacji**

Warszawa 03.07.2024  
(miejsowość, data)

mgr inż. Magdalena Długołęcka

## OŚWIADCZENIE

Jako współautor pracy pt. „Characterization of Extracellular Vesicles from Bronchoalveolar Lavage Fluid and Plasma of Patients with Lung Lesions Using Fluorescence Nanoparticle Tracking Analysis” oświadczam, iż mój własny wkład merytoryczny w przygotowanie, przeprowadzenie i opracowanie badań oraz przedstawienie pracy w formie publikacji stanowi: udział w przygotowaniu koncepcji, przeprowadzenie badań, interpretacja wyników, przeprowadzenie analizy statystycznej, napisanie manuskryptu, przygotowanie i opis figur. Mój udział procentowy w przygotowaniu publikacji określam jako 51%.



.....  
(podpis oświadczającego)

\*w szczególności udziału w przygotowaniu koncepcji, metodyki, wykonaniu badań, interpretacji wyników



Warszawa, 03.07.2024  
(miejsowość, data)

Mgr inż. Jacek Szymański

## OŚWIADCZENIE

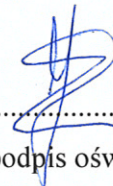
Jako współautor pracy pt. „Characterization of Extracellular Vesicles from Bronchoalveolar Lavage Fluid and Plasma of Patients with Lung Lesions Using Fluorescence Nanoparticle Tracking Analysis” oświadczam, iż mój własny wkład merytoryczny w przygotowanie, przeprowadzenie i opracowanie badań oraz przedstawienie pracy w formie publikacji stanowi: przeprowadzenie badań oraz przygotowanie figury 1 i 10.

Mój udział procentowy w przygotowaniu publikacji określam jako 9%.

Wkład Pani mgr inż. Magdaleny Długołęckiej w powstawanie publikacji określam jako 51%, obejmował on udział w przygotowaniu koncepcji, przeprowadzenie badań, interpretację wyników, przeprowadzenie analizy statystycznej, napisanie manuskryptu, przygotowanie i opis figur.

(merytoryczny opis wkładu kandydata do stopnia w powstanie publikacji)\*

Jednocześnie wyrażam zgodę na wykorzystanie w/w pracy jako część rozprawy doktorskiej Pani mgr inż. Magdaleny Długołęckiej.



.....  
(podpis oświadczającego)

\*w szczególności udziału w przygotowaniu koncepcji, metodyki, wykonaniu badań, interpretacji wyników



Warszawa 03.07.2024  
(miejsowość, data)

Lek. Łukasz Zaręba

## OŚWIADCZENIE

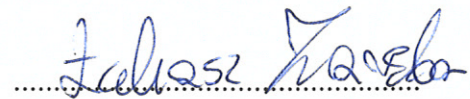
Jako współautor pracy pt. „Characterization of Extracellular Vesicles from Bronchoalveolar Lavage Fluid and Plasma of Patients with Lung Lesions Using Fluorescence Nanoparticle Tracking Analysis” oświadczam, iż mój własny wkład merytoryczny w przygotowanie, przeprowadzenie i opracowanie badań oraz przedstawienie pracy w formie publikacji stanowi: przeprowadzenie badań.

Mój udział procentowy w przygotowaniu publikacji określam jako 8%.

Wkład Pani mgr inż. Magdaleny Długołęckiej w powstanie publikacji określam jako 51%, obejmował on udział w przygotowaniu koncepcji, przeprowadzenie badań, interpretację wyników, przeprowadzenie analizy statystycznej, napisanie manuskryptu, przygotowanie i opis figur.

(merytoryczny opis wkładu kandydata do stopnia w powstanie publikacji)\*

Jednocześnie wyrażam zgodę na wykorzystanie w/w pracy jako część rozprawy doktorskiej Pani mgr inż. Magdaleny Długołęckiej.



(podpis oświadczającego)

\*w szczególności udziału w przygotowaniu koncepcji, metodyki, wykonaniu badań, interpretacji wyników



Warszawa 03.07.2024  
(miejsowość, data)

Mgr Zuzanna Homoncik

## OŚWIADCZENIE

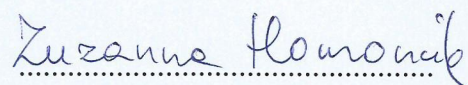
Jako współautor pracy pt. „Characterization of Extracellular Vesicles from Bronchoalveolar Lavage Fluid and Plasma of Patients with Lung Lesions Using Fluorescence Nanoparticle Tracking Analysis” oświadczam, iż mój własny wkład merytoryczny w przygotowanie, przeprowadzenie i opracowanie badań oraz przedstawienie pracy w formie publikacji stanowi: przeprowadzenie badań.

Mój udział procentowy w przygotowaniu publikacji określam jako 8%.

Wkład Pani mgr inż. Magdaleny Długołęckiej w powstawanie publikacji określam jako 51%, obejmował on udział w przygotowaniu koncepcji, przeprowadzenie badań, interpretację wyników, przeprowadzenie analizy statystycznej, napisanie manuskryptu, przygotowanie i opis figur.

(merytoryczny opis wkładu kandydata do stopnia w powstanie publikacji)\*

Jednocześnie wyrażam zgodę na wykorzystanie w/w pracy jako część rozprawy doktorskiej Pani mgr inż. Magdaleny Długołęckiej.



(podpis oświadczającego)

\*w szczególności udziału w przygotowaniu koncepcji, metodyki, wykonaniu badań, interpretacji wyników



Warszawa, 03.07.2024  
(miejsowość, data)

lek. med. Małgorzata Polubiec-Kownacka

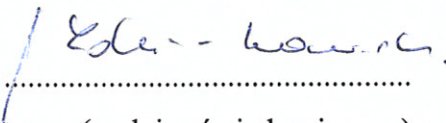
## OŚWIADCZENIE

Jako współautor pracy pt. „Characterization of Extracellular Vesicles from Bronchoalveolar Lavage Fluid and Plasma of Patients with Lung Lesions Using Fluorescence Nanoparticle Tracking Analysis” oświadczam, iż mój własny wkład merytoryczny w przygotowanie, przeprowadzenie i opracowanie badań oraz przedstawienie pracy w formie publikacji stanowi: rekrutacja pacjentów, przeprowadzenie i opis procedury BAL.

Mój udział procentowy w przygotowaniu publikacji określam jako 10%.

Wkład Pani mgr inż. Magdaleny Długołęckiej w powstawanie publikacji określam jako 51%, obejmował on udział w przygotowaniu koncepcji, przeprowadzenie badań, interpretację wyników, przeprowadzenie analizy statystycznej, napisanie manuskryptu, przygotowanie i opis figur. (merytoryczny opis wkładu kandydata do stopnia w powstanie publikacji)\*

Jednocześnie wyrażam zgodę na wykorzystanie w/w pracy jako część rozprawy doktorskiej Pani mgr inż. Magdaleny Długołęckiej.

  
.....  
(podpis oświadczającego)

\*w szczególności udziału w przygotowaniu koncepcji, metodyki, wykonaniu badań, interpretacji wyników



Warszawa, 03.07.2024  
(miejsowość, data)

prof. dr hab. n. med. Joanna Domagała-Kulawik

## OŚWIADCZENIE

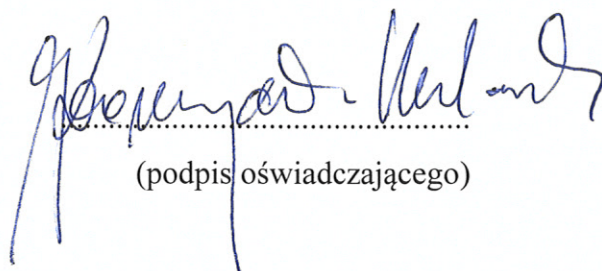
Jako współautor pracy pt. „Characterization of Extracellular Vesicles from Bronchoalveolar Lavage Fluid and Plasma of Patients with Lung Lesions Using Fluorescence Nanoparticle Tracking Analysis” oświadczam, iż mój własny wkład merytoryczny w przygotowanie, przeprowadzenie i opracowanie badań oraz przedstawienie pracy w formie publikacji stanowi: przygotowanie koncepcji badania.

Mój udział procentowy w przygotowaniu publikacji określam jako 5%.

Wkład Pani mgr inż. Magdaleny Długołęckiej w powstawanie publikacji określam jako 51%, obejmował on udział w przygotowaniu koncepcji, przeprowadzenie badań, interpretację wyników, przeprowadzenie analizy statystycznej, napisanie manuskryptu, przygotowanie i opis figur.

(merytoryczny opis wkładu kandydata do stopnia w powstanie publikacji)\*

Jednocześnie wyrażam zgodę na wykorzystanie w/w pracy jako część rozprawy doktorskiej Pani mgr inż. Magdaleny Długołęckiej.



(podpis oświadczającego)

\*w szczególności udziału w przygotowaniu koncepcji, metodyki, wykonaniu badań, interpretacji wyników



Warszawa 03.07.2024  
(miejsowość, data)

dr n. med. i n. o zdr.  
Małgorzata Czystowska-Kuźmicz

## OŚWIADCZENIE

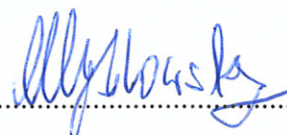
Jako współautor pracy pt. „Characterization of Extracellular Vesicles from Bronchoalveolar Lavage Fluid and Plasma of Patients with Lung Lesions Using Fluorescence Nanoparticle Tracking Analysis” oświadczam, iż mój własny wkład merytoryczny w przygotowanie, przeprowadzenie i opracowanie badań oraz przedstawienie pracy w formie publikacji stanowi: przygotowanie koncepcji, metodologii, zapewnienie zasobów, udział w przygotowaniu i redagowaniu manuskryptu, nadzór nad projektem.

Mój udział procentowy w przygotowaniu publikacji określam jako 9%.

Wkład Pani mgr inż. Magdaleny Długołęckiej w powstawanie publikacji określam jako 51%, obejmował on udział w przygotowaniu koncepcji, przeprowadzenie badań, interpretację wyników, przeprowadzenie analizy statystycznej, napisanie manuskryptu, przygotowanie i opis figur.

(merytoryczny opis wkładu kandydata do stopnia w powstanie publikacji)\*

Jednocześnie wyrażam zgodę na wykorzystanie w/w pracy jako część rozprawy doktorskiej Pani mgr inż. Magdaleny Długołęckiej.



(podpis oświadczającego)

\*w szczególności udziału w przygotowaniu koncepcji, metodyki, wykonaniu badań, interpretacji wyników



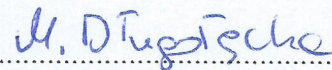
Warszawa 05.09.2024  
(miejsowość, data)

mgr inż. Magdalena Długolecka

## OŚWIADCZENIE

Jako współautor pracy pt. „Factors to consider before choosing EV labeling method for fluorescence-based techniques” oświadczam, iż mój własny wkład merytoryczny w przygotowanie, przeprowadzenie i opracowanie badań oraz przedstawienie pracy w formie publikacji stanowi przygotowanie koncepcji, przegląd literatury, napisanie i udział w redagowaniu manuskryptu.

Mój udział procentowy w przygotowaniu publikacji określam jako 90%.



(podpis oświadczającego)

\*w szczególności udziału w przygotowaniu koncepcji, metodyki, wykonaniu badań, interpretacji wyników



Warszawa 05.09.2024  
(miejsowość, data)

dr n. med. i n. o zdr.  
Małgorzata Czystowska-Kuźmich

## OŚWIADCZENIE

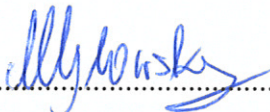
Jako współautor pracy pt. „Factors to consider before choosing EV labeling method for fluorescence-based techniques” oświadczam, iż mój własny wkład merytoryczny w przygotowanie, przeprowadzenie i opracowanie badań oraz przedstawienie pracy w formie publikacji stanowi: udział w przygotowaniu koncepcji, przegląd literatury, redagowanie manuskryptu, nadzór nad projektem.

Mój udział procentowy w przygotowaniu publikacji określam jako 10%.

Wkład Pani mgr inż. Magdaleny Długołęckiej w powstanie publikacji określam jako 90%, obejmował on przygotowanie koncepcji, przegląd literatury, napisanie i udział w redagowaniu manuskryptu.

(merytoryczny opis wkładu kandydata do stopnia w powstanie publikacji)\*

Jednocześnie wyrażam zgodę na wykorzystanie w/w pracy jako część rozprawy doktorskiej Pani mgr inż. Magdaleny Długołęckiej.

  
.....  
(podpis oświadczającego)

\*w szczególności udziału w przygotowaniu koncepcji, metodyki, wykonaniu badań, interpretacji wyników